2001-12

Planetary and topographic Beta effects on the Northern Canary Current System (NCCS)

Towle, Wendy A.

Monterey, California. Naval Postgraduate School

NAVAL POSTGRADUATE SCHOOL
Monterey, California

THESIS

PLANETARY AND TOPOGRAPHIC BETA EFFECTS ON THE NORTHERN CANARY CURRENT SYSTEM (NCCS)

by

Wendy A. Towle

December 2001

Thesis Advisor:	Mary L. Batteen
Second Reader:	R. T. Williams

Approved for public release; distribution is unlimited.

THIS PAGE INTENTIONALLY LEFT BLANK

REPORT DOCUMENTATION PAGE			Form Approved OMB No. 0704-0188
Public reporting burden for this collection of information is estimated to average 1 hour per response, including the time for reviewing instruction, searching existing data sources, gathering and maintaining the data needed, and completing and reviewing the collection of information. Send comments regarding this burden estimate or any other aspect of this collection of information, including suggestions for reducing this burden, to Washington headquarters Services, Directorate for Information Operations and Reports, 1215 Jefferson Davis Highway, Suite 1204, Arlington, VA 22202-4302, and to the Office of Management and Budget, Paperwork Reduction Project (0704-0188) Washington DC 20503.			
1. AGENCY USE ONLY *(Leave blank)*	**2. REPORT DATE** December 2001	**3. REPORT TYPE AND DATES COVERED** Master's Thesis	
4. TITLE AND SUBTITLE: Planetary and Topographic Beta Effects on the Northern Canary Current System (NCCS)			**5. FUNDING NUMBERS**
6. AUTHOR(S) Towle, Wendy A.			
7. PERFORMING ORGANIZATION NAME(S) AND ADDRESS(ES) Naval Postgraduate School Monterey, CA 93943-5000			**8. PERFORMING ORGANIZATION REPORT NUMBER**
9. SPONSORING / MONITORING AGENCY NAME(S) AND ADDRESS(ES) N/A			**10. SPONSORING / MONITORING AGENCY REPORT NUMBER**
11. SUPPLEMENTARY NOTES The views expressed in this thesis are those of the author and do not reflect the official policy or position of the Department of Defense or the U.S. Government.			
12a. DISTRIBUTION / AVAILABILITY STATEMENT Approved for public release; distribution is unlimited.			**12b. DISTRIBUTION CODE**

13. ABSTRACT ***(maximum 200 words)***

To investigate planetary and topographic beta effects on classical as well as unique features in the northern Canary Current system (NCCS), several numerical experiments using the Princeton Ocean Model are explored. To isolate the dependence of Coriolis parameterization (β-plane vs. *f*-plane) from the topographic beta effect, the first (last) two experiments use a flat bottom (topography). In all experiments, classical eastern boundary condition (EBC) features are produced including an offshore surface equatorward meandering jet, coastal surface and subsurface poleward currents, upwelling, meanders, eddies and filaments. Due to the beta effect, the surface coastal jet does not have to be confined to within a Rossby radius of deformation of the coast. The beta effect also plays an important role in the development and westward propagation of Meddies, a unique feature of the NCCS. Bottom topography is shown to play an important role in narrowing, intensifying, and trapping coastal currents. These results show that, while wind forcing is the primary mechanism for generating classical EBC features, planetary and topographic beta also play important roles in the generation, evolution, and maintenance of classical as well as unique features in the NCCS.

14. SUBJECT TERMS Primitive equation model, northern Canary Current System, currents, meanders, eddies, filaments, undercurrent, POM			**15. NUMBER OF PAGES**
			16. PRICE CODE
17. SECURITY CLASSIFICATION OF REPORT Unclassified	**18. SECURITY CLASSIFICATION OF THIS PAGE** Unclassified	**19. SECURITY CLASSIFICATION OF ABSTRACT** Unclassified	**20. LIMITATION OF ABSTRACT** UL

NSN 7540-01-280-5500 Standard Form 298 (Rev. 2-89)
Prescribed by ANSI Std. 239-18

THIS PAGE INTENTIONALLY LEFT BLANK

Approved for public release; distribution is unlimited

PLANETARY AND TOPOGRAPHIC BETA EFFECTS ON THE NORTHERN CANARY CURRENT SYSTEM (NCCS)

Wendy A. Towle
Lieutenant, United States Navy
B.S., United States Naval Academy, 1995

Submitted in partial fulfillment of the
requirements for the degree of

MASTER OF SCIENCE IN METEOROLOGY AND PHYSICAL OCEANOGRAPHY

from the

NAVAL POSTGRADUATE SCHOOL
December 2001

Author: Wendy A. Towle
Wendy A. Towle

Approved by: Mary L. Batteen
Mary L. Batteen, Thesis Advisor

R. T. Williams
R. T. Williams, Second Reader

Mary Batteen
Mary L. Batteen, Chairman
Department of Oceanography

THIS PAGE INTENTIONALLY LEFT BLANK

ABSTRACT

To investigate planetary and topographic beta effects on classical as well as unique features in the northern Canary Current system (NCCS), several numerical experiments using the Princeton Ocean Model are explored. To isolate the dependence of Coriolis parameterization (β-plane vs. *f*-plane) from the topographic beta effect, the first (last) two experiments use a flat bottom (topography). In all experiments, classical eastern boundary condition (EBC) features are produced including an offshore surface equatorward meandering jet, coastal surface and subsurface poleward currents, upwelling, meanders, eddies and filaments. Due to the beta effect, the surface coastal jet does not have to be confined to within a Rossby radius of deformation of the coast. The beta effect also plays an important role in the development and westward propagation of Meddies, a unique feature of the NCCS. Bottom topography is shown to play an important role in narrowing, intensifying, and trapping coastal currents. These results show that, while wind forcing is the primary mechanism for generating classical EBC features, planetary and topographic beta also play important roles in the generation, evolution, and maintenance of classical as well as unique features in the NCCS.

THIS PAGE INTENTIONALLY LEFT BLANK

TABLE OF CONTENTS

THIS PAGE INTENTIONALLY LEFT BLANK

LIST OF FIGURES

THIS PAGE INTENTIONALLY LEFT BLANK

LIST OF TABLES

THIS PAGE INTENTIONALLY LEFT BLANK

I. INTRODUCTION

The Canary Current System (CCS) on the eastern boundary of the central North Atlantic is a classical eastern boundary current (EBC) system. Stretching from ~10°N to ~45°N along the coasts of northwest Africa and the Iberian Peninsula (IP), it marks the closing eastern boundary of the North Atlantic Gyre. Typical of other EBCs, the mean equatorward Canary Current (CC), is a broad (~1000 km), relatively slow (~10-30 cm/s), yearlong surface flow extending to depths of ~500 m (Wooster *et al.*, 1976). The portion of the CC that stretches along the coast of the IP is often referred to as the Portugal Current (e.g., Tomczak and Godfrey, 1994).

As in other EBCs, a poleward undercurrent exists near the coast beneath the CC (e.g., Meincke *et al.*, 1975; Fiuza, 1980) as a relatively narrow (~10-40 km) and weak (~2-10 cm/s) flow, which is strongest between ~100 and ~600 m depth. The depth and strength of the undercurrent varies seasonally and latitudinally. In winter it shoals to the north near Cabo da Roca (see Figures 1a and 1b for geographic locations, and Figure 22.1 of Barton, 1998 for bathymetric contours and coastline geometry for the region), and forms a third flow component commonly referred to as the Iberian Current (Haynes and Barton, 1990). A narrow (~25-40 km), relatively weak (~20-30 cm/s), seasonal surface current, the Iberian Current is found trapped near the coast against the shelf break (Fiuza, 1980; Frouin *et al.*, 1990; Haynes and Barton, 1990) and can occasionally be seen as far south as Cabo de Sao Vicente (Batteen *et al.*, 2000).

A unique feature that distinguishes the CCS from other EBCs is the existence of Mediterranean Outflow (MO) through the Strait of Gibraltar into the adjacent Gulf of Cadiz. A large embayment, the Gulf of Cadiz's pronounced east-west coastline orientation results in weaker upwelling in the Gulf of Cadiz than to the north or south of the Gulf of Cadiz, due to the dominant equatorward trade wind direction. The Gulf of Cadiz also creates a large separation between the two west coast upwelling regimes so that no continuous flow between the two appears to exist (Barton, 1998).

The salty MO plume that exits the Mediterranean Sea through the Strait of Gibraltar is diluted, thickens, and becomes vertically differentiated into two distinct cores

as it flows westward into the Gulf of Cadiz (Iorga and Lozier, 1999). At ~7°W in the Gulf of Cadiz, both a shallow core at depths of ~600-900 m and a deeper core at ~1100-1200 m exist. Both cores continue to flow westward along the southern coast of Spain and turn poleward around Cabo de Sao Vicente (Ambar and Howe, 1979; Iorga and Lozier, 1999). A third, shallower, poleward core of Mediterranean water has also been traced from the Strait of Gibraltar northward to ~38.5°N off western Portugal (Ambar, 1982). In addition, a climatological cyclonic circulation in the southwestern Gulf of Cadiz acts to spread salty MO south of ~34°N (Iorga and Lozier, 1999).

The northern CCS (NCCS) is influenced predominantly by equatorward, upwelling favorable winds produced by the eastern half of the Azores High. Located in the northeastern part of the Atlantic Ocean, the Azores High is a semi-permanent subtropical high pressure system similar in nature and behavior to the North Pacific Subtropical High (Nelson, 1977). As such, the center of the Azores High migrates meridionally with the seasons, reaching its southernmost extent near 27°N in March and ridging north to ~33°N by August. The building and migration of the Azores High cause wind stress values over the NCCS region to vary temporally, resulting in both alongshore and cross-shore variability of the predominantly equatorward winds along the west coast of the IP and the northwest coast of Africa. The east-west pressure contrast between Portugal and the center of the Azores High during summer is ~8 mb. In winter, this pressure gradient weakens to ~1 mb. As a result of this seasonally changing pressure gradient, considerably stronger northerly and northwesterly winds occur in the NCCS region in summer, while northerly and northwesterly winds become weaker to even slight southerly off the Iberian Peninsula in winter (Batteen *et al.*, 2000). The shift in maximum wind stress also causes upwelling favorable winds to shift from ~27°N near the Canary Islands in January, to ~43°N off Portugal by July (Fiuza, 1982).

Like other classical EBCs, observations of the sea surface in the NCCS region have shown highly energetic mesoscale features such as jet-like surface currents, meanders, eddies and filaments over the broad climatological mean flow of the CC. Satellite sea surface images have shown nearshore upwelling during periods of upwelling favorable winds with several narrow filaments of cooler water extending off the coast of

the Iberian Peninsula (Fiuza and Sousa, 1989) and Cape Ghir in northwest Africa (Van Camp *et al.*, 1991; Hagen *et al.*, 1996). In these images, upwelling filaments often extend ~80-150 km offshore, with alongshore spacing of ~80-100 km between filaments (Haynes *et al.*, 1993), and often terminate with dipole eddy pairs (Fiuza *et al.*, 1982; Barton, 1998). Observations have also shown anticyclonic and cyclonic pairs of mesoscale eddies on the order of 100 km off the IP coast (Fiuza, 1984; Stammer *et al.*, 1991). These mesoscale features have been observed during periods of predominantly upwelling favorable winds and appear to be located near prominent coastline irregularities such as capes. These observations provide evidence that wind forcing along coastline irregularities appear to be important mechanisms in the formation and sustainment of many of the mesoscale features found in the NCCS domain and other EBC regions (Batteen *et al.*, 2000).

Unique to the NCCS is the generation of anticyclonic submesoscale coherent vortices (SCVs) or Meddies. Numerical studies suggest that baroclinic instability of the northward dense plume of salty MO along the IP continental slope leads to the generation of Meddies (Kase *et al.*, 1989). As a result of numerous observations over the past decade, the primary generation region of Meddies is widely accepted to be near Cabo de Sao Vicente, off southwest Portugal. Several different trajectories of Meddies have been observed, including a southwestward movement into the Canary Basin, and westward translations south of the Azores (Richardson and Tychensky, 1998).

Over the last two decades numerous modeling studies have focused on the driving mechanism of complex mesoscale activities in EBC regions, including upwelling filaments, highly energetic eddies, and meandering jets. For the California Current System, the classical EBC system, Ikeda *et al.* (1984a, b) and Haidvogel *et al.* (1991) studied baroclinic instability, coastline irregularities, and bottom topography as possible mechanisms, while Batteen *et al.* (1989), McCreary *et al*. (1991), Pares-Sierra *et al.* (1993), Batteen (1997) and Batteen *et al.* (2000) studied wind forcing as a possible generation mechanism.

For over a decade, a high resolution, multi-level, primitive equation model has been used to examine the response to wind forcing of an idealized flat-bottomed oceanic

regime along different eastern ocean boundaries (e.g., Batteen, 1989; Batteen, 1997, Batteen *et al.*, 2000). Results from sensitivity studies have produced various results depending on the type of wind forcing, coastline geometry and Coriolis parameterization used.

For the California Current System, Batteen (1989) used a band of steady alongshore, upwelling favorable winds, either with or without alongshore variability, as forcing on both an *f*-plane and β-plane. This study was conducted using a straight California coast only. Eddies and jets with strong onshore and offshore directed flows were generated, along with a coastal jet and undercurrent on a scale and magnitude consistent with available observed data. The results supported the hypothesis that alongshore varying wind forcing on a β-plane is an important generation mechanism for eddies in the California Current System.

For the California Current System, Batteen (1997) forced the model from rest using seasonal climatological winds along a straight California coast on both an *f*-plane and β-plane. This study also included seasonal climatological wind forcing on an irregular coastline using β-plane only and focused on the role of the beta effect in generating, evolving and maintaining classical mesoscale features in the California Current System. The results of this study showed that a surface equatorward current, upwelling of cooler water along the coast, and a poleward undercurrent develop in response to the prevailing wind direction. In addition, baroclinic and barotropic instabilities develop in the equatorward surface current and poleward flow, resulting in the generation of meanders near the coast, upwelling filaments extending offshore, and the subsequent development of seasonal or semi-permanent cyclonic and anticyclonic eddies farther offshore. While the meridional variability of f (β-plane) and variability in the equatorward component of wind stress were shown to be necessary ingredients for generating realistic vertical and horizontal structures for the cores of the surface equatorward and subsurface poleward currents, irregularities in the coastline geometry were shown to be important for "anchoring" upwelling and filaments, and for enhancing the growth of meanders and eddies. The results from several numerical experiments in this process-oriented study supported the hypothesis that wind forcing and coastline

irregularities on a β-plane are important mechanisms for generation of observed mesoscale features of the California Current System.

In a more recent study Batteen *et al.*, (2000) used the results of four numerical experiments of increasing complexity to investigate the unique and classical features of the NCCS. All four experiments were run on a β-plane. Experiment 1 included seasonal wind forcing on a straight coast, while Experiments 2 and 3 added the effects of irregular coastline geometry to the seasonal wind forcing. The most complex experiment, Experiment 4, added the effects of both thermohaline gradients and annual MO to the seasonal wind forcing and irregular coastline geometry. Consistent with previous studies, wind forcing was shown to be a key generative mechanism for EBC mesoscale features, while capes were shown to be key areas for enhanced upwelling, extensive filament, maximum current velocities and enhanced growth of cyclonic meanders and eddies. Unique features of the NCCS, including the development of anticyclonic meanders and eddies in an embayment like the Gulf of Cadiz and the generations of Meddies from MO, were also highlighted (Batteen *et al.*, 2000).

The objective of this study is to build on previous studies and to investigate planetary and topographic beta effects on the generation, evolution, and maintenance of currents, upwelling, meanders, eddies, filaments, MO, and Meddies in the NCCS. The results of several numerical experiments (e.g., see Table 1) using the Princeton Ocean Model (POM), a bottom following sigma coordinate model is explored. The POM was chosen for this study because it has been widely used to simulate coastal processes associated with continental shelf flows and bottom boundary layer dynamics. In all experiments (e.g., see Figure 1 for model domain), annual wind forcing is used. To isolate the dependence of Coriolis parameterization (β-plane vs. *f*-plane) from the topographic beta effect, the first two experiments use a flat bottom. Experiment 1 (Experiment 2) introduces the effect of running the model on an *f*-plane (β-plane) for the NCCS. The results of Experiment 2 are compared to the results of Experiment 1 to explore the role of the planetary beta effect on the NCCS. Experiment 3 (Experiment 4) is the same as Experiment 1 (Experiment 2) except that bottom topography has been

incorporated. The results of Experiment 4 are compared to the results of earlier experiments to explore the additional role of topographic beta in the NCCS.

This study is organized as follows. In Chapter II we describe the numerical model and the specific experimental conditions. The results of the four main numerical experiments, along with an additional sensitivity experiment, are presented in Chapter III. A summary and discussion is presented in Chapter IV.

II. MODEL DESCRIPTION

A. DATA SETS

The topographic data were obtained from the Institute of Geophysics and Planetary Physics, University of California San Diego (Sandwell D.T. and W.F. Smith, 1996). The data set has a resolution of 2 minutes (e.g., 1/30 of a degree) and is a compilation of 30 years of data soundings obtained by ships. Where the ships' data is sparse, altimetry information was used to interpolate soundings.

Annual temperature and salinity values were obtained from Levitus and Boyer (1994) and Levitus et al. (1994). The data uses a 1 by 1 degree horizontal resolution at the vertical levels shown in Table 2.

For wind forcing, climatological wind fields were obtained from the European Centre for Medium Range Weather Forecasts (ECMWF) near-surface wind analyses (Trenberth et al., 1990). The data uses a 2.5 by 2.5 degree grid.

B. PRE-PROCESSING

The original topography (e.g., see Figure 2) was interpolated with a two-dimensional (2D) linear interpolation filter to the resolution used in the POM model, i.e., 3 by 3.7 km near the coast and 6 by 7.4 km away from the coast with a total of 287 by 241 points. The highest resolution was used where the values of the 'slope parameter' (defined by Mellor, 1998, as $\frac{|\delta H|}{2 * \overline{H}}$, where $\overline{H}$ is the average depth and δH is the difference in depth between two adjacent cells), were the largest in both the latitude and longitude directions. Since over much of the topography the slope parameter was larger than 0.2, which is the suggested maximum value to be used in sigma coordinate models (Mellor, 1998), the topography had to be smoothed with a linear 2D low-pass filter in order to meet this criterium. The new depth of each point calculated with this filter was a non-weighted average of 15 by 15 points surrounding the point. Subsequently depths greater than 2500 m were reassigned to depths of 2500 m, land was assigned the depth of

10 m (to avoid divisions by zero in the model) and the Strait of Gibraltar was closed. The resulting topography is shown in Figure 3.

The annual temperature and salinity values were interpolated for the horizontal spatial resolution of the model and for the 21 vertical sigma levels with a three-dimensional linear interpolation scheme. This had to be done separately for smoothed topography and for flat bottom due to the change in vertical levels for flat bottom and topography. Temperature fields at sigma level one and several cross-sections are shown in Figures 4 through 10.

The daily seasonal winds were averaged over time in order to obtain the annual non-weighted average wind vector field (e.g., see Figure 11). The wind vectors were interpolated for the horizontal spatial resolution of the model with a 2D linear interpolation scheme. The components of the wind stress were than calculated.

C. BRIEF MODEL DESCRIPTION

The Princeton Ocean Model, POM, a well-documented model (e.g., Blumberg and Mellor, 1987; Mellor, 1996), was used in the model studies. POM is a primitive equation, free surface model with a second-moment turbulence closure scheme (Mellor and Yamada, 1982) that, through the use of bottom-following sigma levels, can realistically simulate processes associated with continental shelf flows and bottom boundary layer dynamics in local domains (e.g., bays, estuaries and coastal regions). Recently, the model has been used successfully to simulate decadal processes in entire ocean basins (see Ezer and Mellor, 1994, 1997).

As described earlier, the resolution of the horizontal orthogonal grid varies between 3 by 3.7 km and 6 by 7.4 km. The variable grid allows the use of more (less) points in regions of large (small) gradients.

The 21 sigma levels used are shown in Figure 12 and Table 3. The sigma values range from zero at the surface to minus one at the bottom with the vertical grid spacing proportional to the ocean depth. The vertical resolution has been chosen to be higher near the surface and the bottom in order to resolve both the surface boundary layer and

the bottom boundary layer, which are important in coastal regions. To eliminate the time constrains for the vertical grid related to the higher resolution near surface, bottom and shallow water, an implicit vertical time differencing scheme is used.

The prognostic variables of the model are potential temperature, salinity, density, the three components of velocity, surface elevation, turbulence kinetic energy and length scale. The model has a split time step for the external and internal modes. The external mode solves the equations for the vertically integrated momentum equations. It also provides the sea surface and barotropic velocity components, and has a time step of 6 seconds. The internal mode solves the complete three-dimensional (3D) equations and has a time step of 180 seconds.

A Smagorinsky formulation (Smagorinsky et al., 1965) is used for the horizontal diffusion in which the horizontal viscosity coefficients depend on the grid size, the velocity gradients and a coefficient. In this study a value of 0.2 was assigned to this coefficient, consistent with other POM studies (e.g., Ezer and Mellor, 1997).

D. INITIALIZATION, FORCING AND BOUNDARY CONDITIONS

The model was initialized with annual temperature and salinity values obtained from Levitus and Boyer (1994) and Levitus et al. (1994). Since the model runs reached a quasi-equilibrium state in a relatively short time (~ 40 days, e.g., see Figure 13), zero salinity and temperature fluxes were prescribed at the ocean surface. The climatological surface temperature (e.g., see Figure 4) shows a decrease in temperature from the southwestern to the northeastern corner of the domain. The gradient increases to the north (which will be shown to be important for the formation of the Iberian Current). A cross-section for salinity at 36°N (e.g., see Figure 7) shows the Mediterranean Water signature at ~ 1200 m depth with salinity values of ~ 36.1 psu. In the upper 300 m the North Atlantic Ocean waters are found, with the characteristic high salinity values. A cross-section for temperature at the same location (e.g., see Figure 8) shows below ~1000 m depth a downward sloping of the isotherms approaching the coast which is consistent with the presence of warm Mediterranean Waters and of a poleward flow. In a cross-section near ~ 41.5°N (northern boundary) the signature of the Mediterranean Water is

found at ~ 1000 m depth with a much less zonal extent but with the same value for the maximum salinity (e.g., see Figure 9). The waters at 41.5°N are generally ~0.1 to 0.2 psu less haline than the waters at 36°N. The temperatures for the 41.5°N cross-section (e.g., see Figure 10) still shows a strong Mediterranean Water influence but now at ~ 1000 m depth, consistent with the high salinity values found at this location. A cross-section of salinity at the southern boundary (e.g., see Figure 5) shows the Mediterranean signature at ~ 1200 m depth with salinity values of ~ 35.7 psu, much less than the ones found on the northern boundary. The temperature signature (e.g., see Figure 6) is also less strong than in the northern boundary case (the vertical gradient of temperature near the coast is much higher in the southern boundary case).

The model was forced from rest with the annual ECMWF wind fields, which were interpolated for the model grid. As expected, the wind stress is stronger in the southern region of the model domain and weaker off Iberia and in the Gulf of Cadiz (e.g., see Figure 11).

Correct specification of the open boundary conditions (BC) is very important to achieve realistic results, with no reflections, clamping, spurious currents or numerical alteration of the total volume of water in the model. The problem is that there is not a general criteria that can give the answer to what boundary conditions are the best for a specific model or study. For models with a free surface, such as used here, one of the important criteria is that the BCs should be transparent to the waves. In this model, a gradient boundary condition (Chapman, 1985), which allows geostrophic flow normal to the boundary, worked best for the elevation. For the baroclinic velocity components normal to the boundary, an explicit wave radiation scheme based on the Sommerfield radiation condition was used. For inflow situations, the model was forced with annual temperature and salinity values obtained from Levitus and Boyer (1994) and Levitus *et al*. (1994), while in outflow situations an advection scheme was used.

For the barotropic velocity components, a Flather radiation plus Roed local solution (FRO) was used. Palma and Matano (2000) showed good results with the FRO during BC tests to determine the BCs response to an alongshelf wind stress. Palma and Matano (1998) also showed that the FRO BC had good reflection properties and results in

a test that determined the BC response to the combined action of wind forcing and wave radiation. His tests were executed with the barotropic version of POM and compared with benchmark results (no boundary conditions).

E. REDUCTION OF PRESSURE GRADIENT FORCE ERROR

Velocity errors induced by the pressure gradient force are unavoidable in three-dimensional (3D) sigma coordinate models. There are two types of sigma coordinate errors, the sigma error of the first kind (SEFK) and of the second kind (SESK), as defined by Mellor (1998). The first one goes to zero prognostically by advecting the density field to a new state of equilibrium. The second one, a vorticity error, is the most important because it does not vanish with time, and is present in both 2D and 3D cases.

There are several techniques to reduce the pressure gradient errors:

1 - Smoothing the topography can reduce both SEFK and SESK. In particular, the slope parameter should not be greater than 0.2 (Mellor, 1998). Greater values of this parameter can induce currents over 1 m/s.

2 – Using the highest possible resolution can reduce the errors, since the pressure gradient error decreases with the square of the horizontal and vertical grid size (Mellor *et al*., 1994).

3 – Subtracting the horizontally averaged density before the computation of the baroclinic integral reduces the SESK (Mellor, 1998).

4 – Using a curvilinear grid that follows the bathymetry reduces the SESK (Mellor, 1998).

In this study the first three techniques were used. The last technique, the use of a curvilinear grid, could not be used, because of the unique geography of the Gulf of Cadiz, which would have given rise to singularity points.

The results of using the first three techniques are shown in Figures 14 and 15. The model was initialized with the horizontally averaged annual climatological temperatures and salinities. A realistic coastline and realistic topography were used, and there was no wind or thermohaline forcing.

With the horizontal averages of the climatology and no forcing, we should expect that nothing will happen, i.e., the initial state of rest should be maintained with time. Due to pressure gradient force errors, however, this will not be the case and there will be resultant velocities as the result of these errors.

In Figure 14 the velocity has been plotted versus time. The velocity error is shown to increase faster in the first 3 days, and become almost constant after day 7. The size of the error reduces to less than 0.5 cm/s by day 10. To show where the errors are present in the model domain, the velocity field at sigma level 1 is shown in Figure 15. As expected, maximum velocities of ~ 0.5 cm/s are found within ~ 30 km from the coast where the slope parameter is the largest. These results have shown that with the use of the three techniques, the pressure gradient error has been considerably reduced. Before the use of these techniques, model runs showed pressure gradient errors of ~ 100 cm/s in the coastal regions (not shown).

III. RESULTS FROM MODEL SIMULATIONS

A. EXPERIMENT 1 – RESULTS OF f-PLANE WIND FORCING

In Experiment 1 (see Table 1), the model was initialized with the horizontally averaged annual climatological temperatures and salinities. A realistic coastline and flat bottom (constant depth of 2500 m) were used, and the model was forced with annual climatological winds.

A quasi-steady state for the kinetic energy was achieved by day 30 (not shown). As expected, the strong winds at the equatorward end of the model have caused cooler temperatures associated with strong upwelling in the coastal region south of Cape Beddouzza (e.g., see Figure 16). Throughout the model domain, there are predominantly equatorward currents. The stronger currents (e.g., maximum speeds of ~ 60 cm/s) tend to be found near coastal promontories in the coastal regions off Cape Beddouzza and Cape Ghir. Between ~ 1000 m depth (e.g., see Figure 17) and the bottom (e.g., see Figure 18), the current along the coast is poleward, in the opposite direction of the surface flow. A typical cross-section of meridional velocity (e.g., see Figure 19) shows the core of the poleward undercurrent at ~ 1700 m depth with a speed of ~ 10 cm/s underlying the equatorward surface current with a core speed of ~ 35 cm/s.

By day 40, two cyclonic eddies have developed near Cabo da Roca and Cabo Sao Vicente (e.g., see Figure 20). Simultaneously, the core of the surface equatorward current has intensified to ~ 45 cm/s, while the core of the poleward undercurrent has deepened and decreased in intensity to ~ 6 cm/s, (e.g., compare Figures 19 and 21). As a result, there are no strong vertical and horizontal shears between the surface equatorward and subsurface poleward currents. Consequently, except off coastal promontories, only weak meanders and filaments are discernible along the coast, in the vicinity of the equatorward jet.

By day 60, instead of propagating westward as would occur on a beta-plane, the two cyclonic eddies (e.g., see Figure 22) remain embedded in the equatorward current, and are still discernible at ~ 1200 m depth (e.g., see Figure 23). The sharp angle in the coastline at Cabo Sao Vicente and the large extent of the Gulf of Cadiz (which is a large

embayment and a unique feature of the NCCS) cause the eddies to move in a predominantly southward direction but not along the coast. Note that a relatively large anticyclonic eddy has developed in the Gulf of Cadiz, by day 60, east of the cyclonic eddy off Cabo Sao Vicente. Just as cyclonic features tended to form off capes in the NCCS, an anticyclonic feature tended to form in the large embayment.

The widths of the coastal jet and undercurrent are consistent with the first internal Rossby radius of deformation, $\frac{\sqrt{gH}}{f}$ (where g is the gravity, H is the water depth, and f is the Coriolis parameter), in concurrence with the expected behavior of eastern boundary currents on an *f*-plane (Gill, 1982). This radius is ~ 30 km for the model domain, as calculated by the method of Feliks (1985). In addition, the equatorward coastal jet and poleward undercurrent development agree well with the *f*-plane wind forcing results of McCreary *et al*. (1987) and McCreary (1981).

B. EXPERIMENT 2 – RESULTS OF BETA PLANE WIND FORCING

In Experiment 2 (see Table 1), instead of an *f* –plane, the model was run on a β-plane with the same model forcing conditions as in Experiment 1. The results of Experiment 2 were run to isolate the important role that the beta effect plays in setting up more realistic coastal currents.

As expected, upwelling first occurs in the south where the stronger winds exist (e.g., refer to Figure 11). In addition to the west coast of Morocco, upwelling is enhanced near prominent capes to the north on the west coast (e.g., off Cabo da Roca in Figure 24). The coldest waters are found south of Cape Ghir and Cabo da Roca (e.g., Figure 24). In Experiment 1, the region of enhanced upwelling was confined south of Morocco (e.g., see Figure 16). In addition, the offshore extent of coastal upwelling is much wider than in Experiment 1, particularly off Cape Ghir where the offshore extent is ~ 120 km. Consequently, the inshore coastal temperatures are also cooler than in Experiment 1.

A typical cross-section (e.g., see Figure 25) of the currents shows that there is a surface coastal equatorward jet that extends to ~ 180 m depth near the coast and ~ 800 m

depth offshore. The surface current is within ~ 120 km of the coast and has core velocities of ~ 20-25 cm/s. Below the equatorward current is a subsurface poleward undercurrent within ~ 50 km of the coast which as a core velocity of ~ 7 cm/s at 1200 m. In contrast to the results on an f-plane in Experiment 1, the core of the poleward undercurrent is shallower, while the core of the equatorward current has weaker velocities (e.g., compare Figures 19 and 25).

In Experiment 1, there was only weak development of filaments. In contrast, Experiment 2 shows the formation of prominent filaments (e.g., see Figure 26), which preferentially develop off the capes. For example, there is evidence of filament activity off Cabo da Roca, the southwest tip of Iberia, and off Cape Ghir (e.g., see Figure 26). A comparison of temperature fields for both experiments (e.g., compare Figures 20 and 26) shows that the upwelling has a greater westward extent than in Experiment 1. For example, in Experiment 2, the offshore extent of the 17°C isotherm is at ~ 300 km off Cape Ghir, while in Experiment 1 the 17°C isotherm was confined to ~ 60 km off Cape Ghir. In both experiments the minimum offshore extent of upwelling is in the Gulf of Cadiz region, as expected, since the winds are relatively weak in this region (e.g., see Figure 11).

The continued widening of the equatorward coastal jet (e.g., see Figures 24, 26 and 27) is consistent with the results of McCreary *et al*. (1987) and Batteen *et al*. (1989). They showed that, due to the beta effect, the surface coastal jet does not necessarily have to be confined to within a Rossby radius of deformation of the coast (the latter, a result seen in the *f*-plane Experiment 1). The beta effect also allows the existence of freely propagating planetary waves, i.e., Rossby waves (Gill, 1982). The offshore propagation of these waves contributes to the generation of an alongshore pressure gradient field, which aids the development of a subsurface rather than a deep undercurrent along the eastern boundary. As a result, the beta effect changes both the vertical and horizontal structures of the surface and subsurface currents.

In particular, as the core of the undercurrent, (which is initially beneath the equatorward jet) intensifies, it shoals and displaces the equatorward jet offshore (e.g., see Figures 28-30). Consequently, strong vertical and horizontal shears in the upper layers

between the equatorward jet and the undercurrent develop. Meanders, upwelling filaments, and eddies subsequently develop in the baroclinically and barotropically unstable coastal environment. Note that neither vertical nor horizontal shears existed between the deep and intense equatorward jet and the even deeper poleward undercurrent in Experiment 1 run on an *f*-plane. As a result, the equatorward jet was unmodified by the poleward subsurface flow, and away from prominent capes and embayments, no significant mesoscale features were seen in Experiment 1.

Apparent in the model results by day 40 is the development of two anticyclonic eddies (i.e., Meddies) at ~ 1200 m depth (e.g., see Figure 31), one off the coast of Cabo Sao Vicente and another one off the coast of Cabo da Roca. A cross-section of salinity at the same location (e.g., see Figure 34) shows that the Meddy has a salty core of ~ 35.8 psu, which is associated with the signature of MO (present in the initial annual climatology). It has been suggested (e.g., Kase *et al*., 1989) that the Meddies are generated by the basic instability of the equatorward coastal jet and the poleward undercurrent. The relatively salty MO core of the undercurrent below ~ 500 m depth, which makes water in the core saltier than water above or below it, could lead to a local baroclinic instability process, resulting in the generation of Meddies. A time sequence of velocity cross-sections for the Meddy off Cabo Sao Vicente (e.g., see Figures 25, 32, and 33) shows the Meddy shallowing with time, just as the undercurrent shallowed with time (e.g., see Figures 28-30).

The relatively deep origin, salty signature depth and anticyclonic rotation of the eddy west of Cabo Sao Vicente are consistent with observations of Meddies in this region (e.g., Richardson and Tychensky, 1998). The Meddy observed off Cabo da Roca is consistent with the results of Kase *et al*., (1989), who observed eddies in the MO off Iberia.

The development of the Meddy off Cabo Sao Vicente in Figure 31 is also consistent with another Meddy generation theory. Pichevin and Nof (1996) suggested that a Meddy generation mechanism can occur when the MO curves back on itself west of Cabo Sao Vicente producing a flow-force that cannot be balanced without growth and shedding of eddies. The beta effect plays an important role in the Meddy generation

model of Pichevin and Nof (1996) because it arrests the growth of Meddies and removes them from their generation region (In contrast, *f*-plane experiments by Pichevin and Nof (1996) develop a constantly growing coastal eddy at the tip of Cabo Sao Vicente).

In Experiment 2, the beta effect acted as a necessary force in promoting the generation and growth of Meddies and causing their removal from the source region. Generation and growth were promoted by local baroclinic instabilities in the MO and by the MO curving back on itself in a region of relatively weak coastal currents. Removal from the Cabo Sao Vicente generation region was a result of the free offshore propagation of planetary waves, in the vicinity of the relatively benign coastal currents. Meddy generation was not simulated in the *f*-plane Experiment 1; instead, there was the domination of the intense equatorward jet through the potential Meddy generation region (e.g., compare Figures 23 and 31).

C. EXPERIMENT 3 – RESULTS OF f-PLANE WIND FORCING WITH TOPOGRAPHY

Experiment 3 (see Table 1) mimics Experiment 1 on an *f*-plane, except that instead of a flat bottom, topography was added with the same model forcing conditions. The results of Experiment 3 were run to isolate the effect of topographic beta and demonstrate its role in the NCCS.

Unique to Experiment 3 were the following: Two isolated cyclonic eddies develop and propagate off Cabo da Roca and Figueira da Foz. A time sequence of surface temperature and velocity fields (e.g., see Figures 35-37) show that, although the eddies detach from the coast, they only propagate westward as far as the edge of the slope bottom bathymetry (e.g., see Figure 2). Additionally, the equatorward surface current increases from speeds of ~ 60 cm/s in Experiment 1 compared to speeds of ~ 80 cm/s in Experiment 3. A comparison of the results from Experiments 1 and 3 shows that the current is narrower in Experiment 3 and remains trapped on the shelf.

A typical cross-section of velocity (e.g., see Figure 38) shows an equatorward current, which has strengthened and deepened to ~ 500 m depth, overlying a poleward undercurrent, which has its core near the bottom of the slope. Because of this deep

structure of the undercurrent, there is no strong vertical and/or horizontal shear between the surface currents and the undercurrent. The only mesoscale features seen in Experiment 3 are discernible off Cabo da Roca and Figueira da Foz (i.e., the detached cyclonic eddies). Also, due to the lack of vertical shear, no Meddies are seen in Experiment 3 (e.g., see Figure 39 which shows the deep signature of the two cyclonic eddies off the shelf but no anticyclonic Meddies).

Similar to the *f*-plane Experiment 1, Experiment 3 shows the occurrence of coastal upwelling off the west coasts and a continuously strengthening equatorward jet that prevents other classical mesoscale features associated with upwelling systems (such as filaments) from occurring (e.g., see Figures 35-37). At depth, the deep equatorward jet also prevents other unique NCCS features from occurring, including the typical westward and poleward spreading of the MO, and the development of Meddies.

The addition of bottom topography in Experiment 3 has isolated the role of topographic beta. Consequently, there is a stronger coastal current due to the topography trapping the current on the shelf. The eddies that develop off Figueira da Foz and Cabo da Roca are strictly due to the topography and propagate only as far as the edge of the bottom slope bathymetry.

As in the *f*-plane Experiment 1, the widths and depths are consistent with an internal Rossby radius of deformation, $\frac{\sqrt{gH}}{f}$. Instead of being restricted to ~ 30 km, however, the radius of deformation can vary due to changes in topography. For example, the eddies that develop off Figueira da Foz and Cabo da Roca are offshore of 30 km and stop at the edge of the bottom slope bathymetry.

D. EXPERIMENT 4 – RESULTS OF BETA PLANE WIND FORCING WITH TOPOGRAPHY

Experiment 4 (see Table 1) mimics Experiment 2 on a β-plane, except that instead of a flat bottom, topography was added with the same model forcing conditions. The results of Experiment 4 were compared to the results of earlier experiments to explore the effects of both planetary and topographic beta in the NCCS.

The velocities in the coastal areas in the bottom topography Experiment 4 are generally much more intense than the flat bottom Experiment 2 (e.g., compare Figures 24 and 40 at day 30. Note that the velocity scaling used in Experiment 4 is double that of Experiment 2). The velocities in Experiment 4 also have the highest magnitudes at ~ 15 km offshore (near the shelf break) instead of right off the coast as in the flat bottom Experiment 2. As in the flat bottom experiment, due to the stronger equatorward winds, the strongest currents are found in the coastal region south of Cape Beddouzza. The temperatures at the surface are also very similar for the two experiments (e.g., compare Figures 24 and 40), both in the location of the strongest upwelling regions (i.e., south of Cape Beddouzza) and in the horizontal extent of the upwelling. One of the main differences between the two experiments occurs off Figueira da Foz where the upwelling is present farther from the coast in Experiment 4 (e.g., compare Figures 26 and 41). The main reason for this phenomenon is the location of a prominent topographic feature at this location (e.g., see Figure 2).

A comparison of the 17°C isotherm in both Experiments 2 and 4 (e.g., compare Figures 26 and 41) shows that the extent of upwelling is generally much less than in the flat bottom case, particularly off Cape Ghir. This can be explained by the presence of the bottom topography that traps the flow and opposes the tendency for westward propagation due to the planetary beta effect. Note that the filament that was present in this region in Experiment 2 is now absent in Experiment 4 (e.g., compare Figures 26 and 41). This also shows that the trapping of the currents due to topography is much stronger than planetary beta.

Note the presence of relatively strong cyclonic eddies near the capes off Iberia, which were much weaker in Experiment 2 (e.g., compare Figures 26 and 41). This shows that bottom topography plays an important role in their intensification.

Unlike Experiment 2, which had meanders throughout the coastal domain by day 60 (e.g. see Figure 27), the only evidence of mesoscale phenomena in this experiment are the two cyclonic eddies off Cabo da Roca and Figueira da Foz (e.g., see Figure 42). Off Cape Ghir and off the coast of Portugal between Cabo da Roca and Cabo Sao Vicente, the flow is maintained much closer to shore in Experiment 4 (e.g., compare Figures 27

and 42). In contrast, the flow is farther offshore in the Gulf of Cadiz, where the slope of the topography is much broader than in the rest of the coastal domain.

Typical cross-sections from both Experiments 2 and 4 (e.g., see Figures 25 and 43) show that the poleward undercurrent is generally much weaker in Experiment 4 than in Experiment 2. For example, at day 30, the undercurrent is less than 1 cm/s at ~ 1200 m depth in Experiment 4; while in Experiment 2 the undercurrent is ~ 6 to 7 cm/s at the same depth. The core of the undercurrent in Experiment 4 is also much deeper. For example, at day 30 the core is at ~ 2300 m depth while in Experiment 2 it is at ~ 1200 m depth.

Meddy formation also occurs much later in Experiment 4 than in Experiment 2. Instead of having Meddies form by day 30 as in Experiment 2, Meddies do not form until ~ day 60. The Meddies form off Cabo da Roca and off Figueira da Foz (e.g., see Figure 44); however, unlike Experiment 2, no Meddy forms off Cabo Sao Vicente (e.g., see Figure 31). As the flat bottom Experiment 2 showed, the sharpness of the coastline was necessary to the formation of Meddies off Cabo Sao Vicente. In Experiment 2 the Meddies also appeared to be generated due to the curvature of the MO back on itself, consistent with the theory suggested by Pichevin and Nof (1996). It is speculated that the smoothing of topography may have smoothed the irregularities of the coastline at 1200 m depth preventing Meddy development.

E. DISCUSSION

One feature missing in all four experiments was the development of the Iberian Current. Since all four experiments used horizontally averaged temperature and salinity climatology, it was hypothesized that full temperature and salinity climatology is a key ingredient for the formation of this current.

To explore this, an additional experiment, hereafter called Experiment 5, was completed that mirrored Experiment 4 using the same model forcing conditions, except that the model was initialized with the full annual instead of the horizontally averaged climatological temperatures and salinities (e.g., see Figures 4-10). This model run, which had the most realistic model forcing conditions, as expected, depicted classical EBC

features including an equatorward (poleward) surface (subsurface) current, coastal upwelling, meanders, filaments, (e.g., see Figures 45-48) as well as Meddies (not shown). The Iberian Current, not seen in earlier experiments, was discernible off the coast of Portugal (e.g., see Figures 46 and 47) showing that thermohaline gradients played a key role in the formation of this current.

The development of generally weaker (i.e., from ~ 80 to 60 cm/s) surface velocities at the coast in this experiment, compared to those in Experiment 4 (e.g., compare Figures 40-42 with Figures 45-47), are consistent with two factors. First, geostrophic inflow produces flow along the coast in opposite directions of the surface and subsurface coastal currents. This results in a reduction of the coastal current speeds. Second, the horizontal variability of density contributes to the enhancement of poleward alongshore variability, giving rise to a greater enhancement and surfacing of the undercurrent (e.g., see Figure 48), which subsequently reduces the flow of the surface equatorward velocities.

The strongest and shallowest poleward undercurrent of all experiments was produced in Experiment 5 (compare Figures 19, 25, 38, and 43 with Figure 48). A comparison of typical cross-sections for this experiment (e.g., see Figures 48 and 49) shows that the undercurrent has intensified to speeds of ~ 20 cm/s and has its core located at shallower depths ranging from ~ 500-800 m.

THIS PAGE INTENTIONALLY LEFT BLANK

IV. SUMMARY AND DISCUSSION

The objective of this study was to build on previous studies and to investigate planetary and topographic beta effects in the NCCS. The results of several numerical experiments (see Table 1) using the POM, a bottom following sigma coordinate model, was explored. The POM was chosen for this study because it has been widely used to simulate coastal processes associated with continental shelf flows and bottom boundary layer dynamics. In all experiments, annual wind forcing was used. To isolate the dependence of Coriolis parameterization (β-plane vs. *f*-plane) from the topographic beta effect, the first two experiments used a flat bottom. Experiment 1 (Experiment 2) introduced the effect of running the model on an *f*-plane (β-plane) for the NCCS. The results of Experiment 2 were compared to the results of Experiment 1 to explore the role of the planetary beta effect on the NCCS. Experiment 3 (Experiment 4) was the same as Experiment 1 (Experiment 2) except that bottom topography has been incorporated. The results of Experiment 4 were compared to the results of earlier experiments to explore the additional role of topographic beta in the NCCS.

In Experiment 1 the intensification of the surface equatorward current led to a deepening and weakening of the poleward undercurrent. As a result, no strong vertical and horizontal shears existed between the surface and subsurface currents. Consequently, except off coastal promontories, only weak meanders and filaments were discernible along the coast. Cyclonic (anticyclonic) eddies developed off Cabo da Roca and Cabo Sao Vicente (in the Gulf of Cadiz). Instead of propagating westward, the cyclonic eddies remained embedded in the equatorward current and traveled in a predominantly southward direction. The widths of the coastal jet and undercurrent were consistent with the first internal Rossby radius of deformation, which is ~30 km in the region.

In Experiment 2 classical EBC features were produced including an offshore surface equatorward meandering jet, coastal surface and subsurface poleward currents, upwelling, meanders, eddies and filaments. In addition, this experiment depicted unique NCCS features such as the poleward spreading of the MO. The beta effect played an important role in the development and westward propagation of Meddies (also unique to

the NCCS), in the Cabo Sao Vicente and Cabo da Roca regions. Due to the beta effect, the surface coastal jet was not confined to within a Rossby radius of deformation of the coast.

A comparison between Experiments 1 and 2 showed the effect of planetary beta and its role in westward propagation. In particular, the coastal surface and subsurface currents and upwelling regions extended farther westward from the coast than in Experiment 1. There was also increased mesoscale activity including prominent filaments, meanders, and eddies all along the coast.

In Experiment 3, bottom topography was incorporated to isolate the role of topographic beta. A stronger coastal current developed due to the effect of topography trapping the current on the shelf. Two cyclonic eddies that developed off Figueira da Foz and Cabo da Roca were also due to the topography. While the eddies initially moved westward, they stopped at the edge of the bottom slope bathymetry.

A comparison between Experiment 1 and 3, both run on an *f*-plane, showed the occurrence of coastal upwelling off the west coasts and a continuously strengthening equatorward jet that prevented other classical mesoscale features associated with upwelling systems (such as filaments) from occurring. In particular, at depth, the deep equatorward jet prevented other unique NCCS features from occurring, including the typical westward and poleward spreading of the MO, and the development of Meddies.

In Experiment 4, both beta plane and bottom topography were incorporated to explore planetary and topographic beta effects in the NCCS. While planetary beta tends to move features westward, topographic beta tends to trap features over the topography. As a result, in regions where the topographic beta competed with the planetary beta, such as off west coasts, the offshore extent of coastal features, such as upwelling and filaments, was limited. Off the northern and southern coasts of the Gulf of Cadiz, where there was no planetary beta effect, bottom topography played an important role in narrowing, intensifying and trapping the coastal currents.

In Experiment 5, the additional effect of full climatology was investigated. This model run depicted classical EBC features (such as surface and subsurface coastal currents, upwelling, meanders, filaments, and eddies) as well as unique NCCS features

(such as Meddies). In addition, this experiment showed that geostrophic inflow set up by thermohaline gradients produced a weaker surface coastal current and a stronger undercurrent. This was also the only experiment that produced the surface poleward Iberian Current. These results show that while wind forcing is the primary mechanism for generating classical EBC features, planetary and topographic beta also play important roles in the generation, evolution, and maintenance of classical as well as unique features in the NCCS.

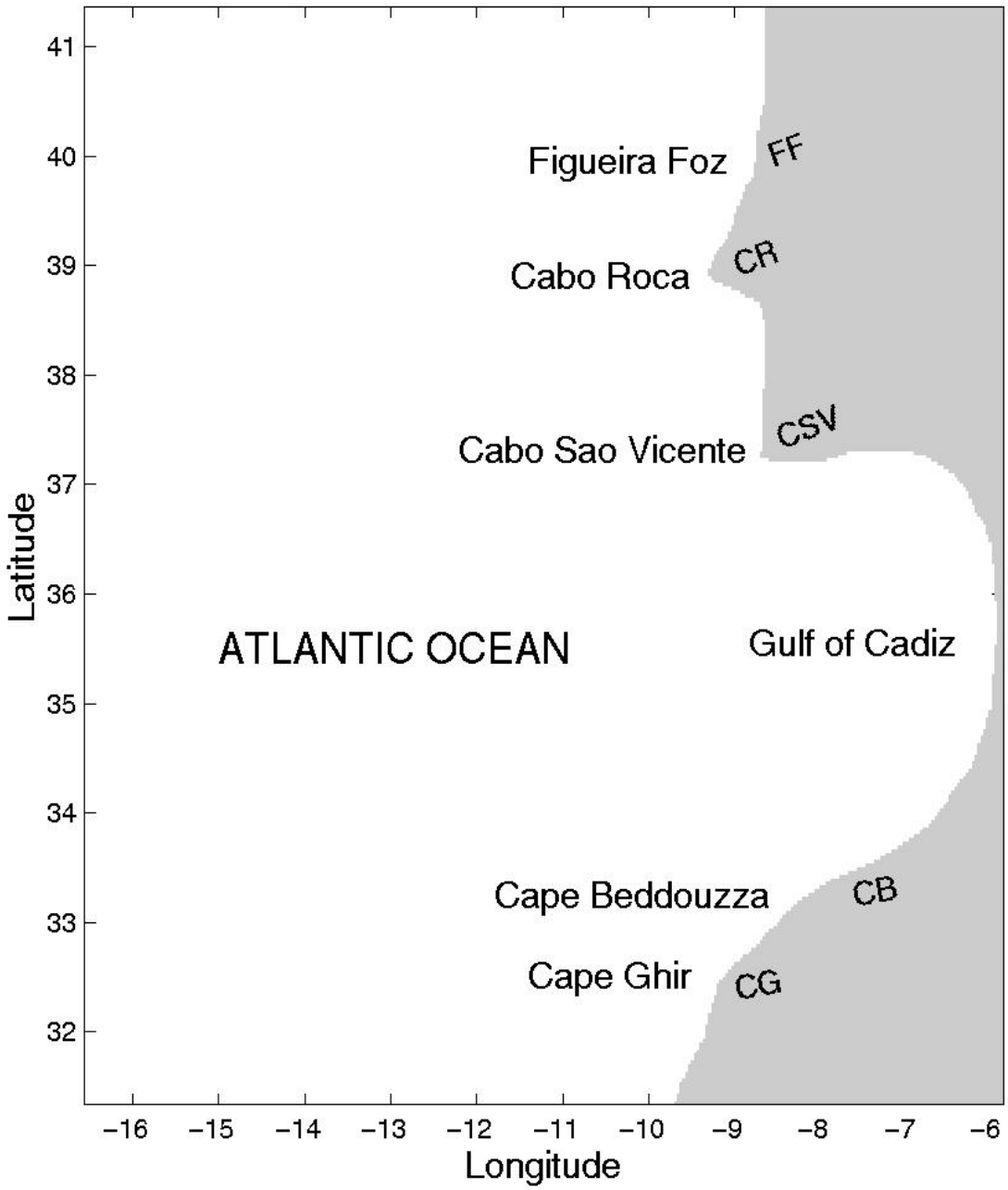

Figure 1. The model domain for the northern Canary Current System (NCCS) is bounded by 31.5°N to 41.5°N, 6°W to 16.5°W. Geographical locations (with abbreviated names used in the following figures) and prominent features are labeled. The model domain has a closed boundary along the entire coast and three open boundaries.

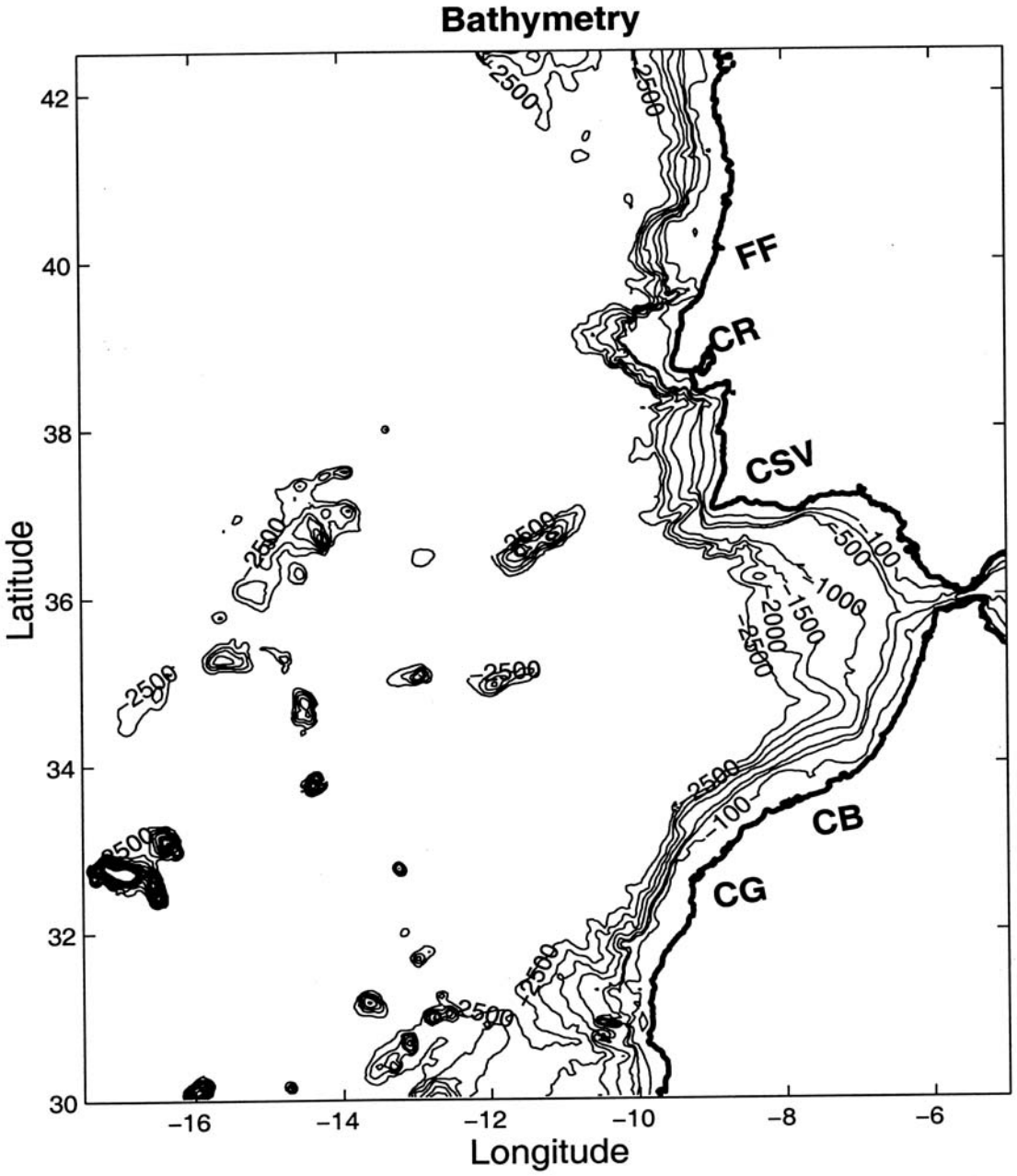

Figure 2. Original topography (from Sandwell D.T. and W.F. Smith, 1996), with a resolution of 2 minutes (i.e., 1/30 of a degree).

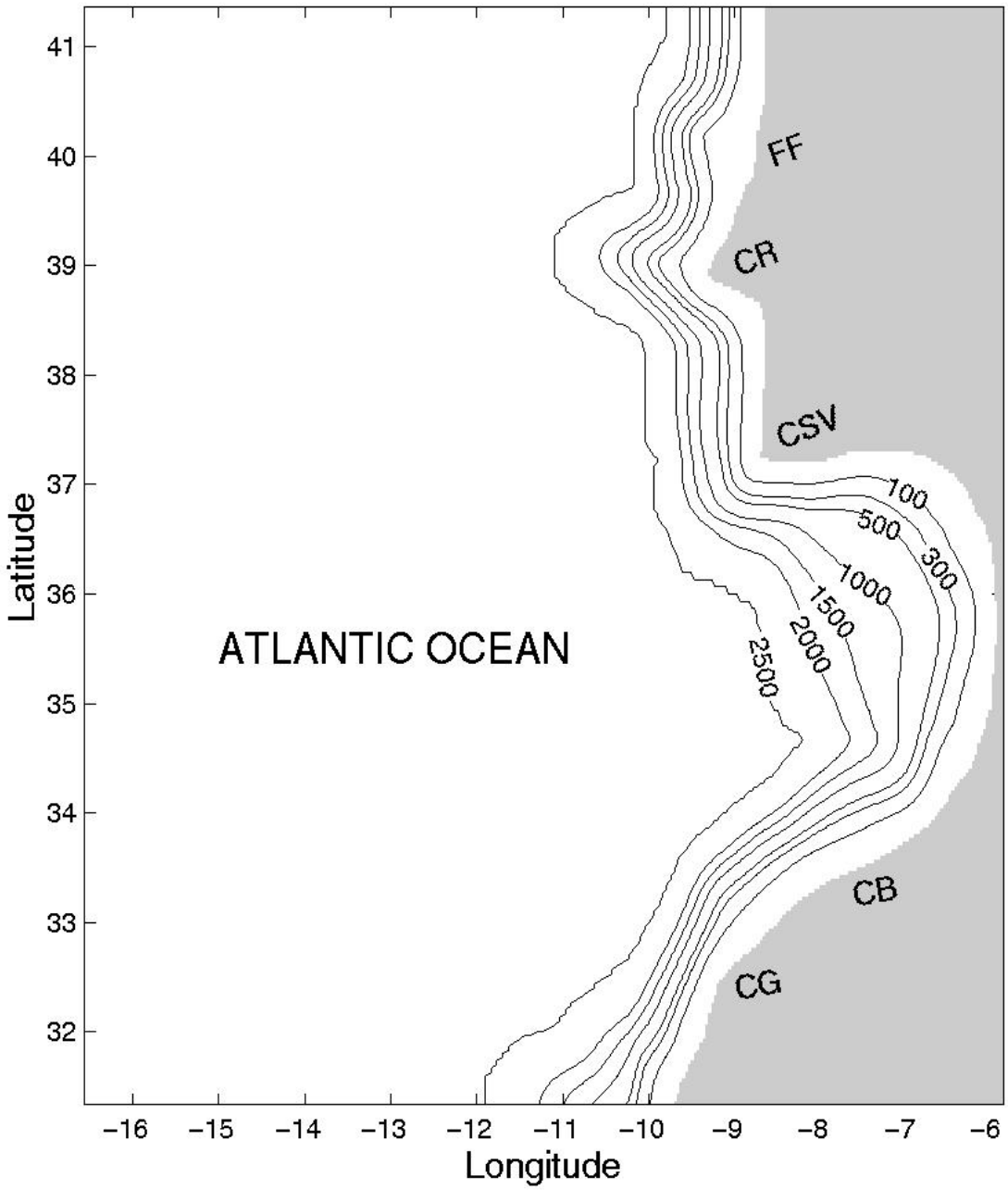

Figure 3. Smoothed topography obtained after applying a linear two-dimensional low-pass filter and reassigning 2500 m depth to depths greater than 2500 m.

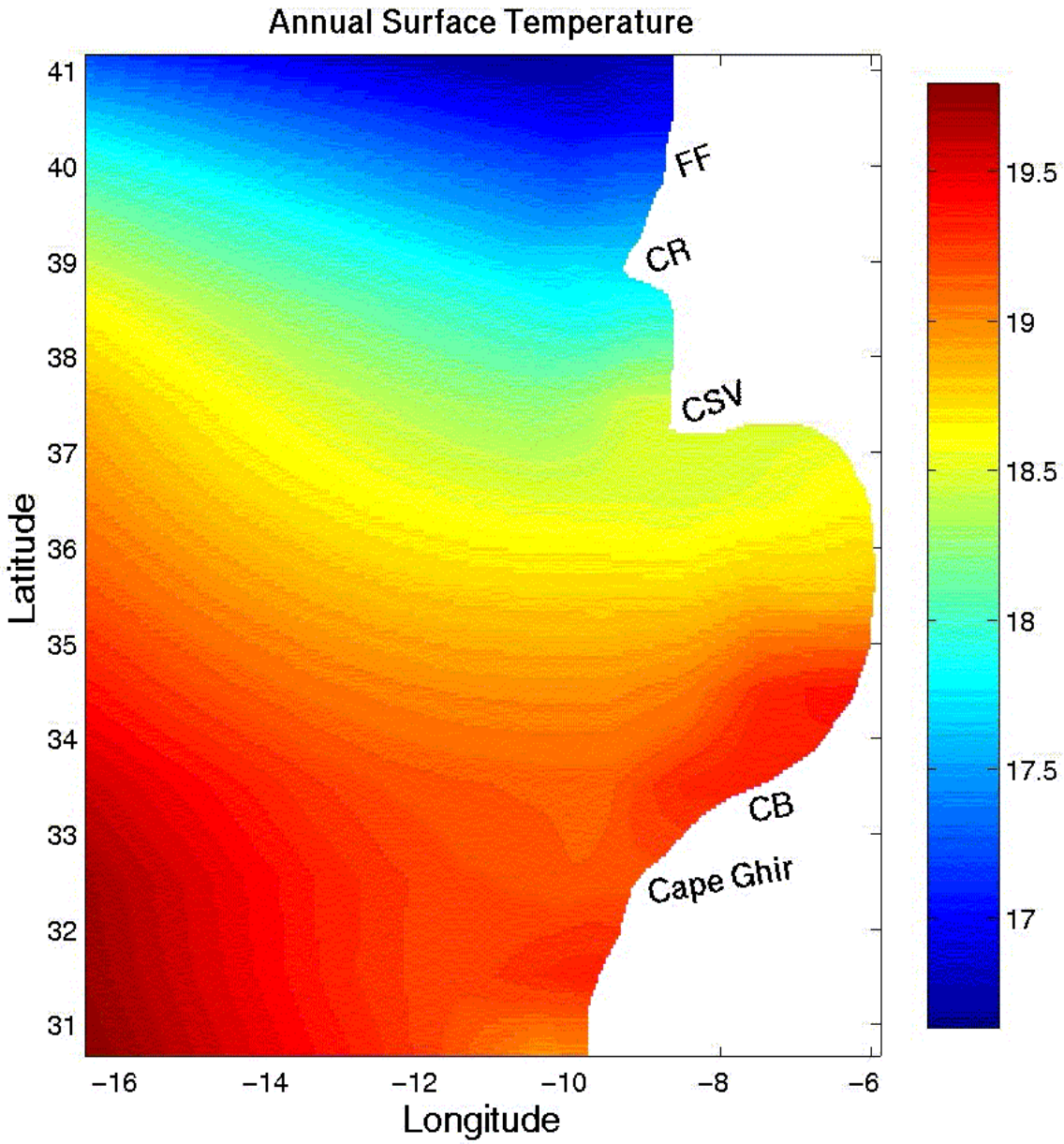

Figure 4. Levitus annual climatological surface temperature.

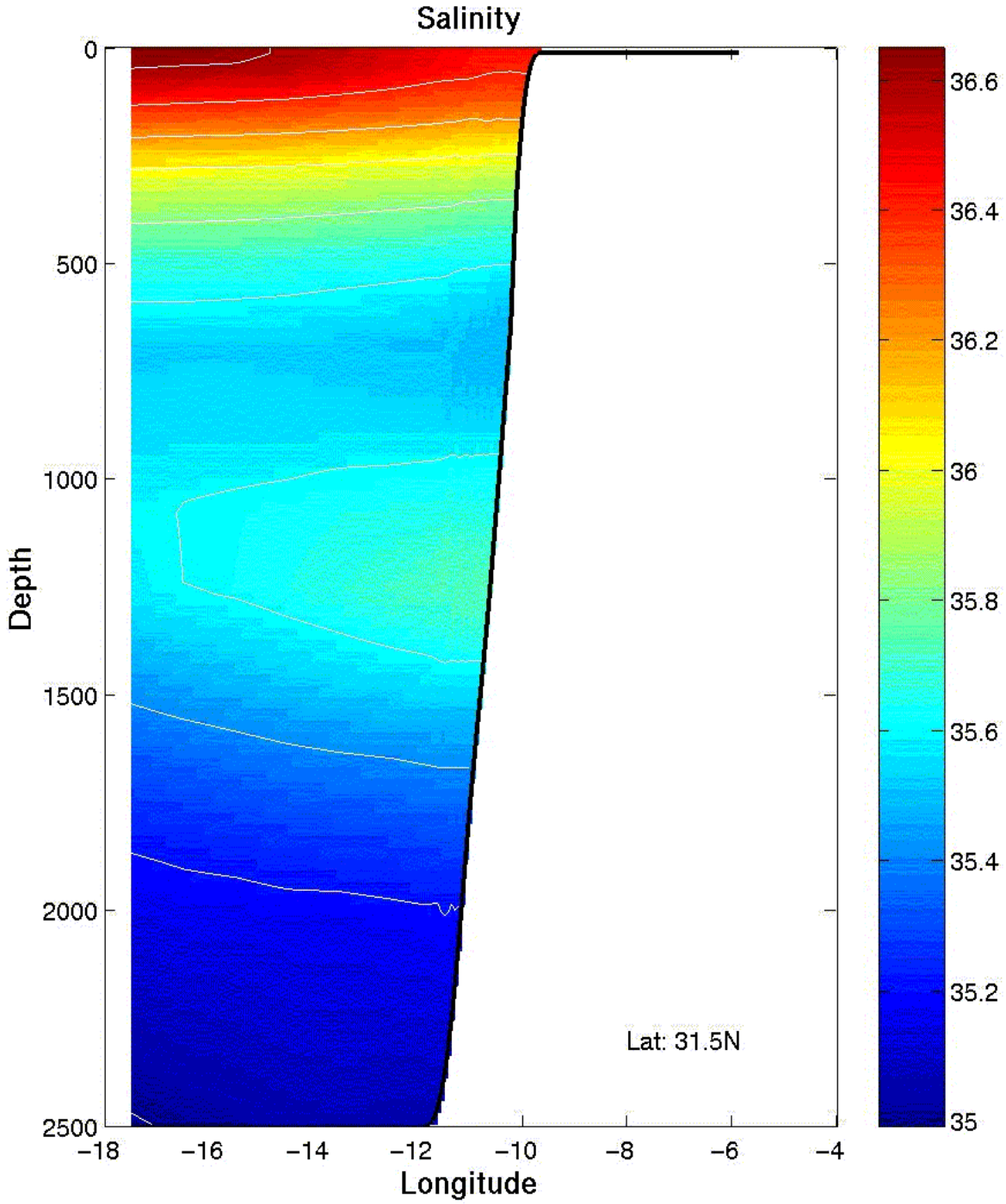

Figure 5. Cross-section at 31.5°N of Levitus annual climatological salinity.

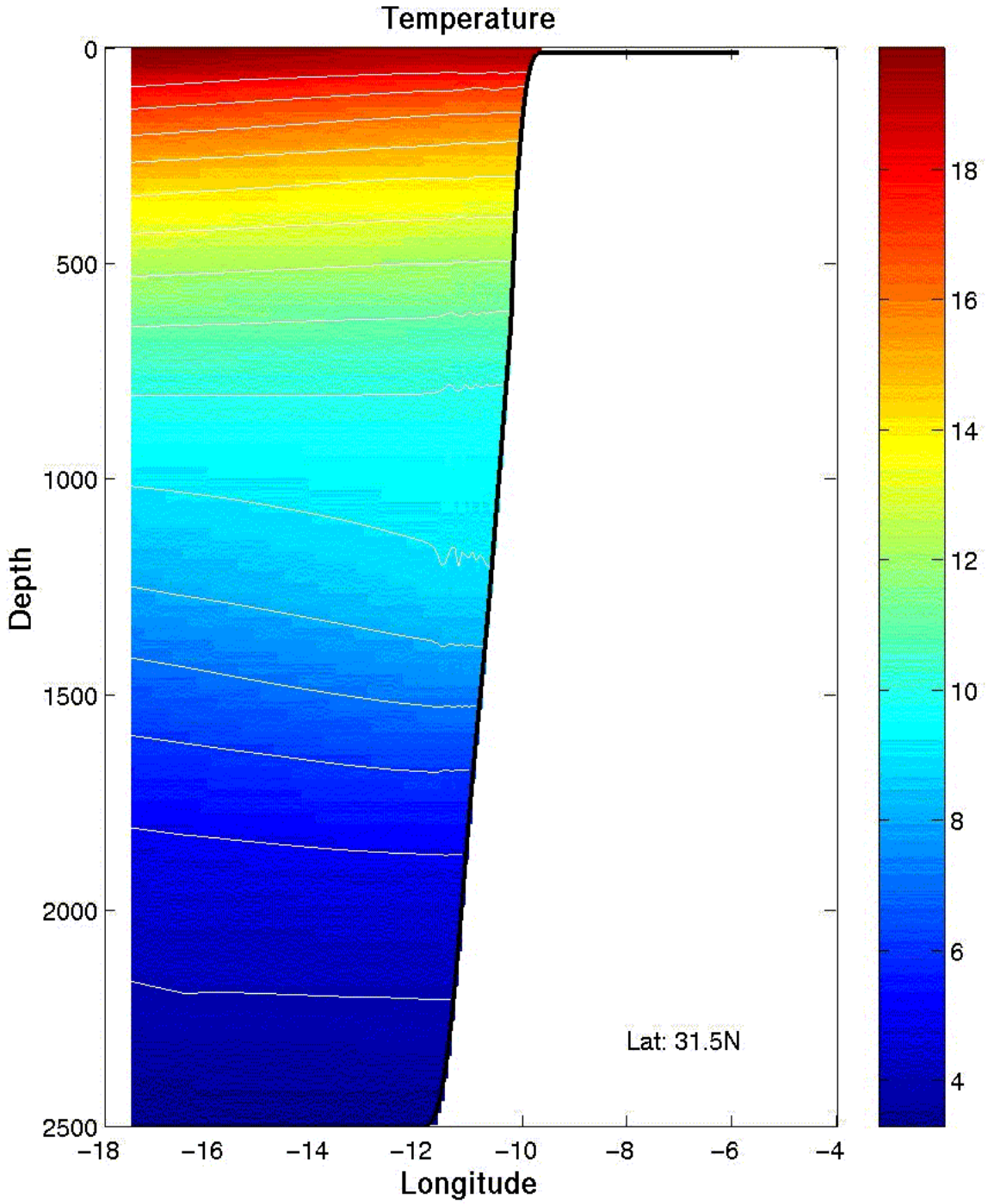

Figure 6. Cross-section at 31.5°N of Levitus annual climatological temperature.

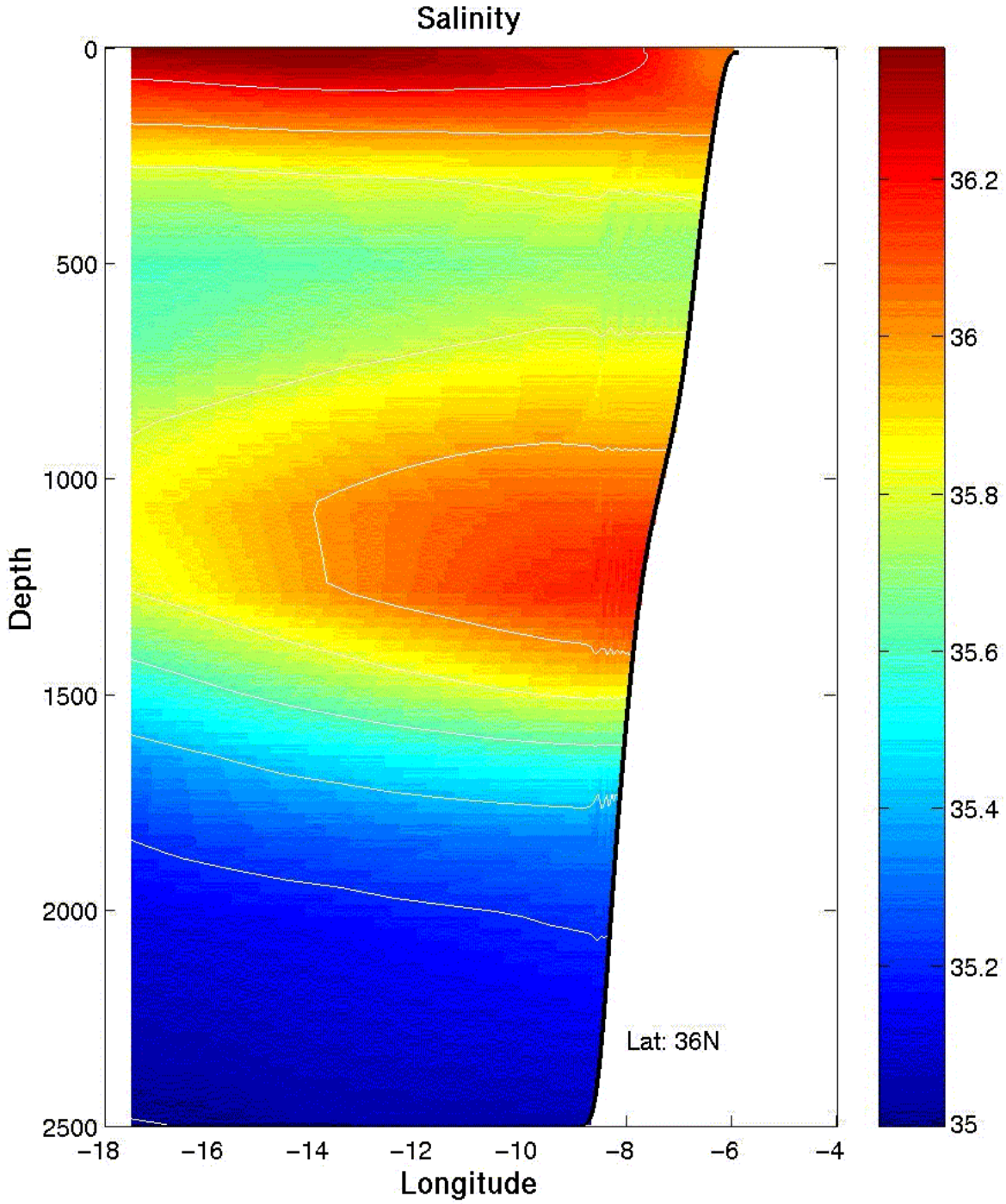

Figure 7. Cross-section at 36°N of Levitus annual climatological salinity.

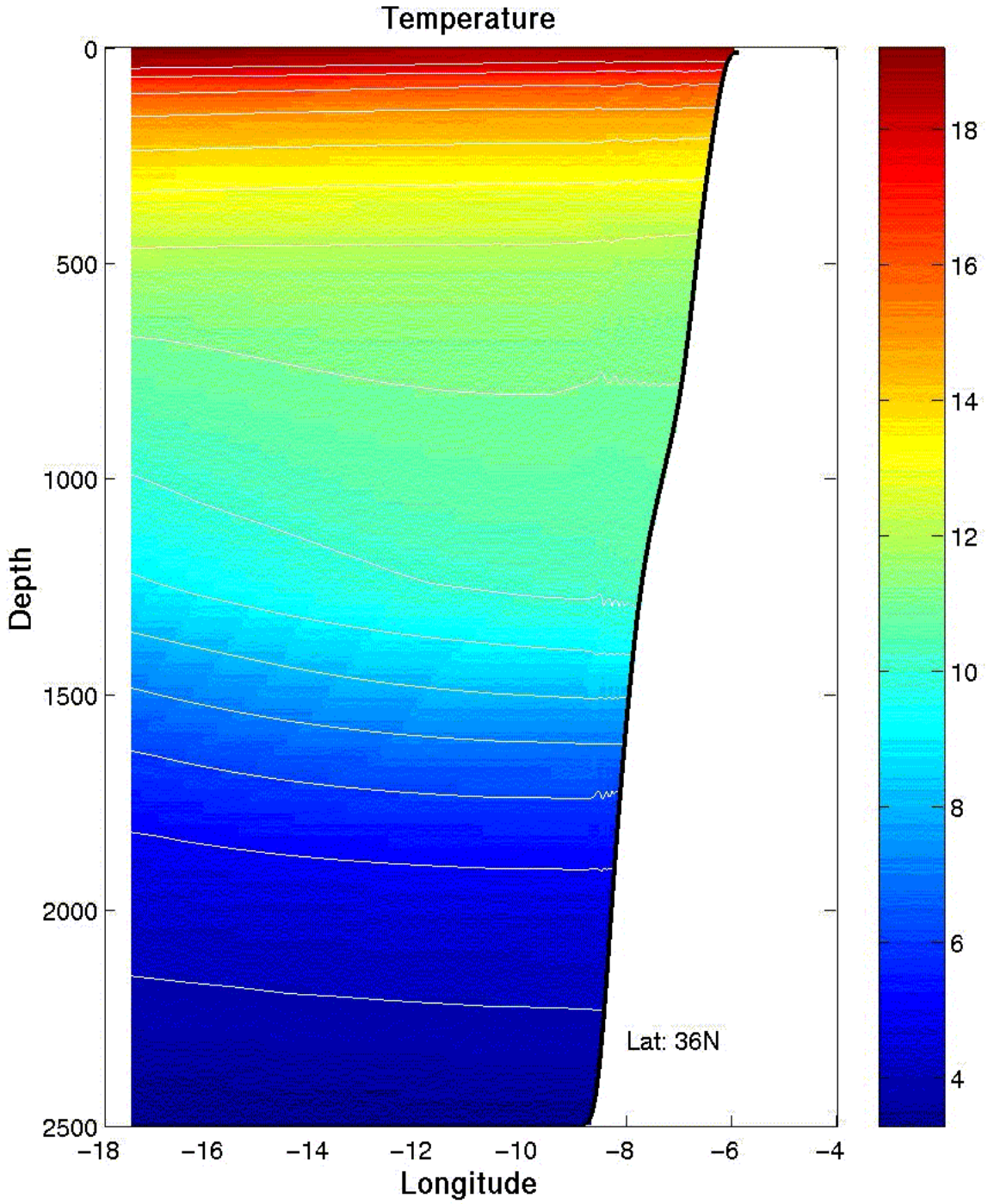

Figure 8. Cross-section at 36°N of Levitus annual climatological temperature.

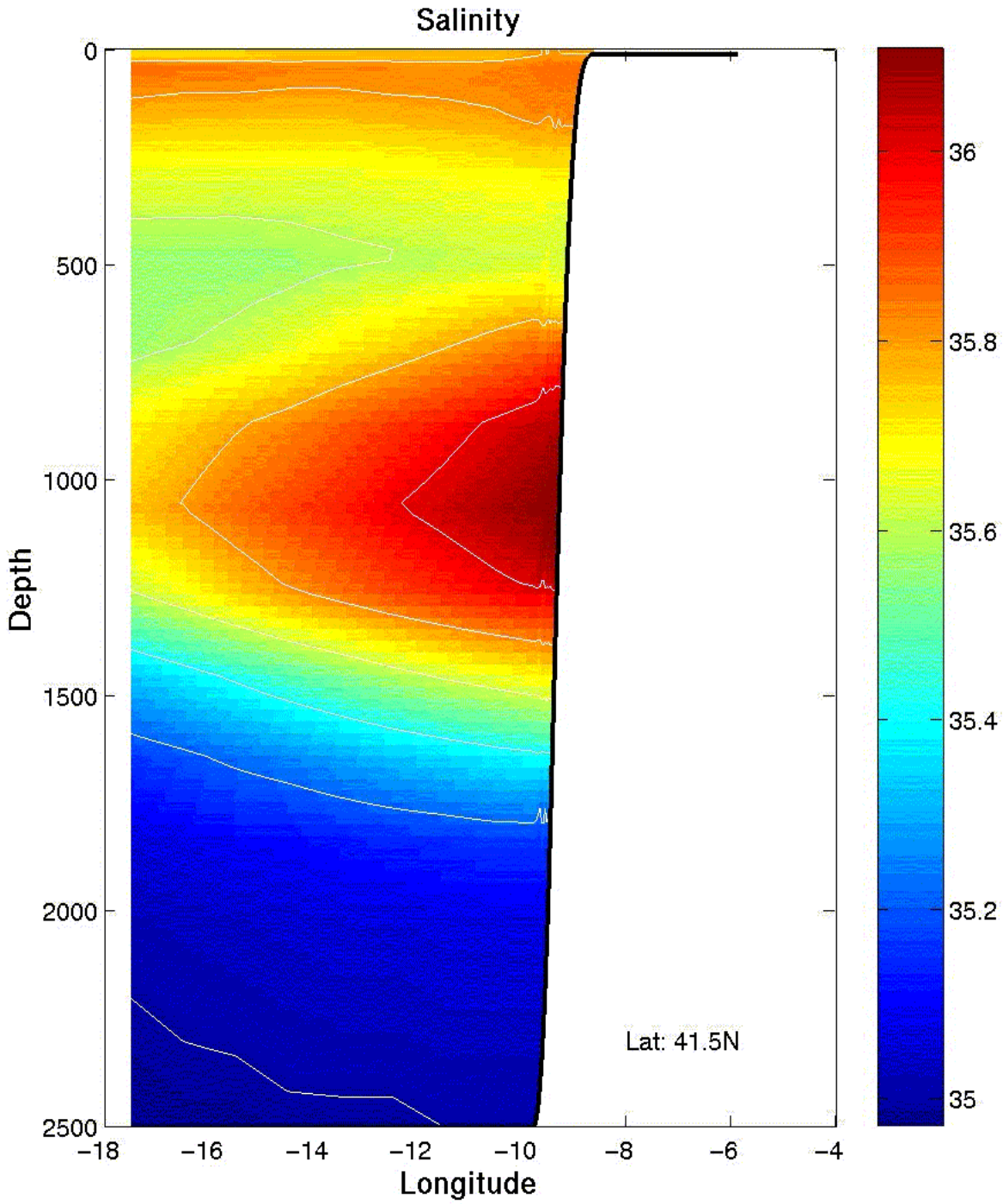

Figure 9. Cross-section at 41.5°N of Levitus annual climatological salinity.

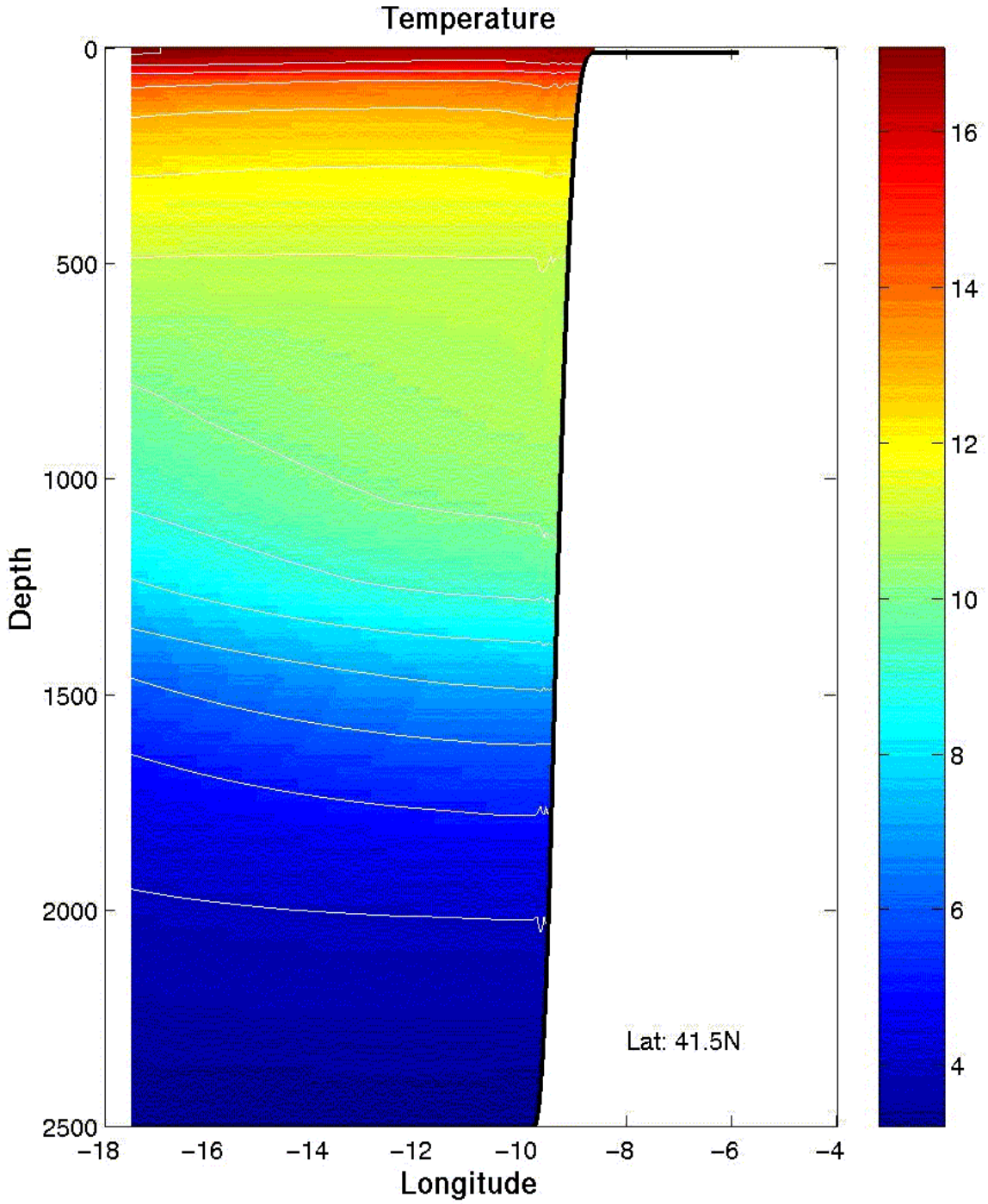

Figure 10. Cross-section at 41.5°N of Levitus annual climatological temperature.

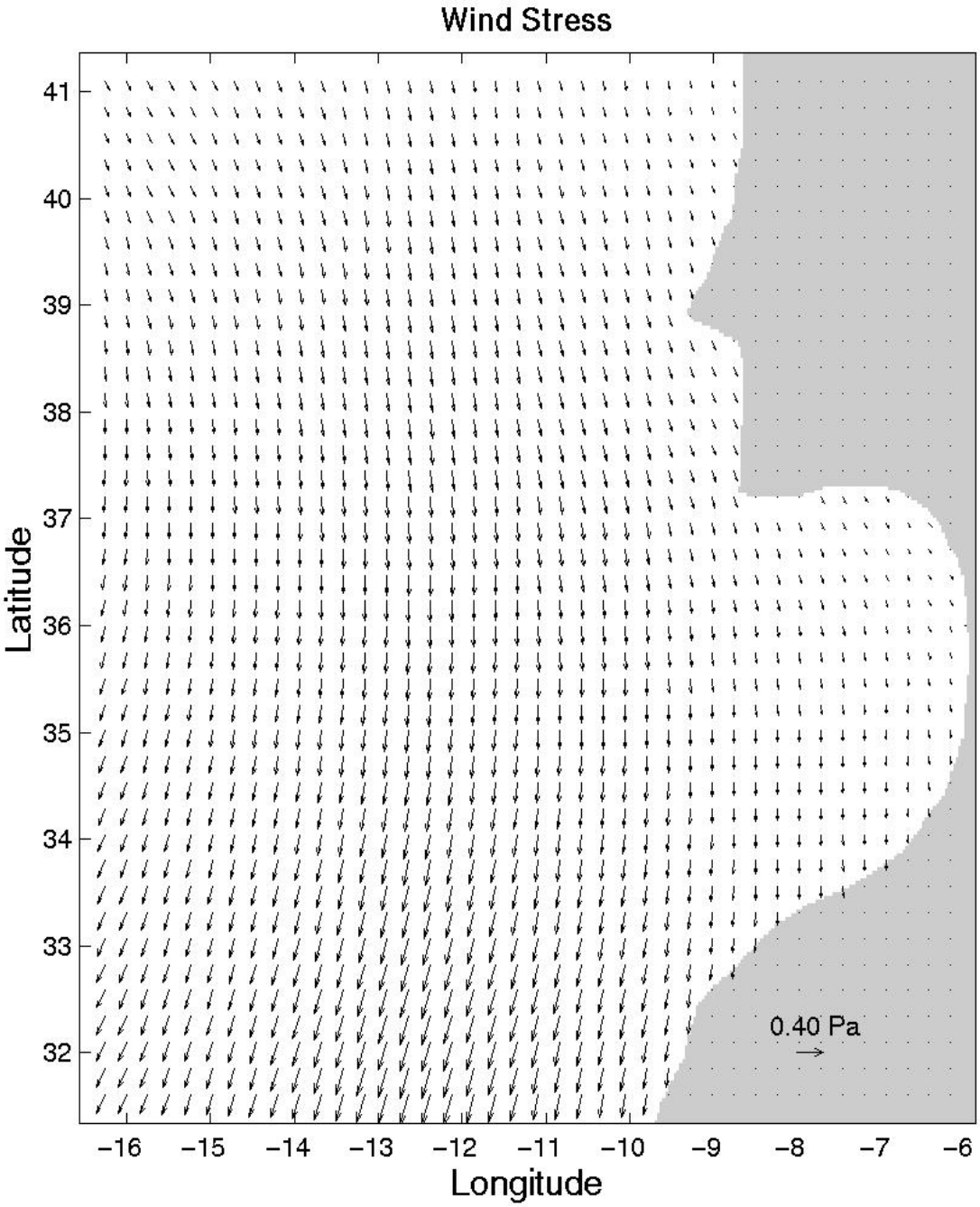

Figure 11. Wind stress in Pascal calculated from annual climatological ECMWF winds obtained from Trenberth *et al*. (1990).

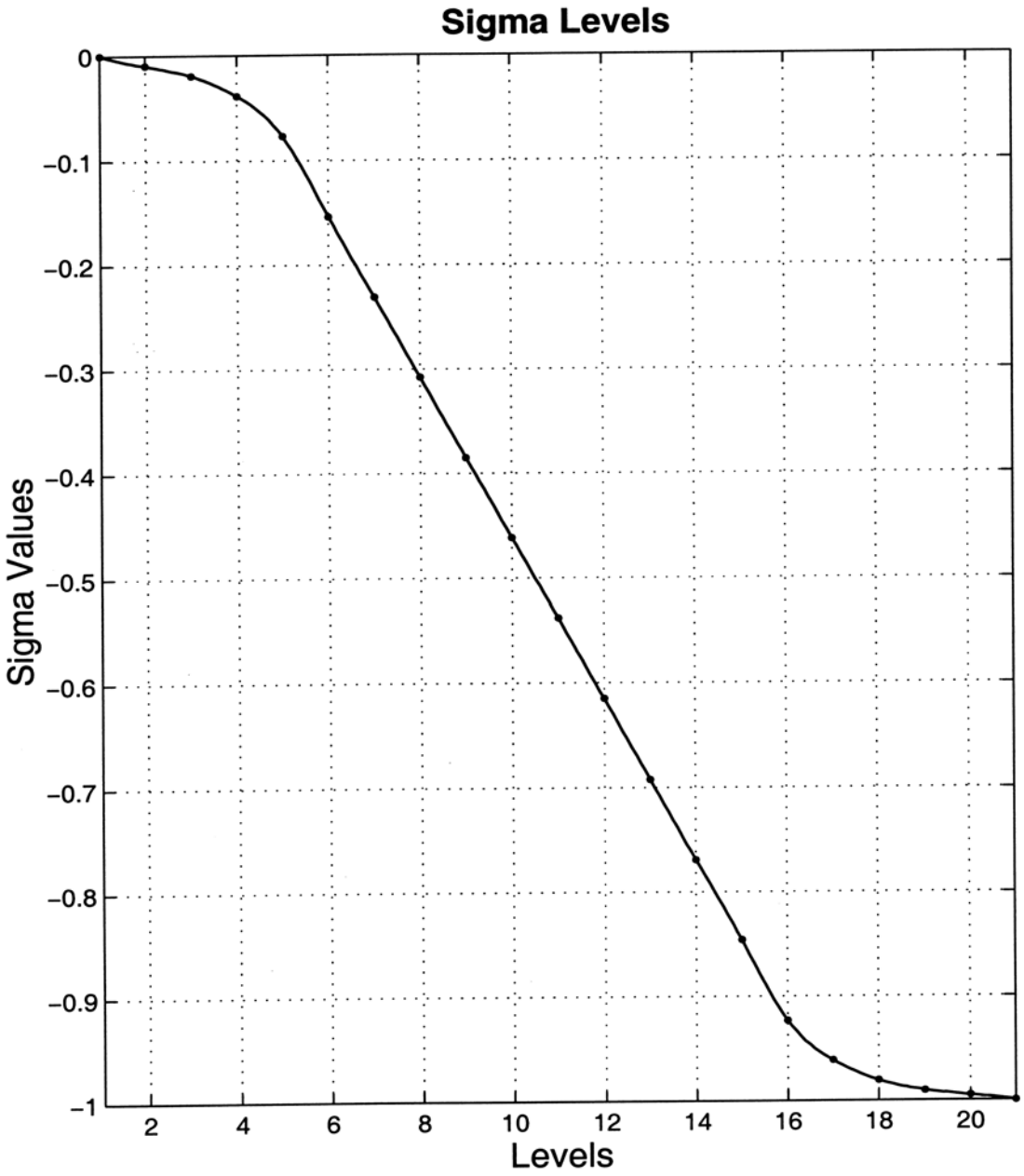

Figure 12. Plot of the 21 sigma levels.

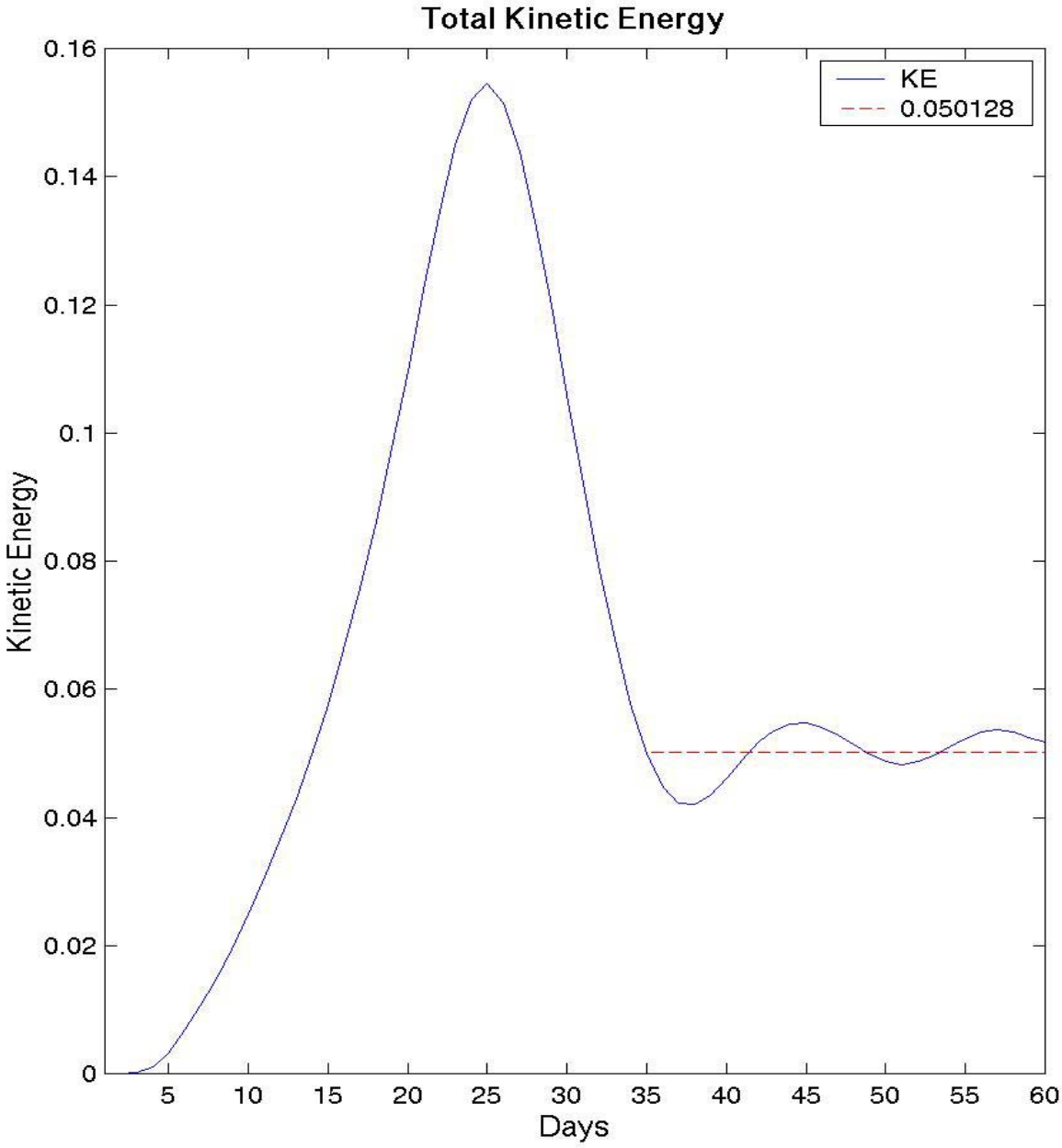

Figure 13. Plot of the total kinetic energy shows a steady and rapid increase of kinetic energy for the first 25 days. During this period the flow develops currents in model simulations but no mesoscale features. Between days 25 and 35, the kinetic energy decreases to about 1/3 of the maximum value. This loss, which is consistent with Roed, (1999), can be explained by a transfer of kinetic energy to available gravitational energy and then to eddy gravitational energy and eddy kinetic energy. After day 35, the development of eddies is discernible in the model simulation.

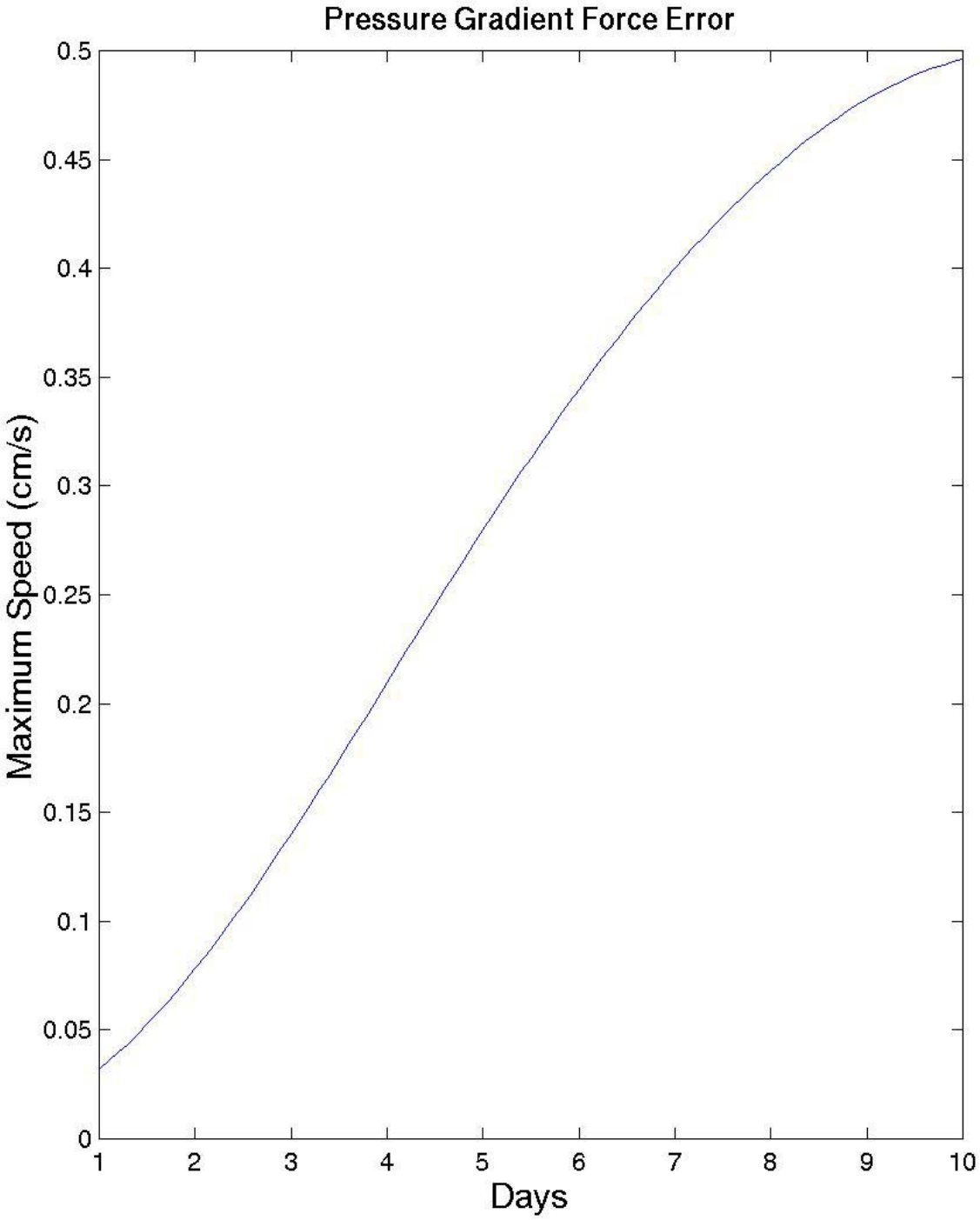

Figure 14. Plot of the maximum velocity error versus time due to the pressure gradient force error.

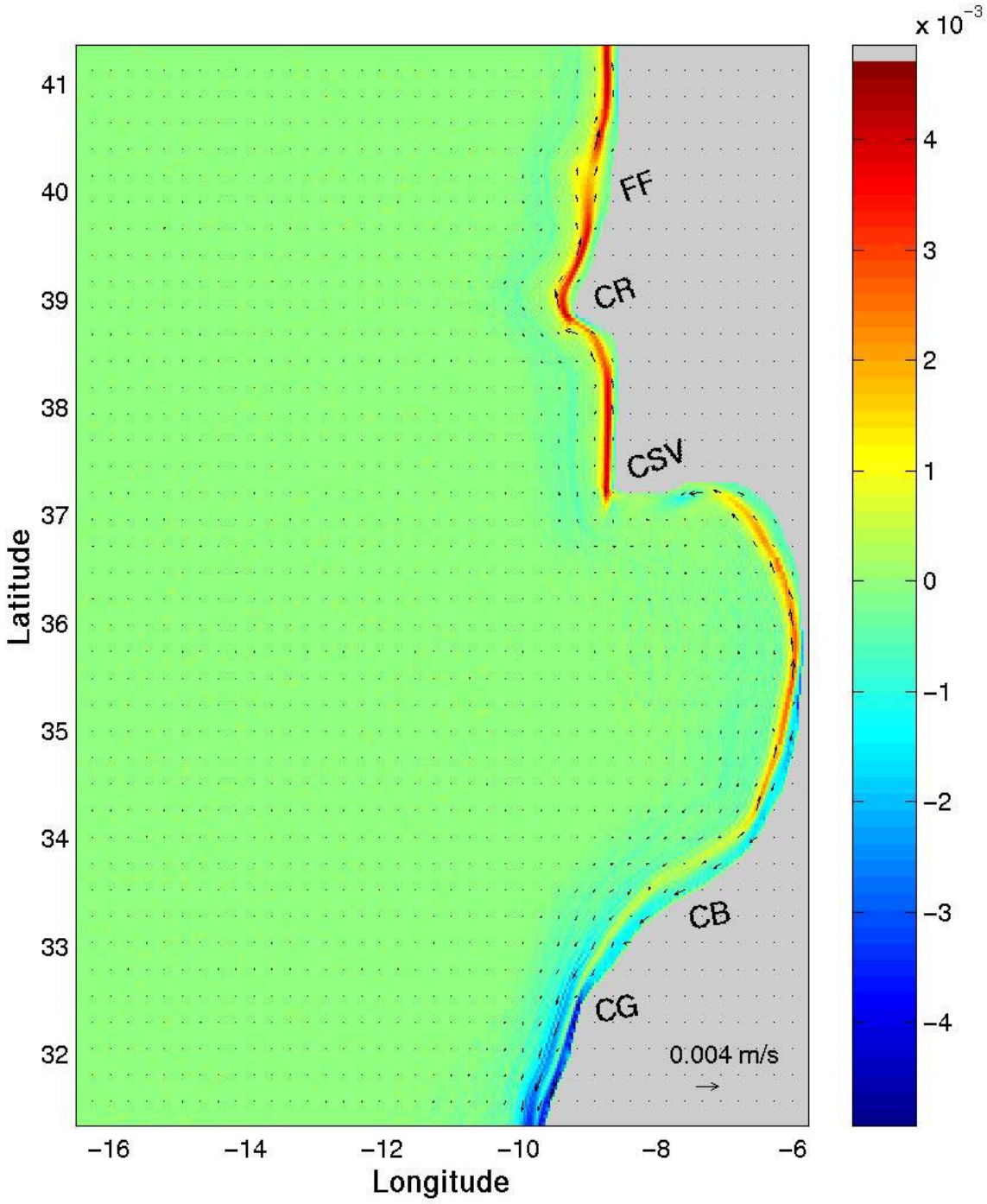

Figure 15. Surface velocity error due to the pressure gradient force error on day 10.

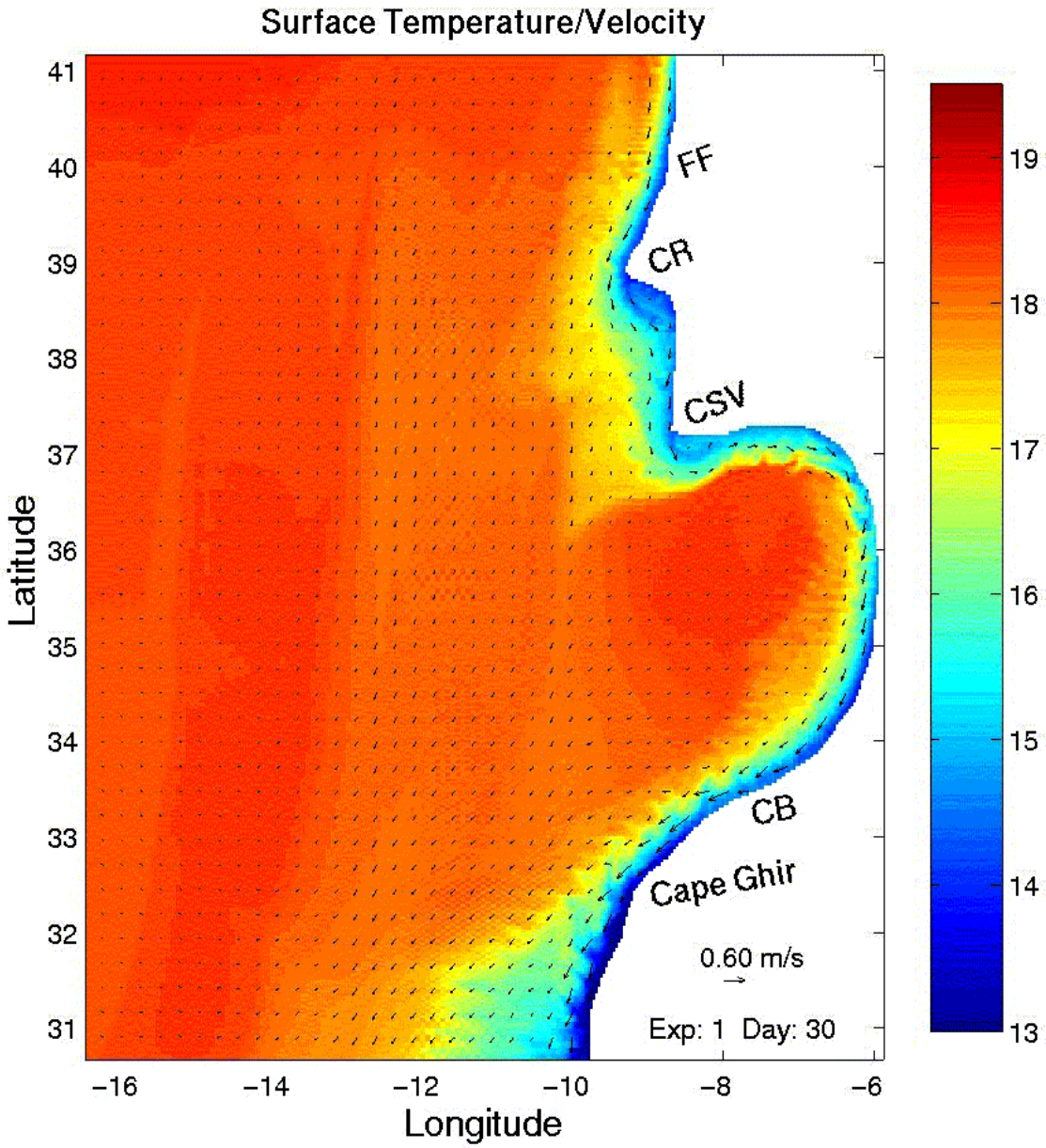

Figure 16. Surface velocity vectors (arrows) and temperatures (in color) for Experiment 1 on day 30.

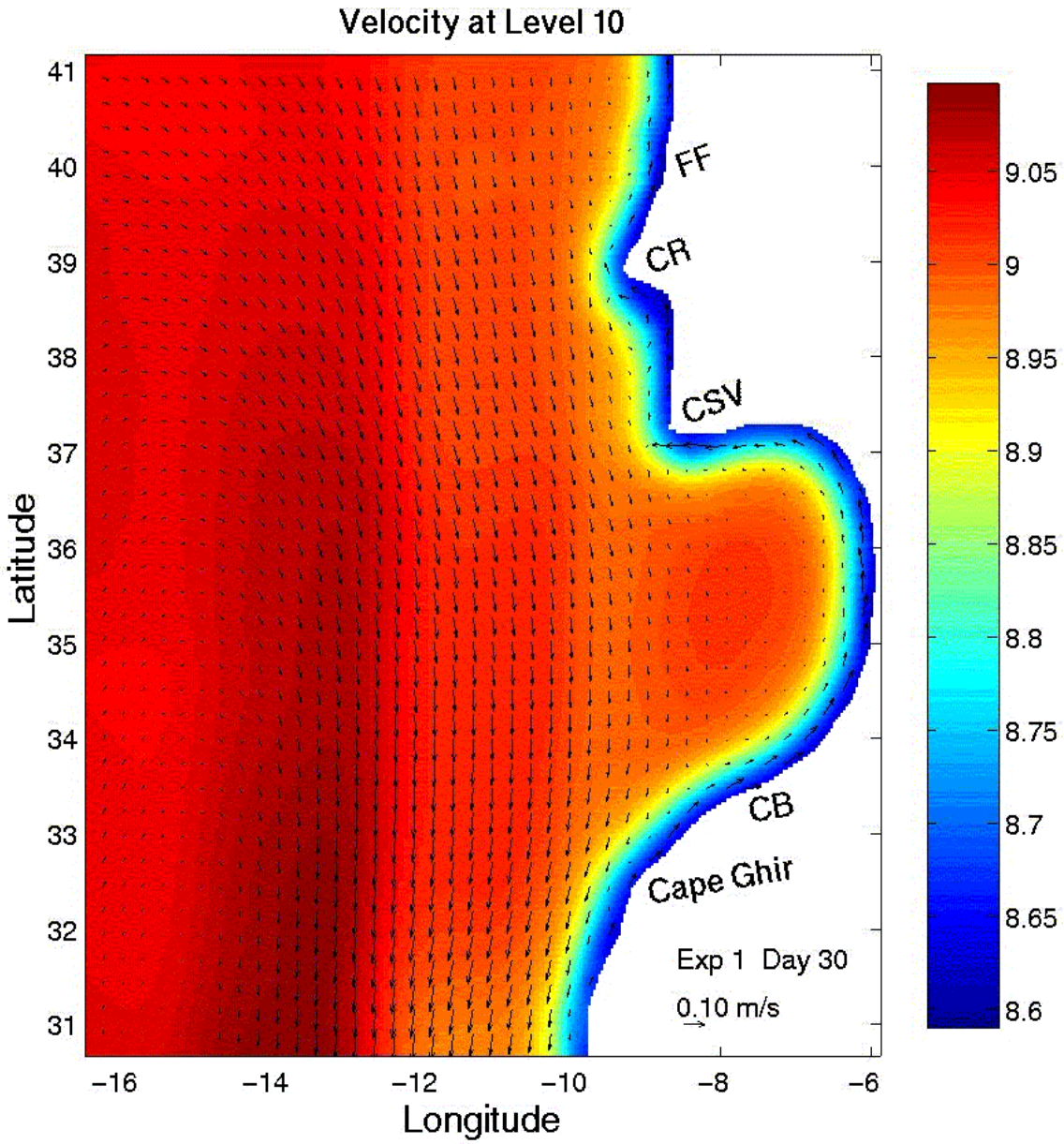

Figure 17. Temperature (in color) and velocity vectors (arrows) at sigma level 10 for Experiment 1 on day 30.

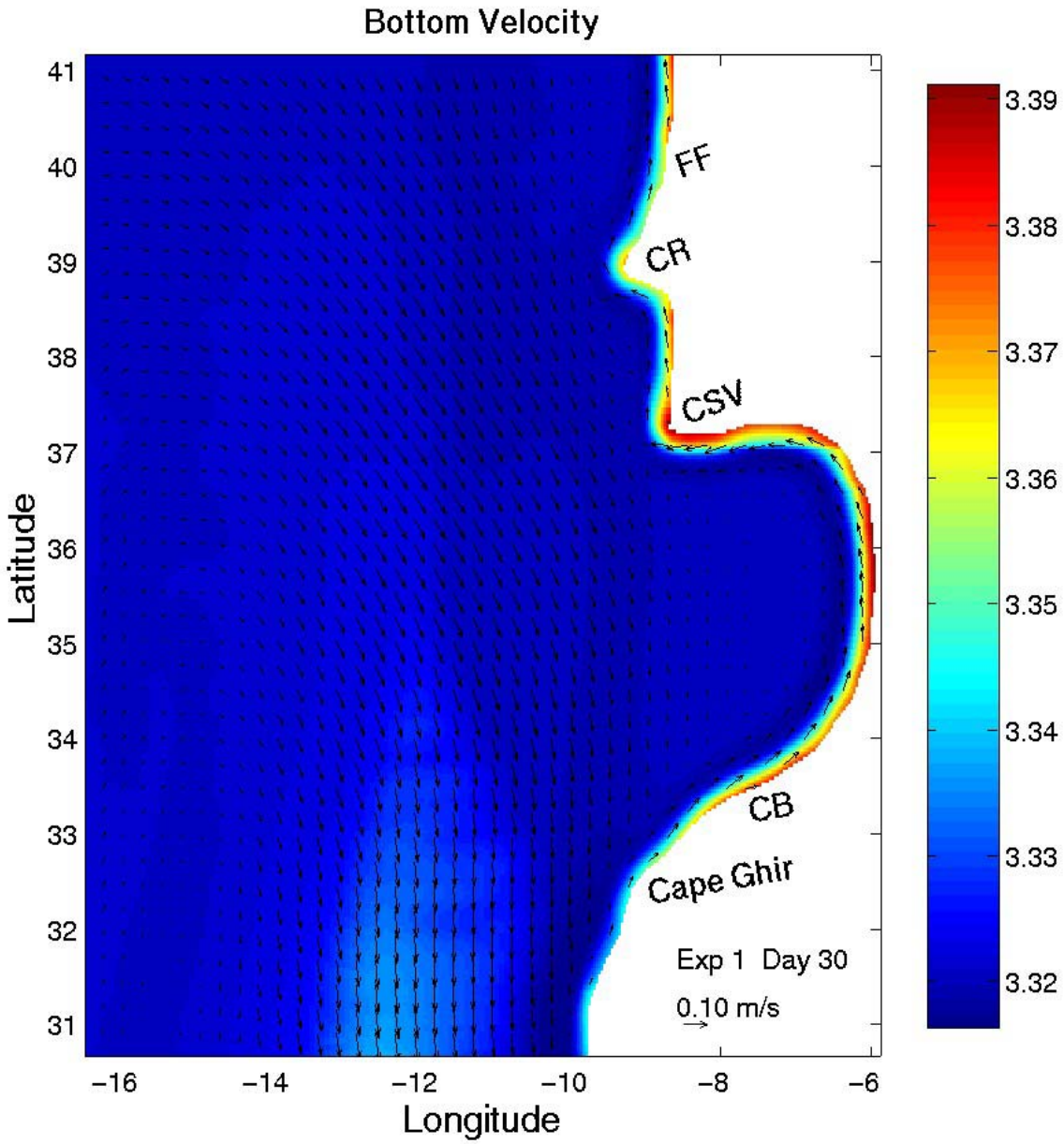

Figure 18. Temperature (in color) and velocity vectors (arrows) at sigma level 20 for Experiment 1 on day 30.

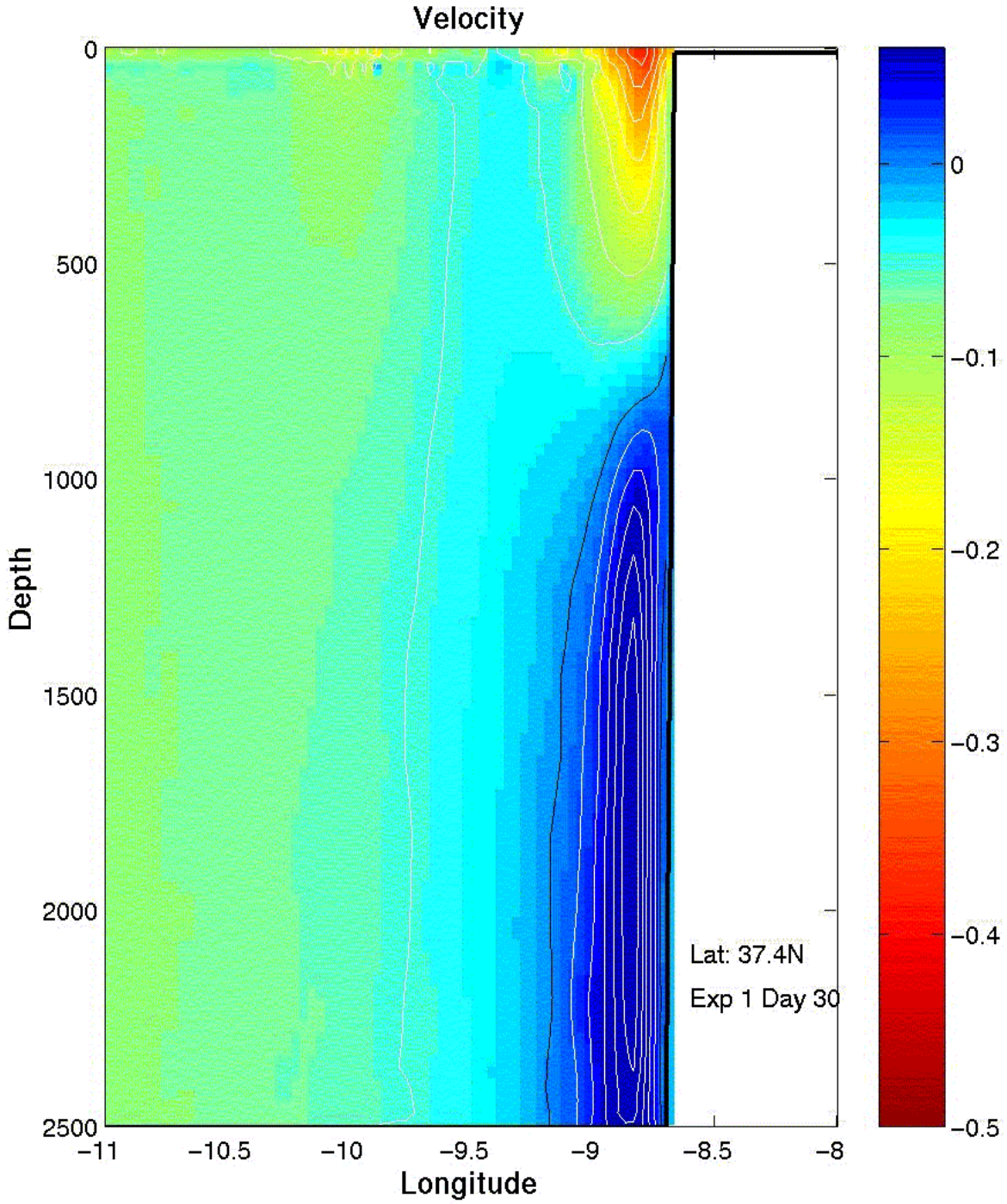

Figure 19. Cross-section of meridional velocity (v) at 37.4°N for Experiment 1 on day 30. Equatorward (poleward) flow is denoted by red (blue) color with contour intervals of 5 cm/s (2 cm/s)

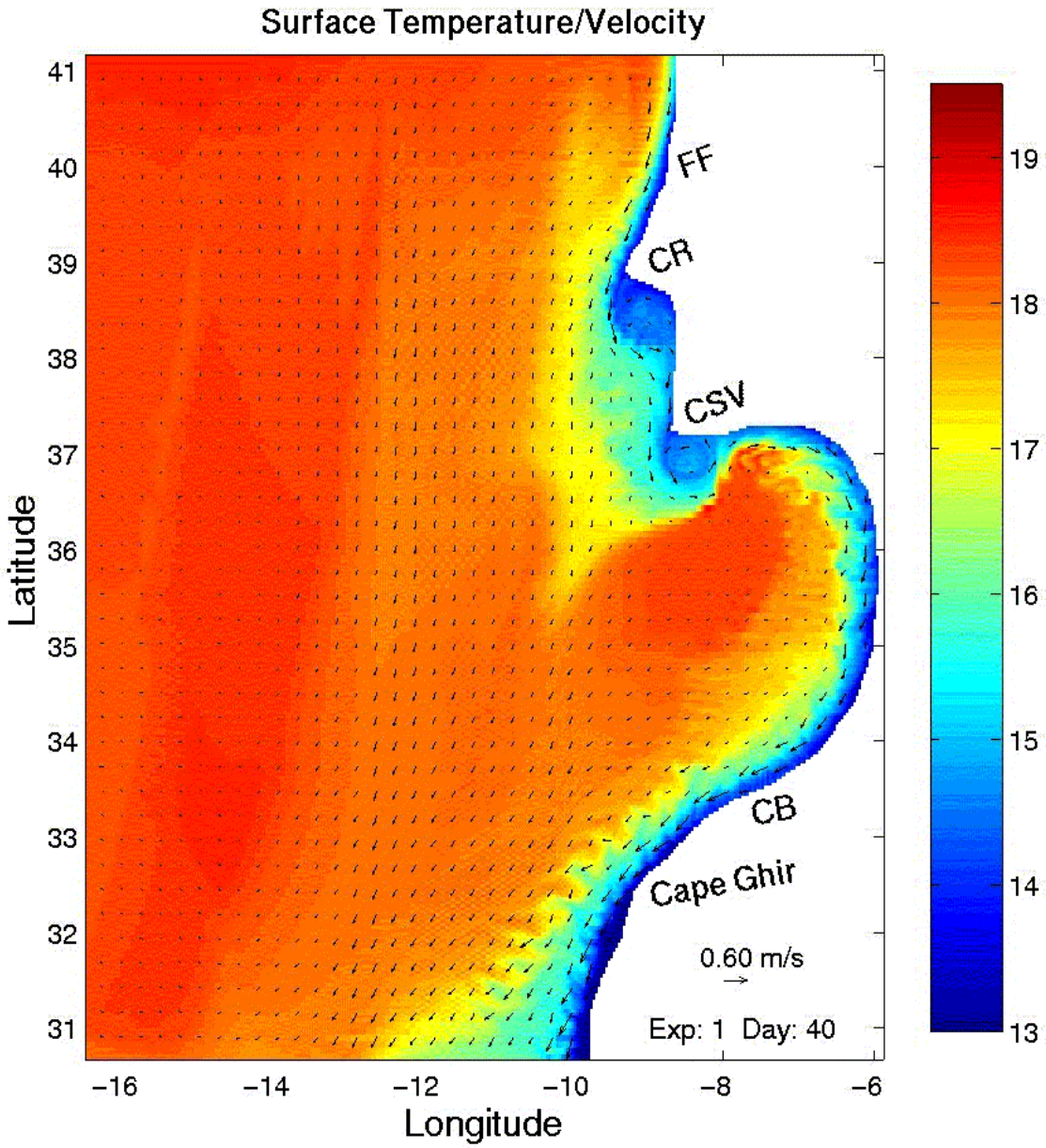

Figure 20. Surface velocity vectors (arrows) and temperatures (in color) for Experiment 1 on day 40.

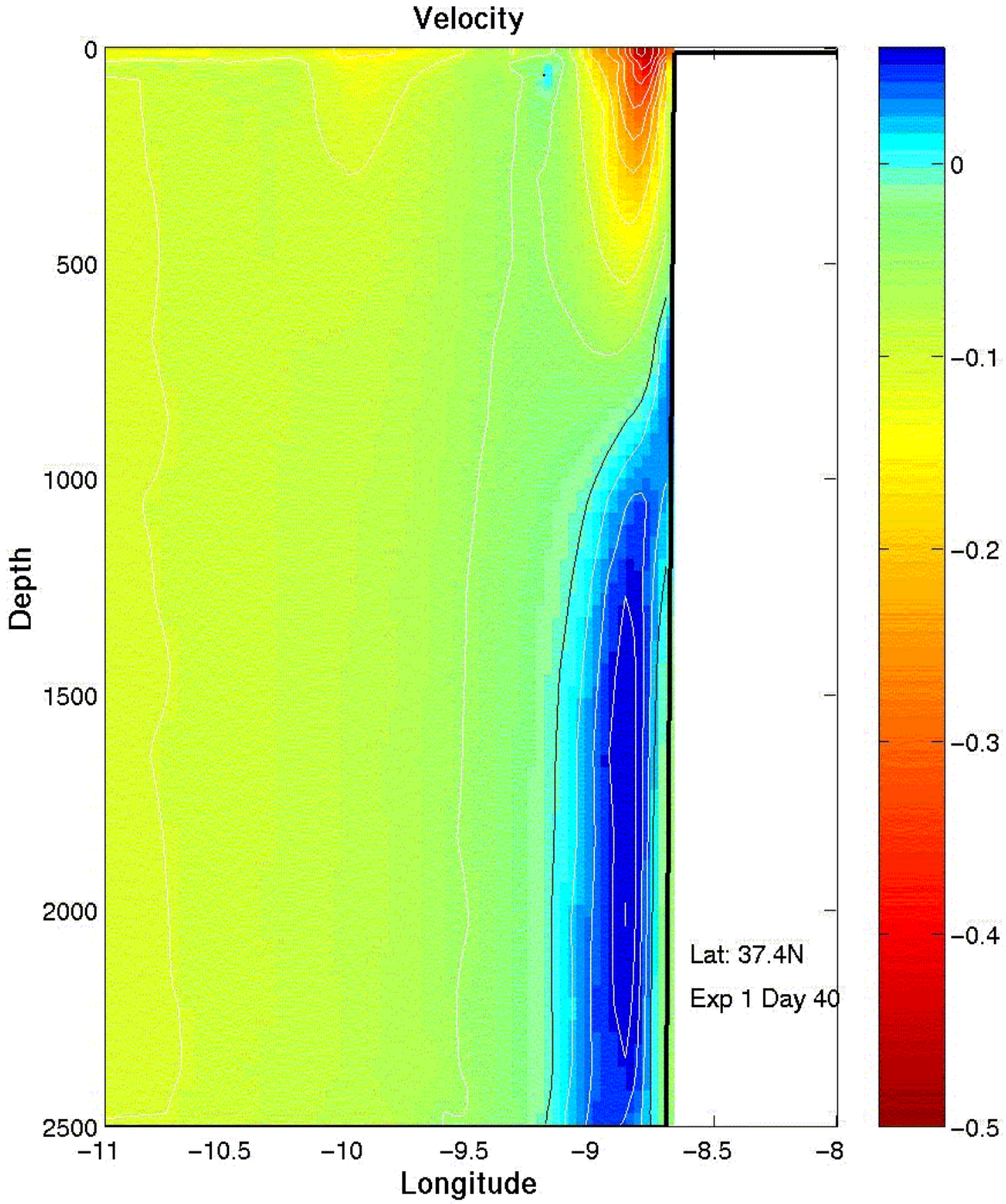

Figure 21. Cross-section of meridional velocity (v) at 37.4°N for Experiment 1 on day 40. Equatorward (poleward) flow is denoted by red (blue) color with contour intervals of 5 cm/s (2 cm/s).

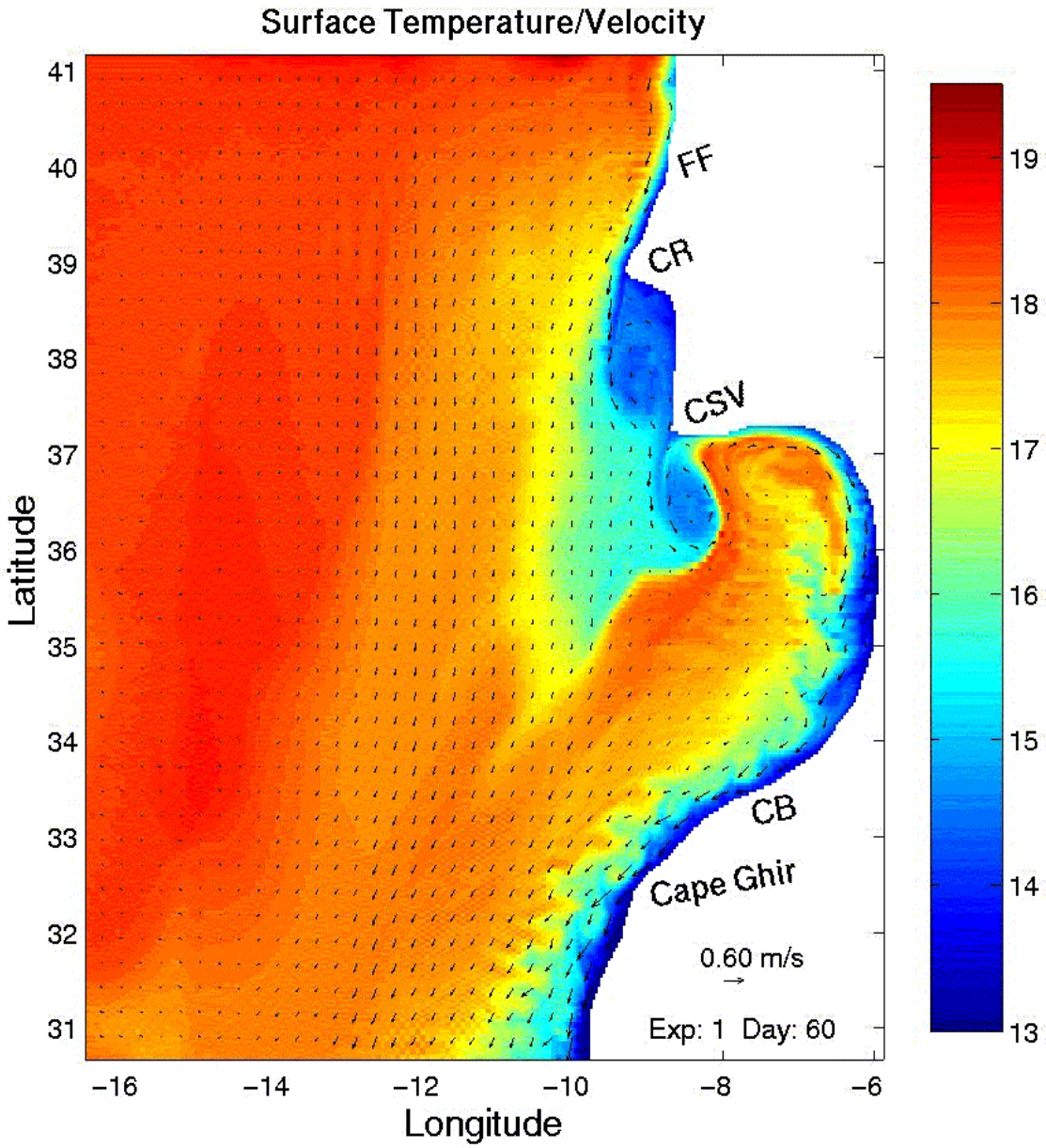

Figure 22. Surface velocity vectors (arrows) and temperatures (in color) for Experiment 1 on day 60.

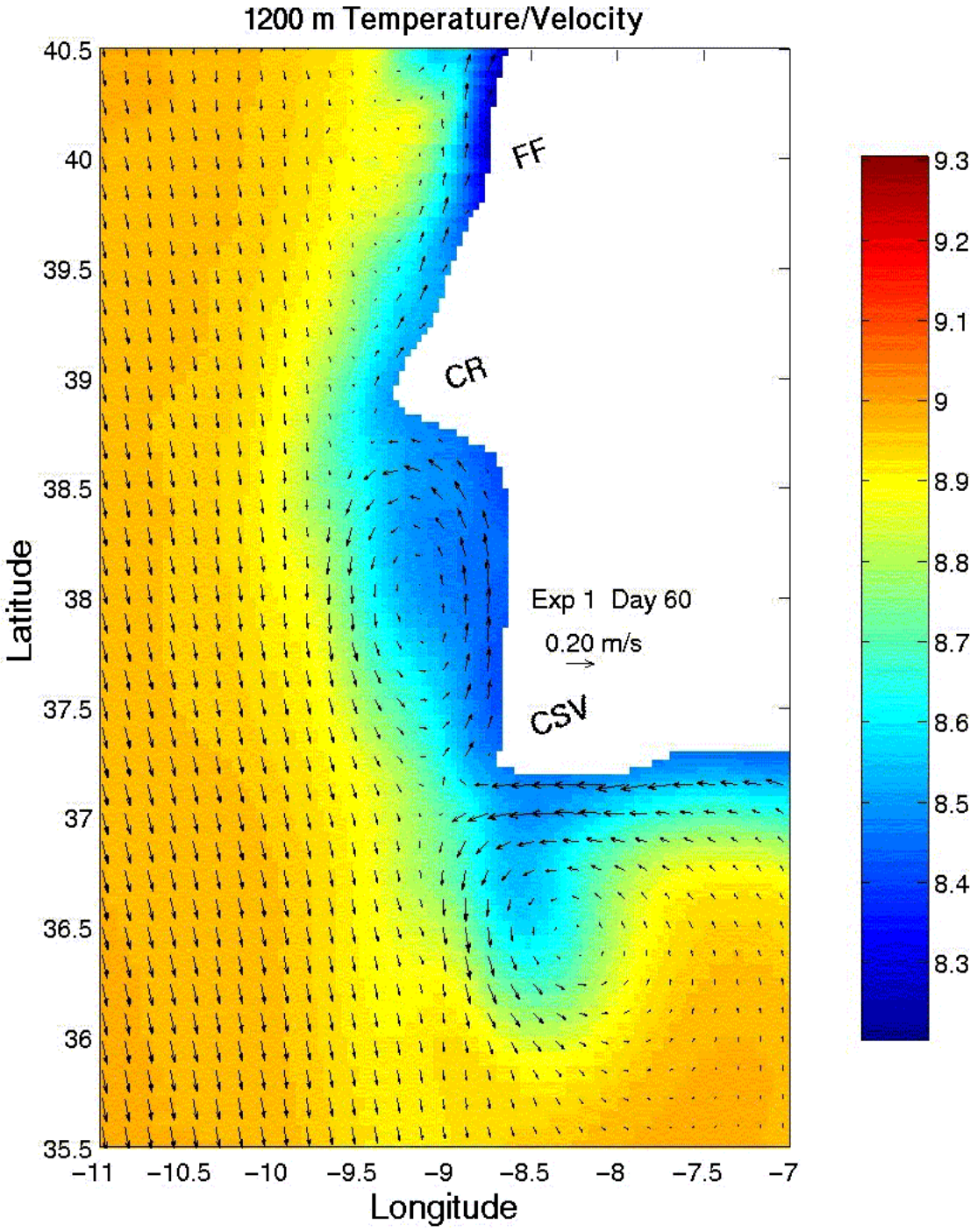

Figure 23. 1200 m velocity vectors (arrows) and temperature (in color) for Experiment 1 on day 60.

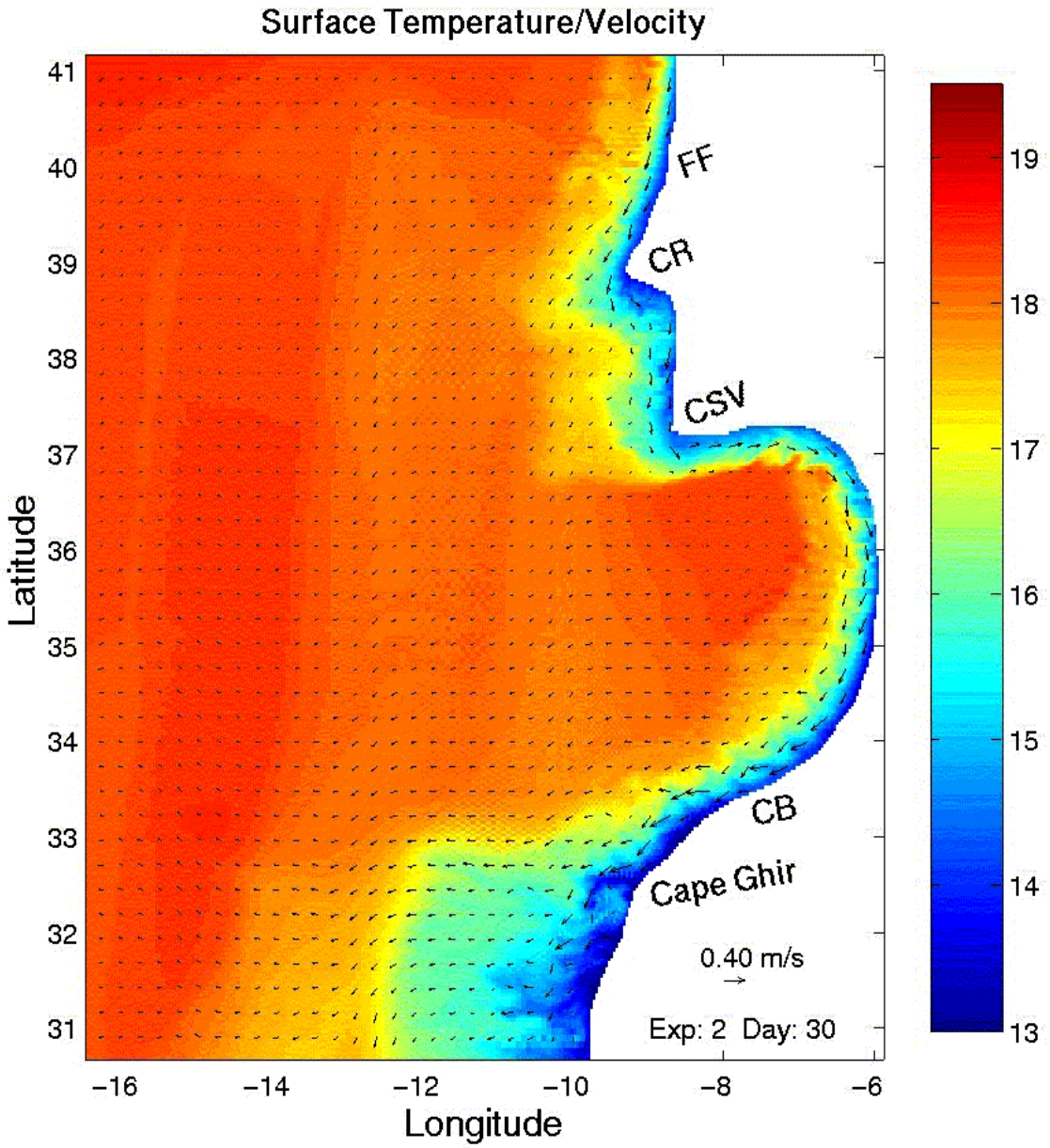

Figure 24. Surface velocity vectors (arrows) and temperatures (in color) for Experiment 2 on day 30.

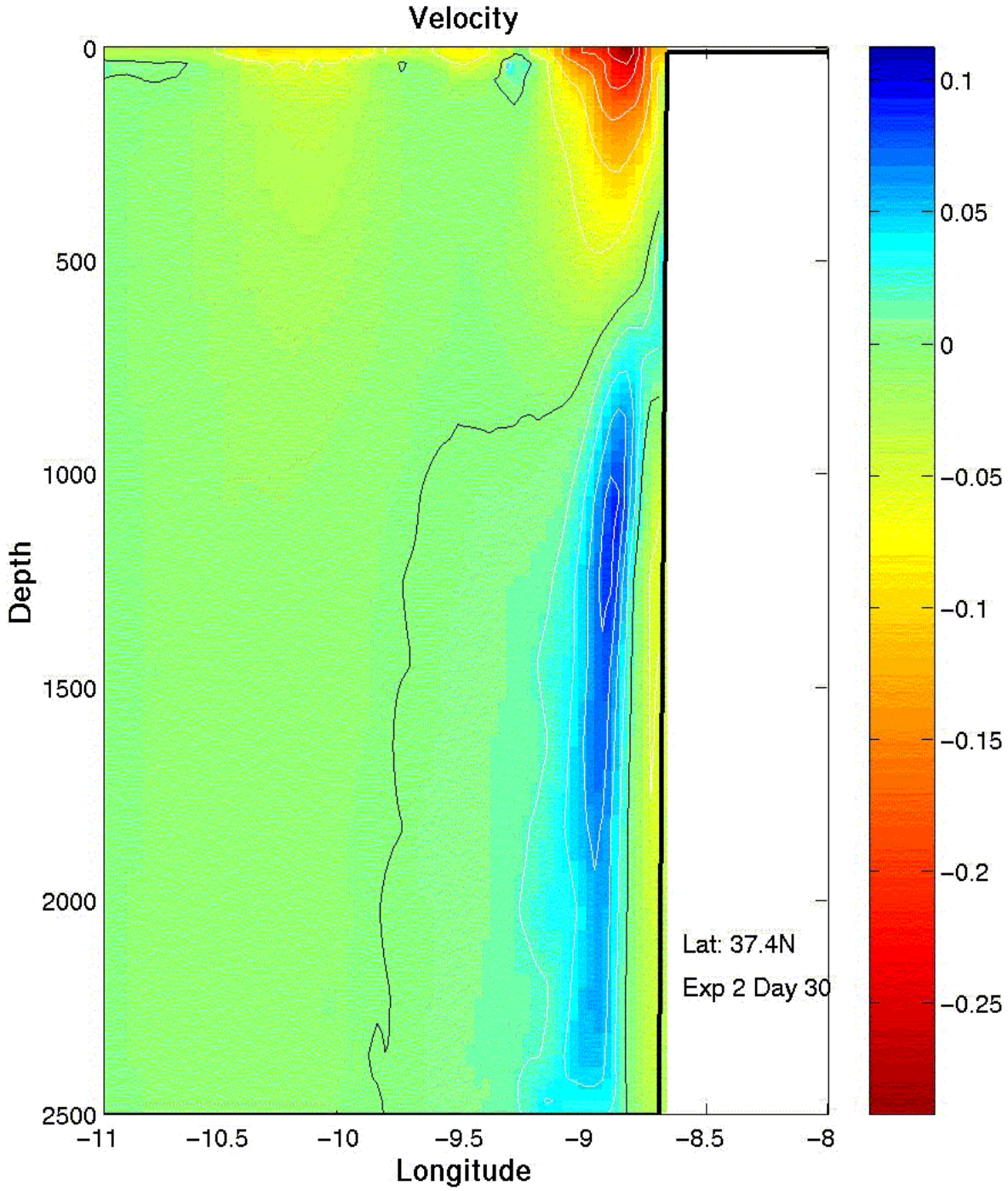

Figure 25. Cross-section of meridional velocity (v) at 37.4°N for Experiment 2 on day 30. Equatorward (poleward) flow is denoted by red (blue) color with contour intervals of 5 cm/s (2 cm/s).

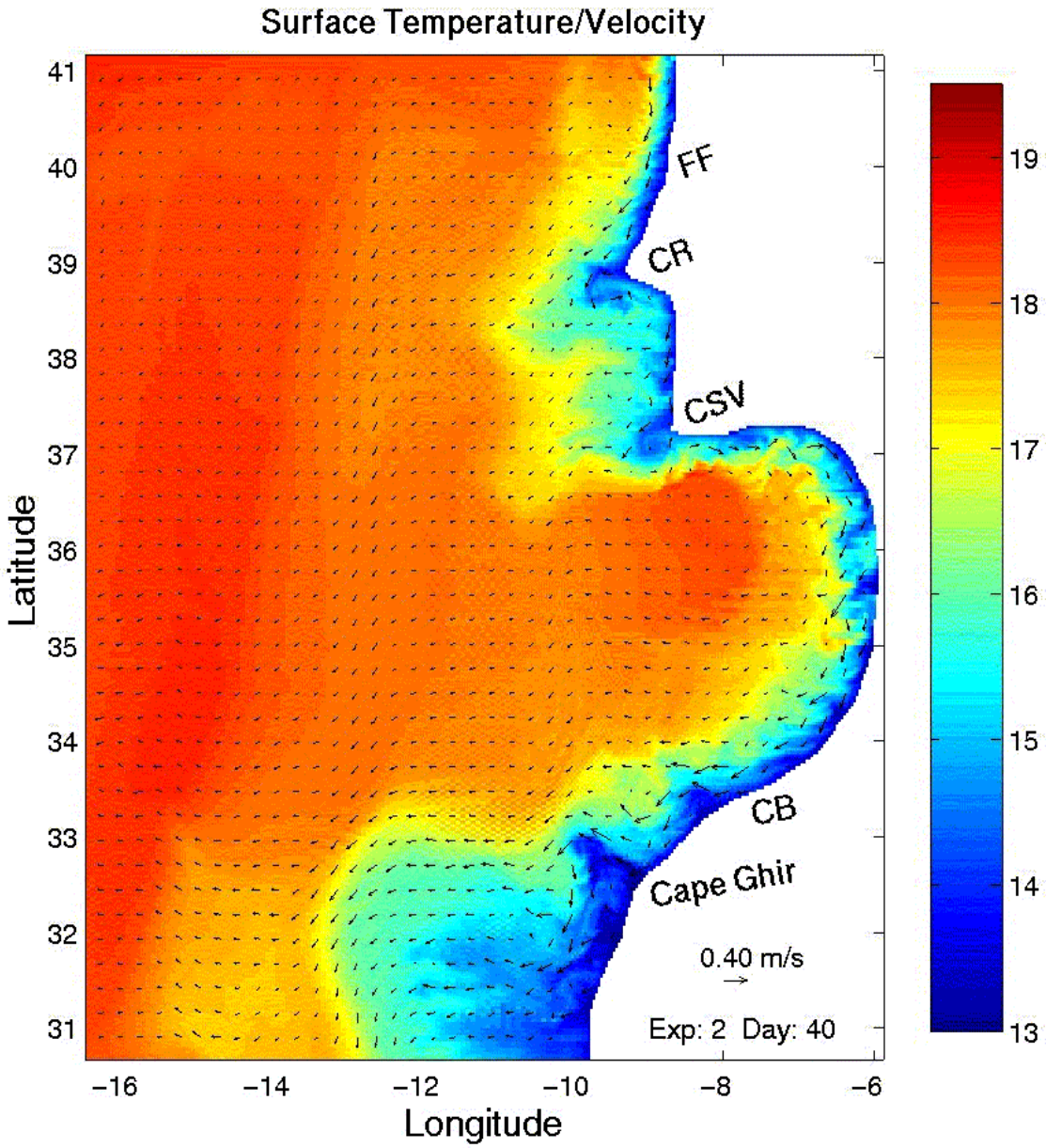

Figure 26. Surface velocity vectors (arrows) and temperatures (in color) for Experiment 2 on day 40.

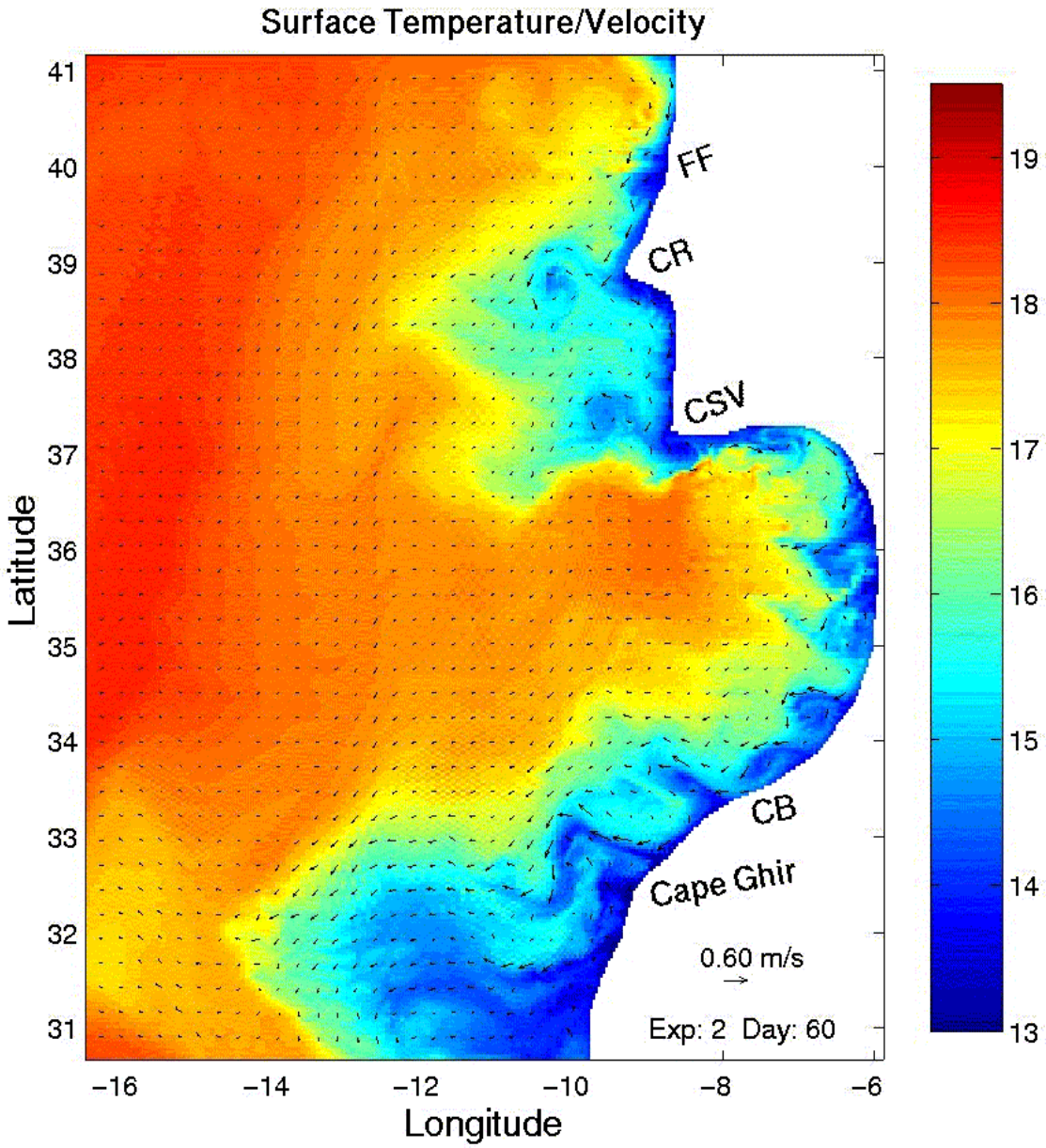

Figure 27. Surface velocity vectors (arrows) and temperatures (in color) for Experiment 2 on day 60.

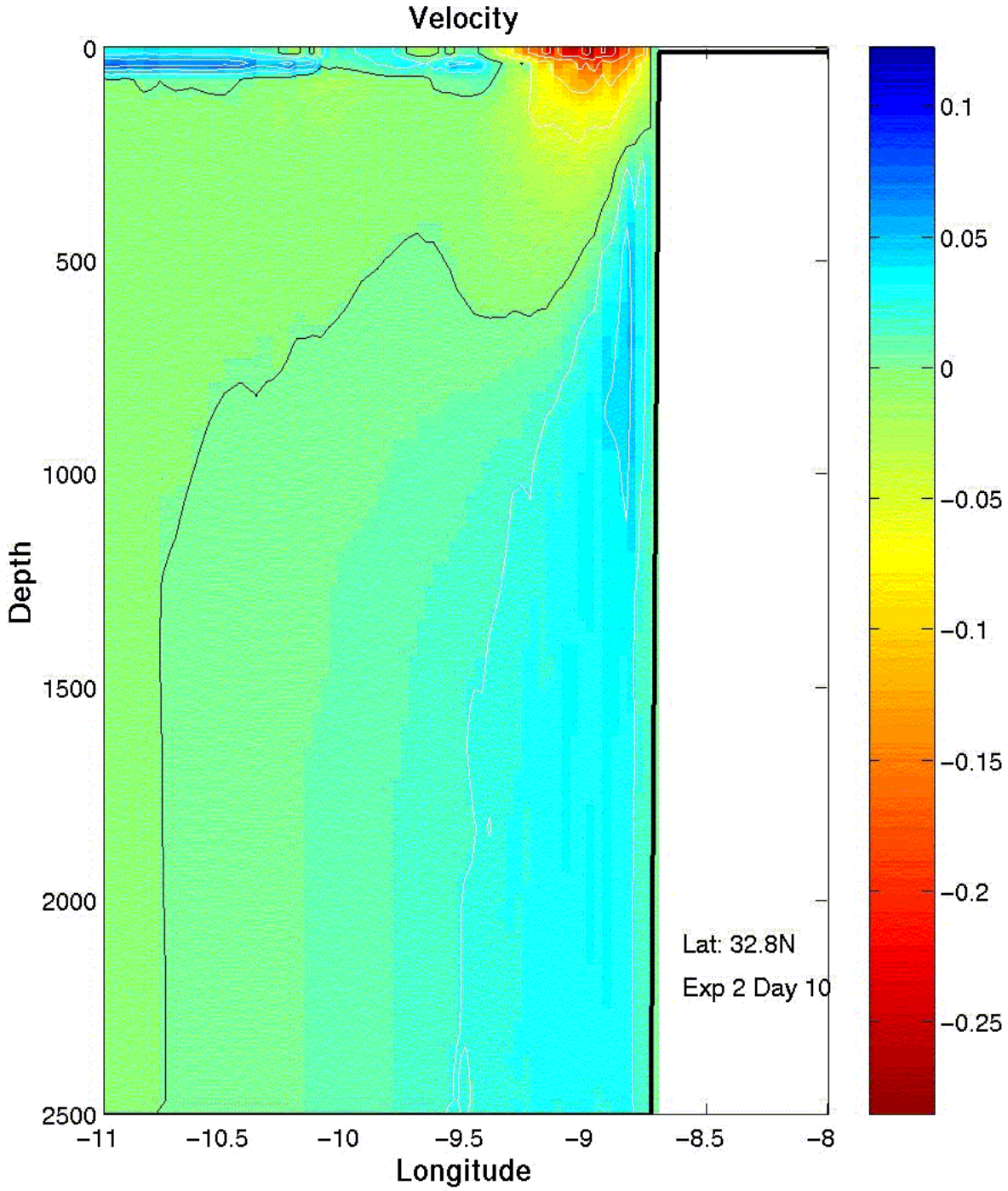

Figure 28. Cross-section of meridional velocity (v) at 32.8°N for Experiment 2 on day 10. Equatorward (poleward) flow is denoted by red (blue) color with contour intervals of 5 cm/s (2 cm/s).

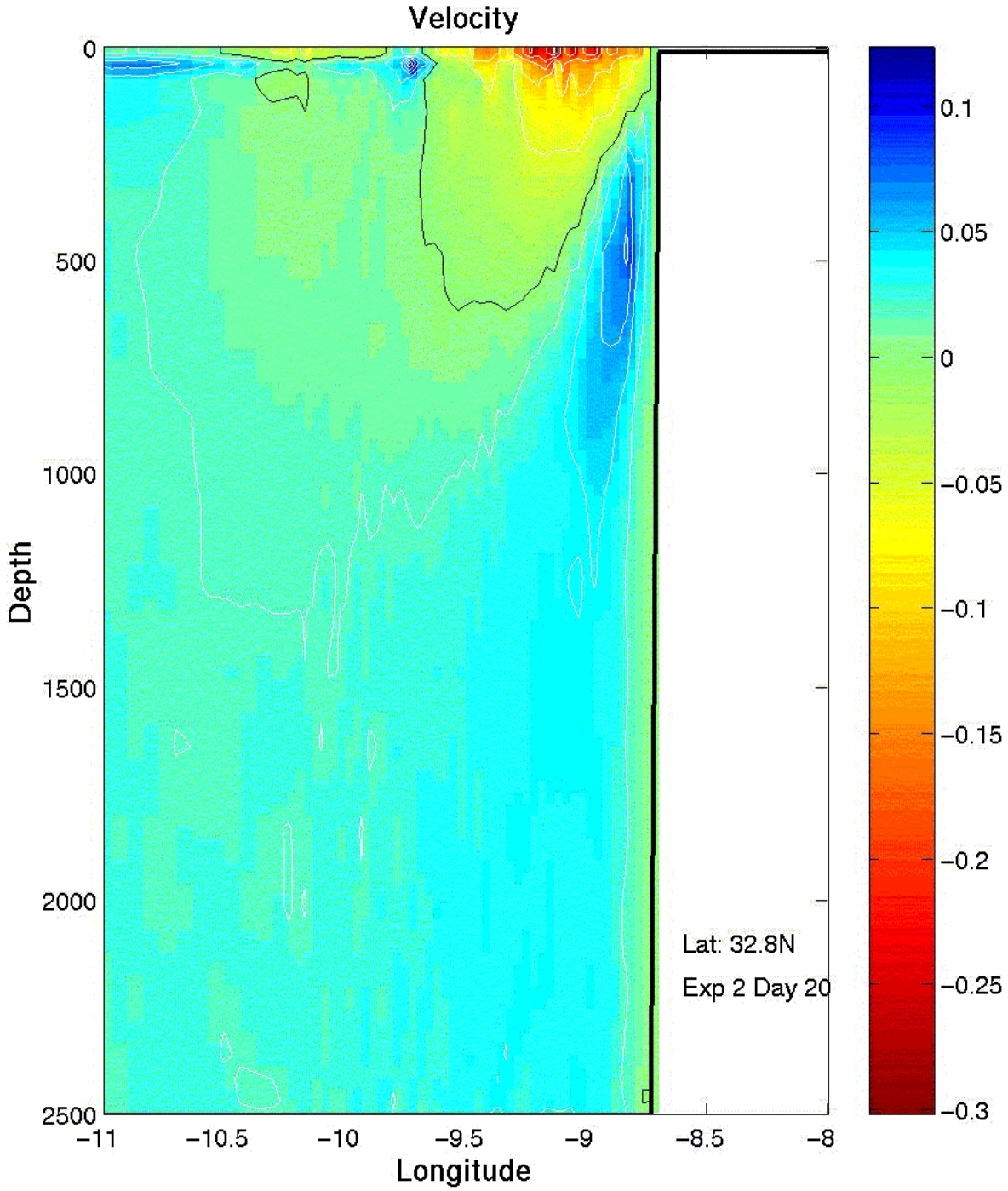

Figure 29. Cross-section of meridional velocity (v) at 32.8°N for Experiment 2 on day 20. Equatorward (poleward) flow is denoted by red (blue) color with contour intervals of 5 cm/s (2 cm/s).

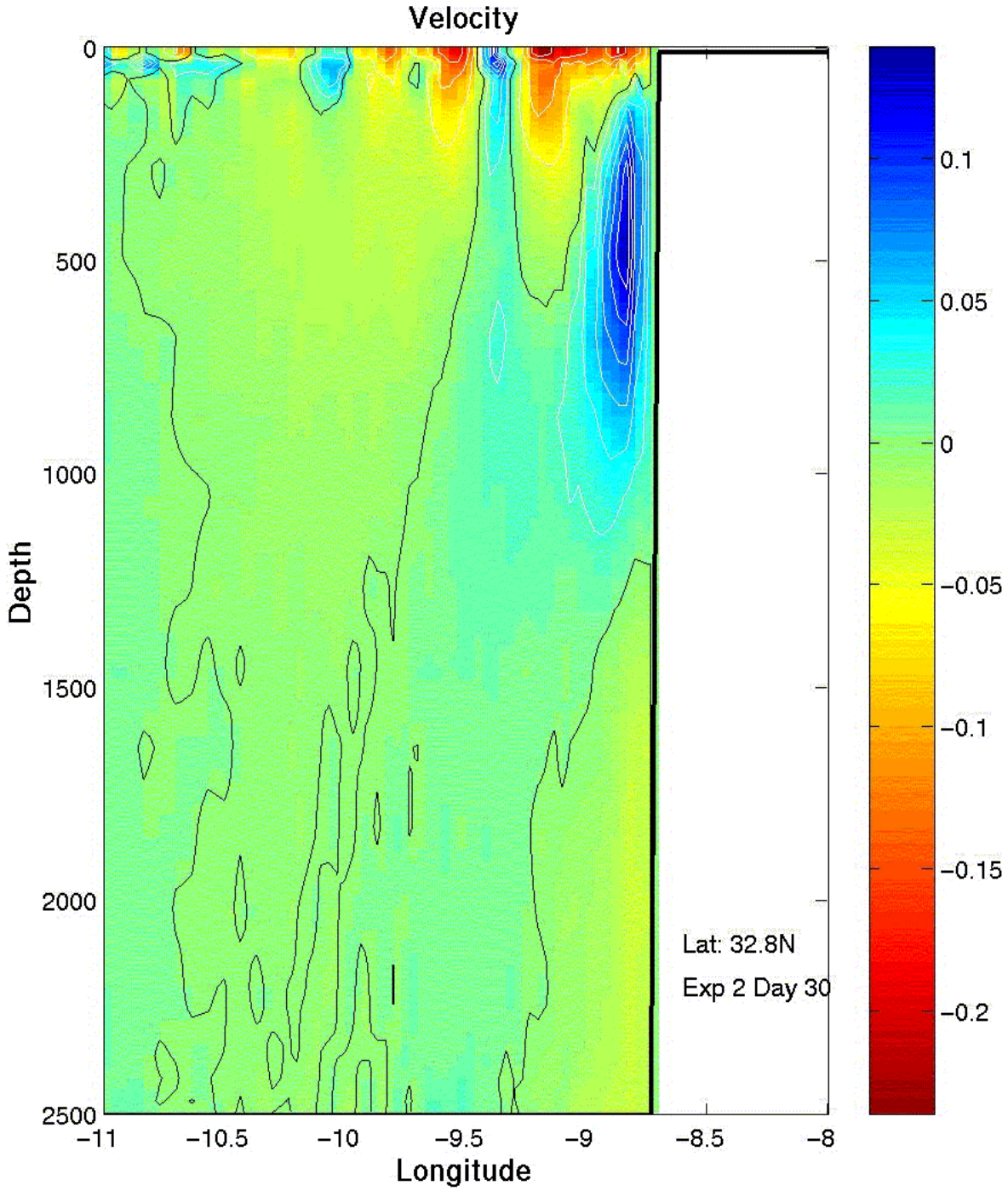

Figure 30. Cross-section of meridional velocity (v) at 32.8°N for Experiment 2 on day 30. Equatorward (poleward) flow is denoted by red (blue) color with contour intervals of 5 cm/s (2 cm/s).

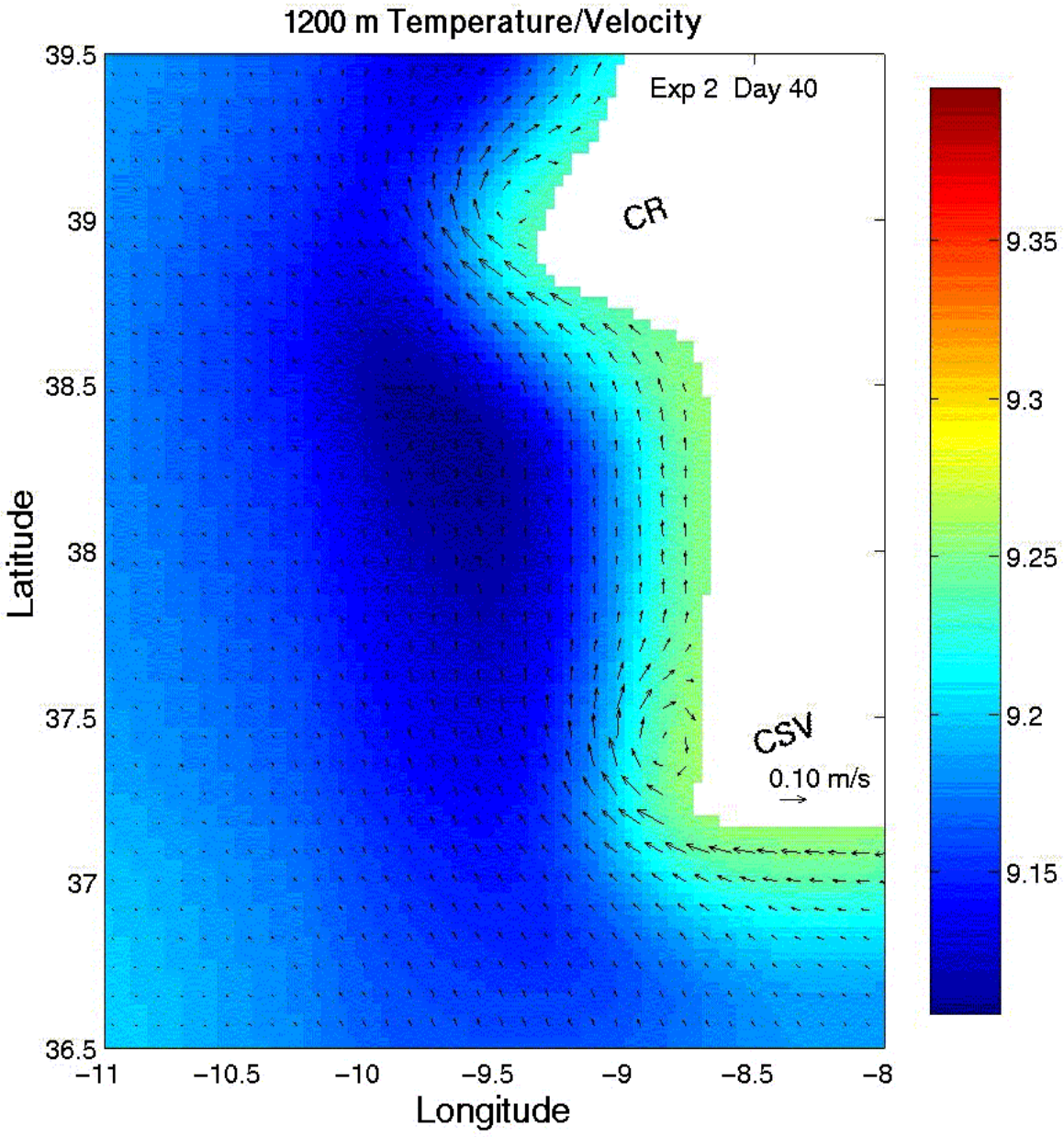

Figure 31. 1200 m velocity vectors (arrows) and temperatures (in color) for Experiment 2 on day 40.

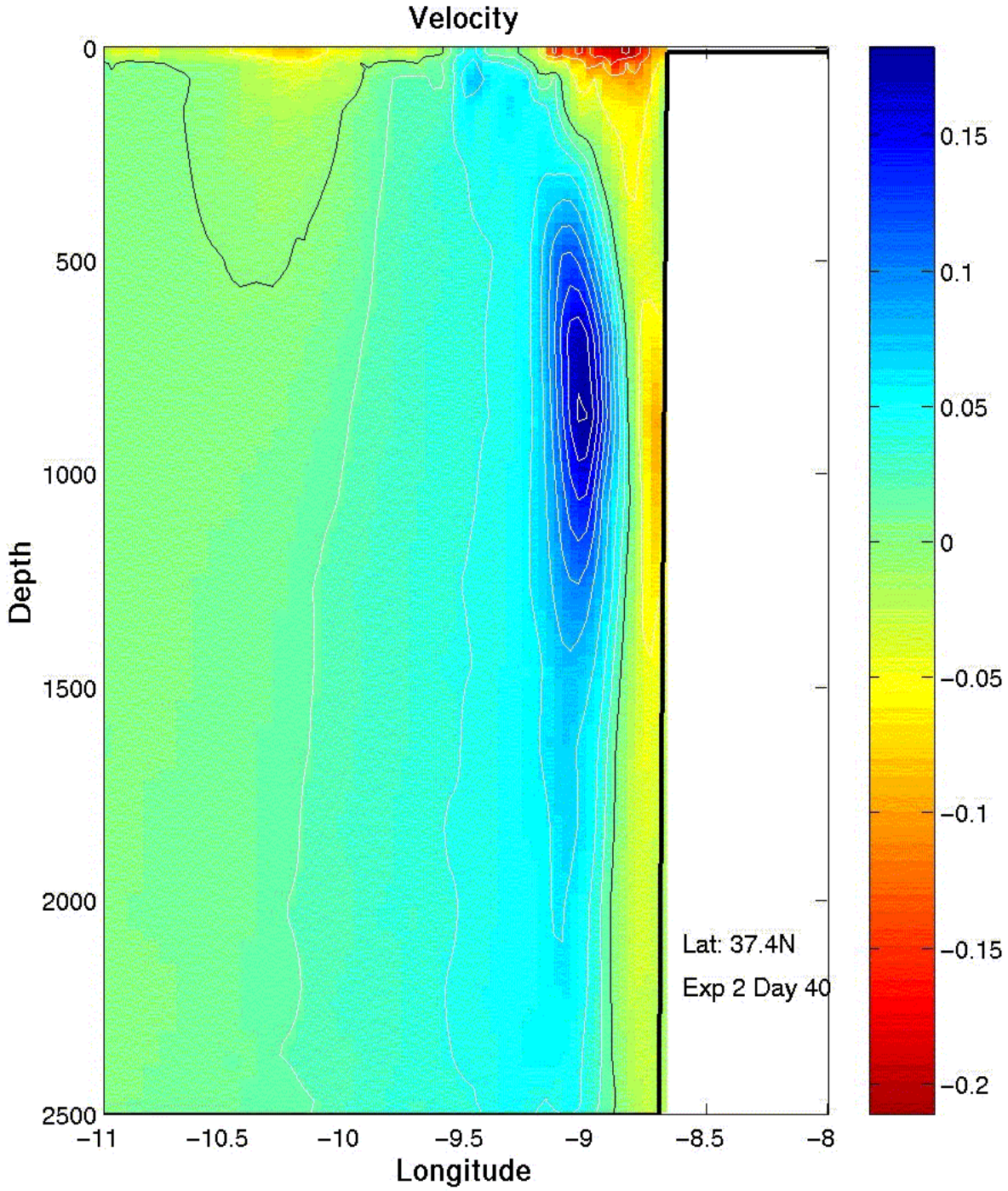

Figure 32. Cross-section of meridional velocity (v) at 37.4°N for Experiment 2 on day 40. Equatorward (poleward) flow is denoted by red (blue) color with contour intervals of 5 cm/s (2 cm/s).

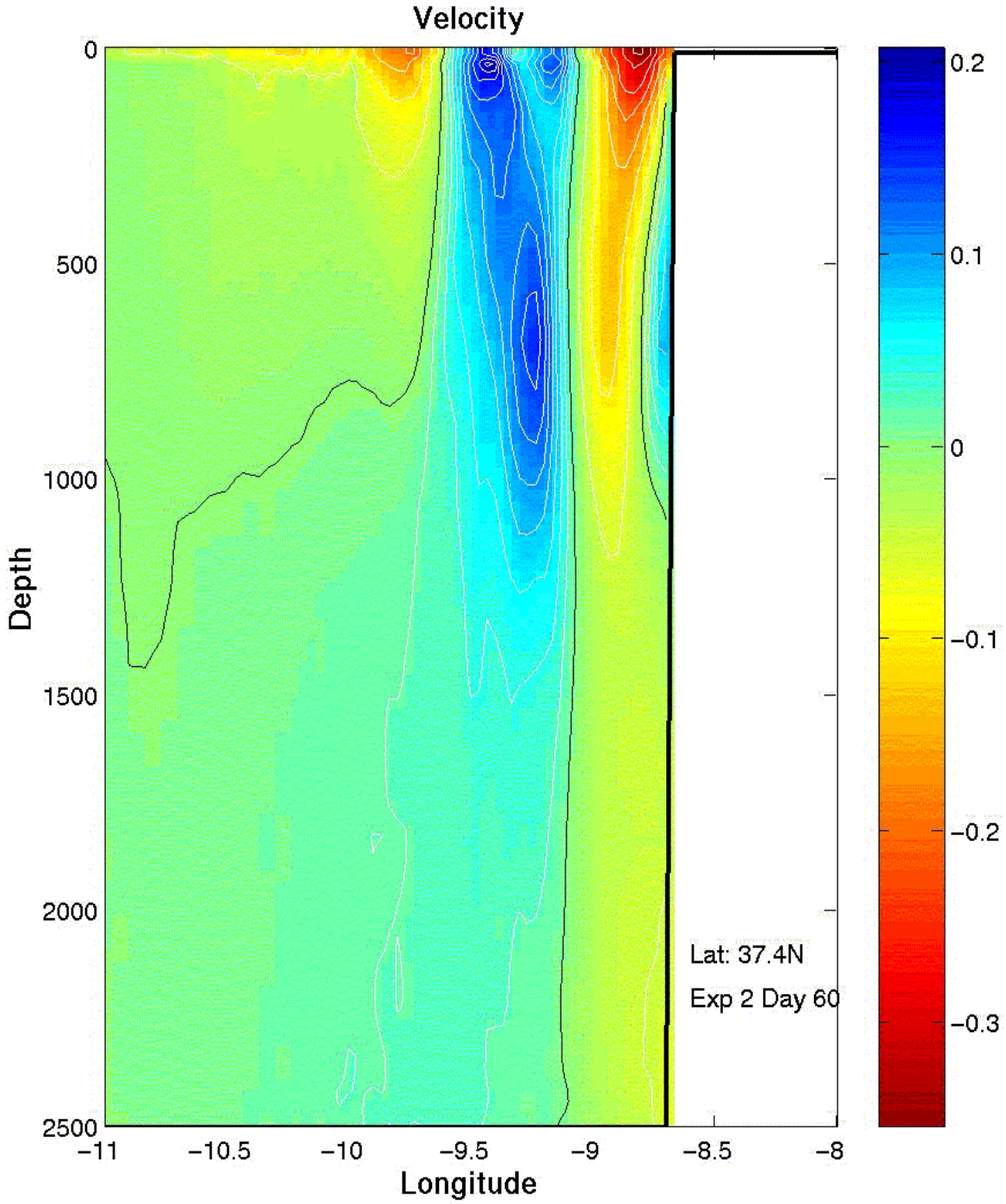

Figure 33. Cross-section of meridional velocity (v) at 37.4°N for Experiment 2 on day 60. Equatorward (poleward) flow is denoted by red (blue) color with contour intervals of 5 cm/s (2 cm/s).

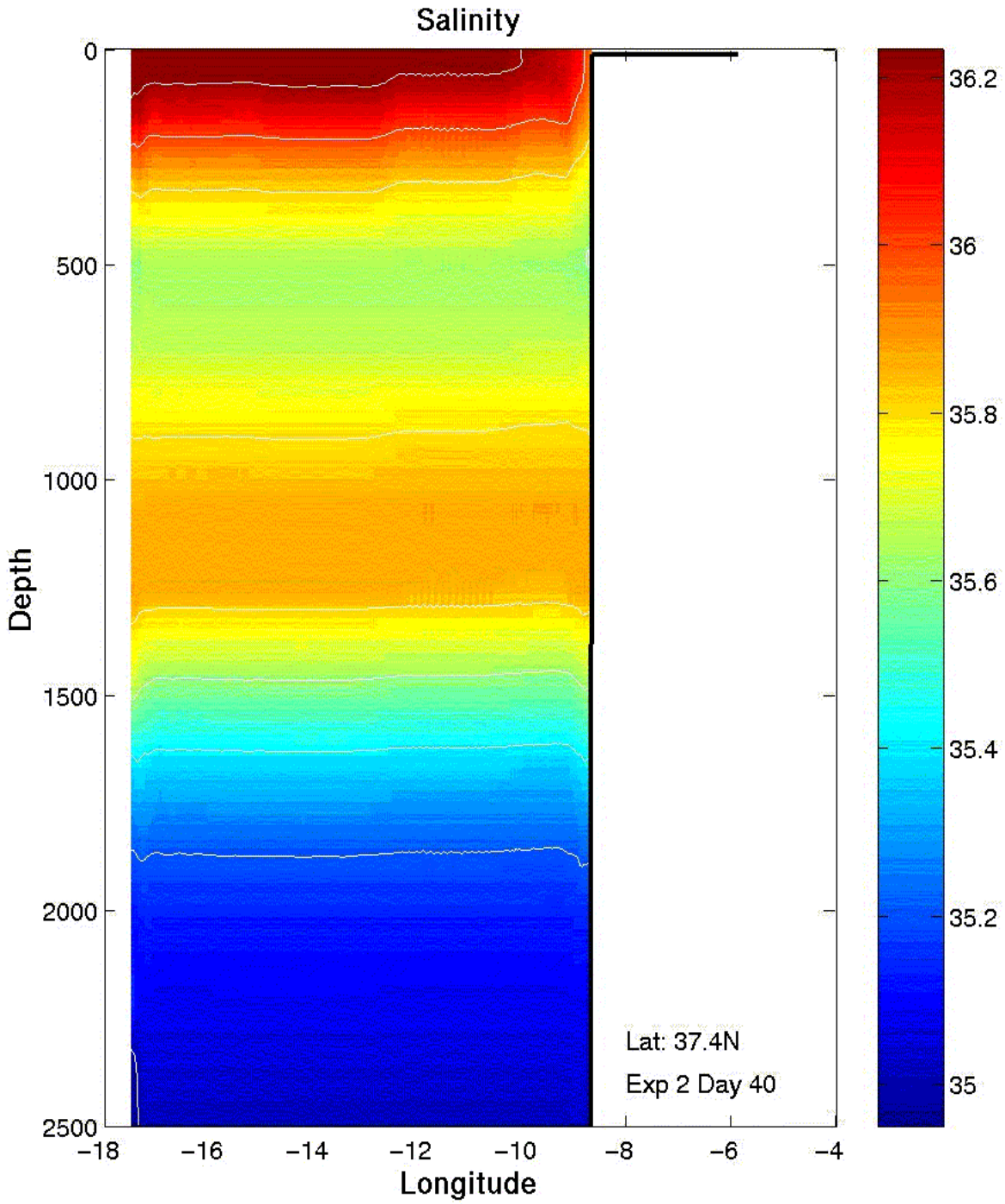

Figure 34. Cross-section at 37.4°N of salinity for Experiment 2 on day 40.

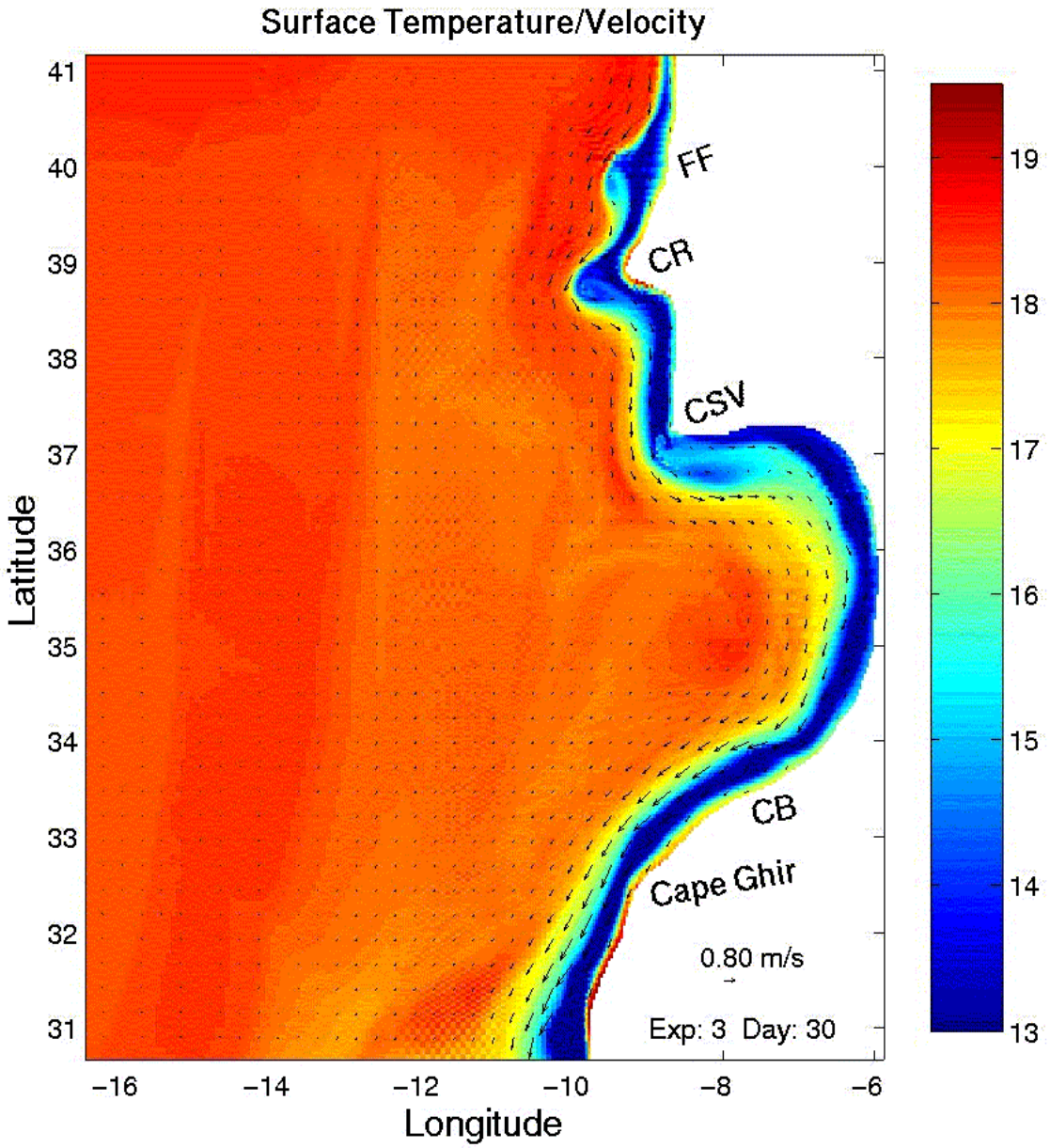

Figure 35. Surface velocity vectors (arrows) and temperatures (in color) for Experiment 3 on day 30.

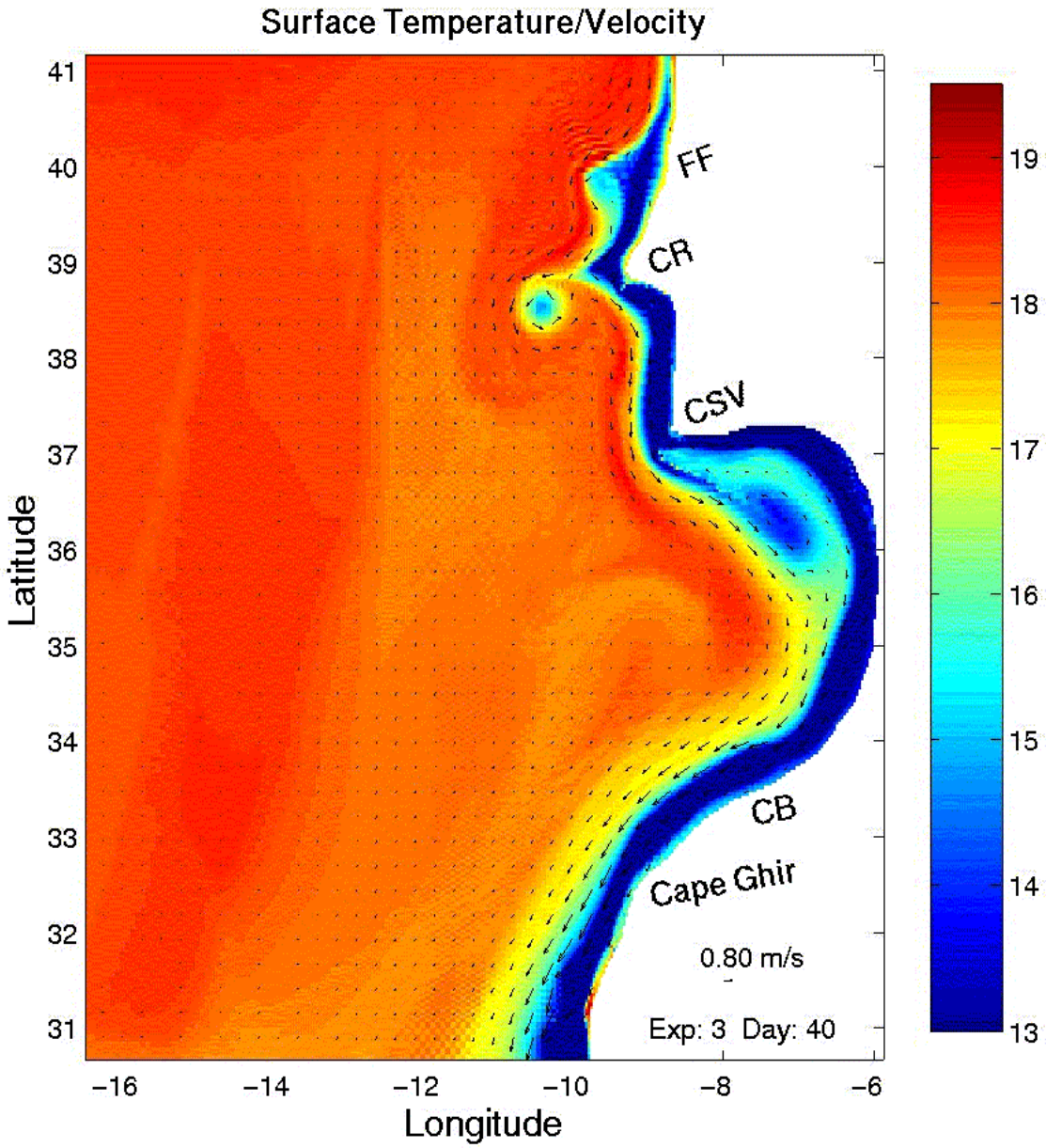

Figure 36. Surface velocity vectors (arrows) and temperatures (in color) for Experiment 3 on day 40.

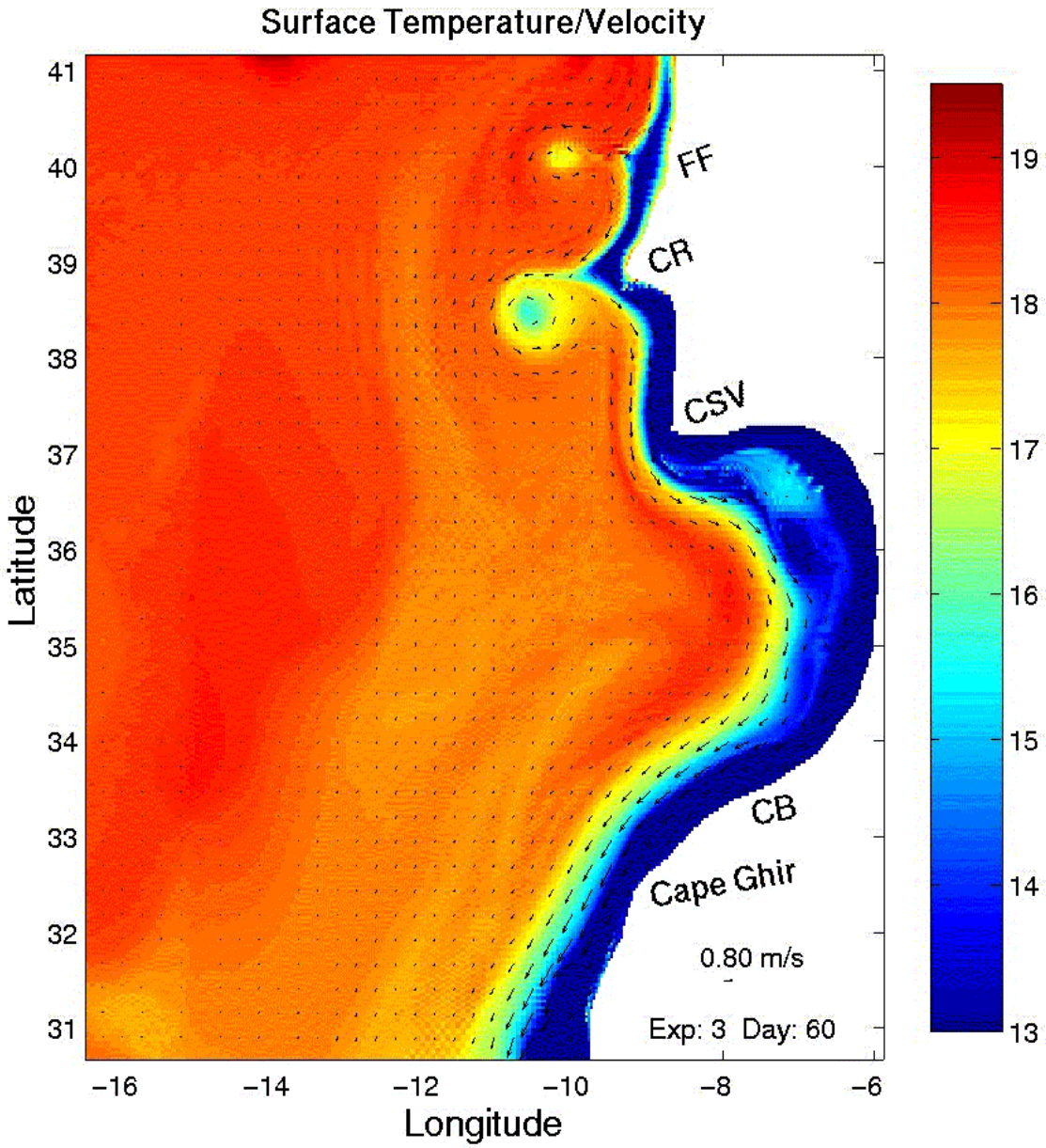

Figure 37. Surface velocity vectors (arrows) and temperatures (in color) for Experiment 3 on day 60.

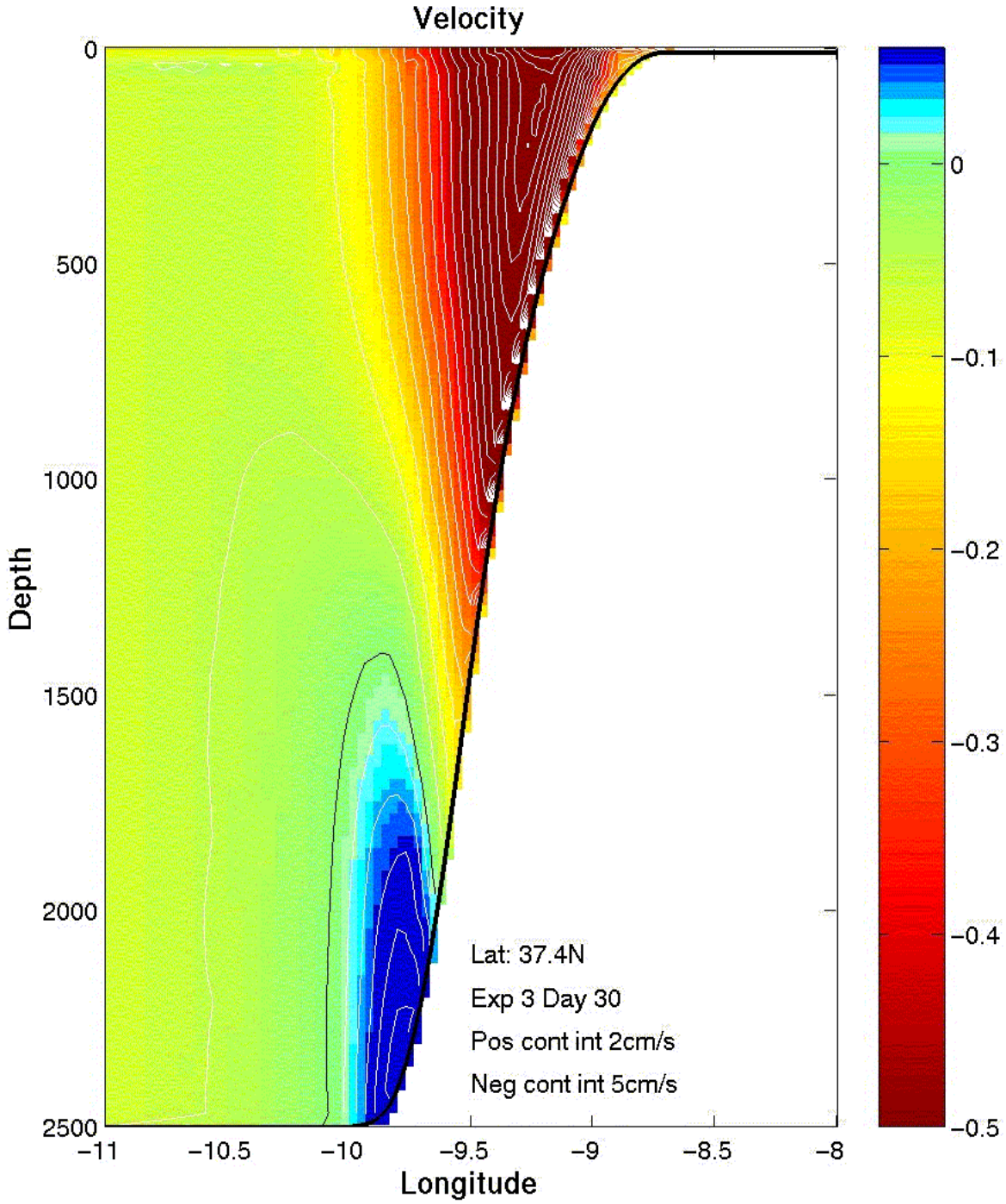

Figure 38. Cross-section of meridional velocity (v) at 37.4°N for Experiment 3 on day 30. Equatorward (poleward) flow is denoted by red (blue) color with contour intervals of 5 cm/s (2 cm/s).

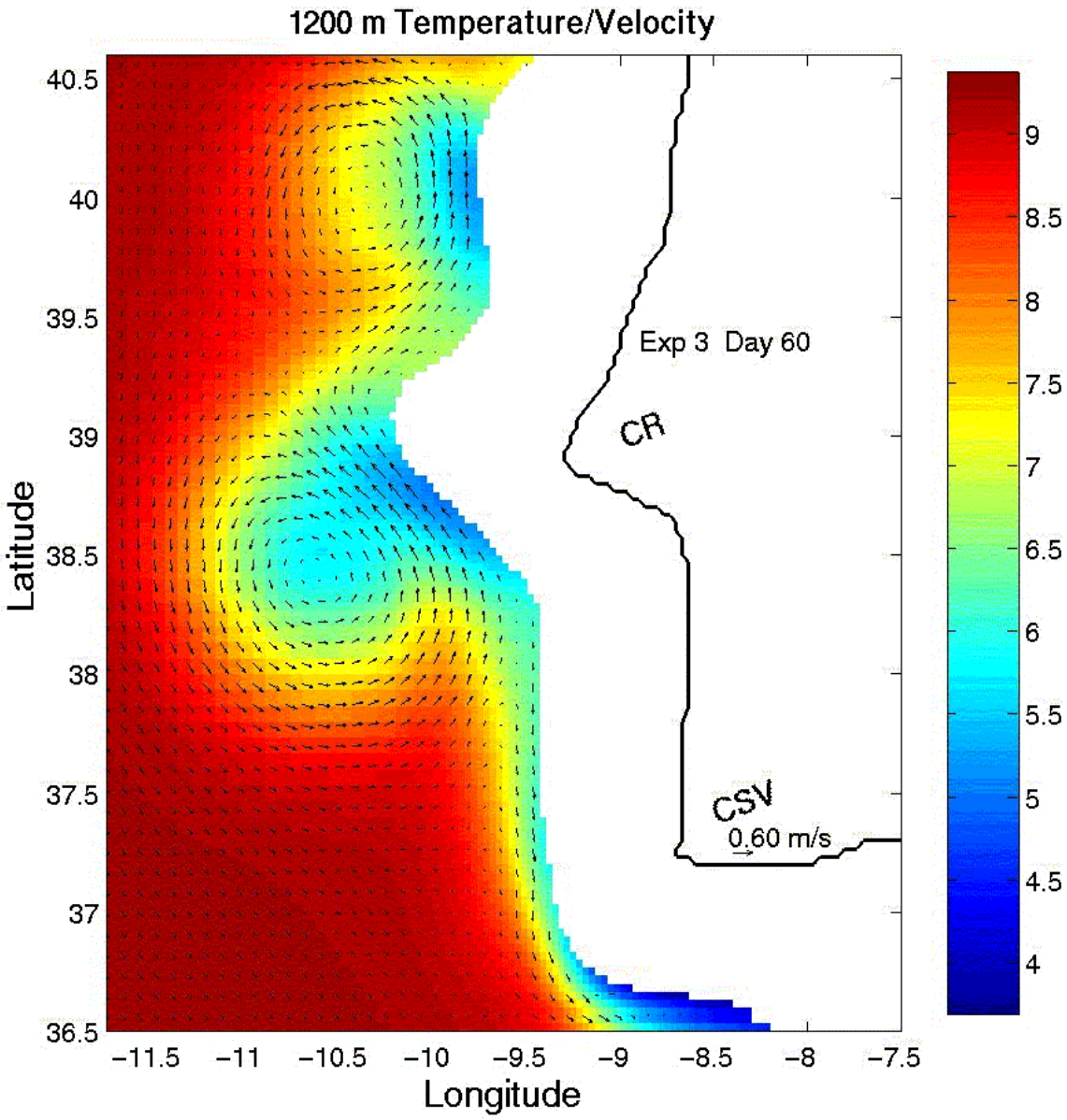

Figure 39. 1200 m velocity vectors (arrows) and temperatures (in color) for Experiment 3 on day 60.

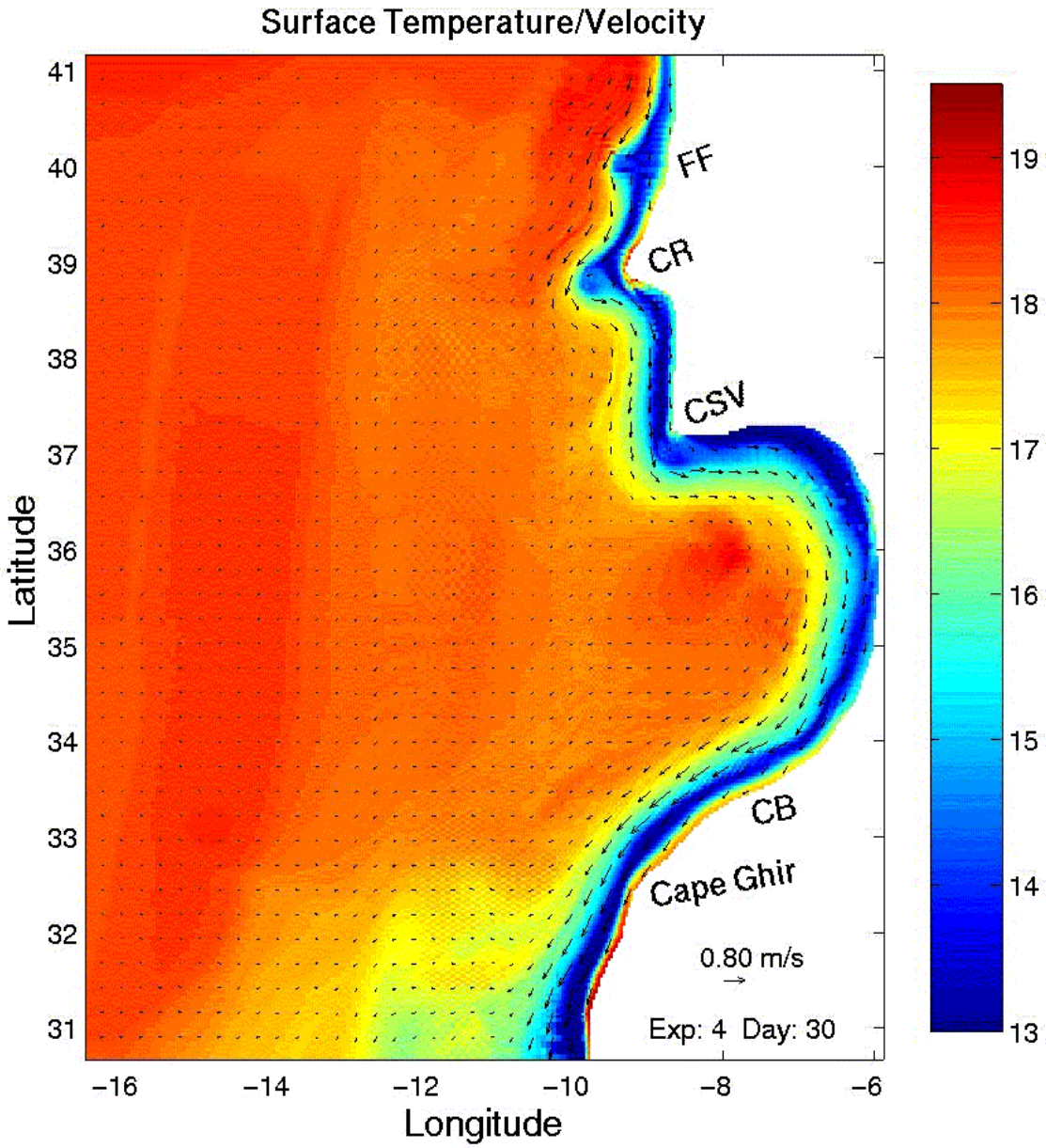

Figure 40. Surface velocity vectors (arrows) and temperatures (in color) for Experiment 4 on day 30.

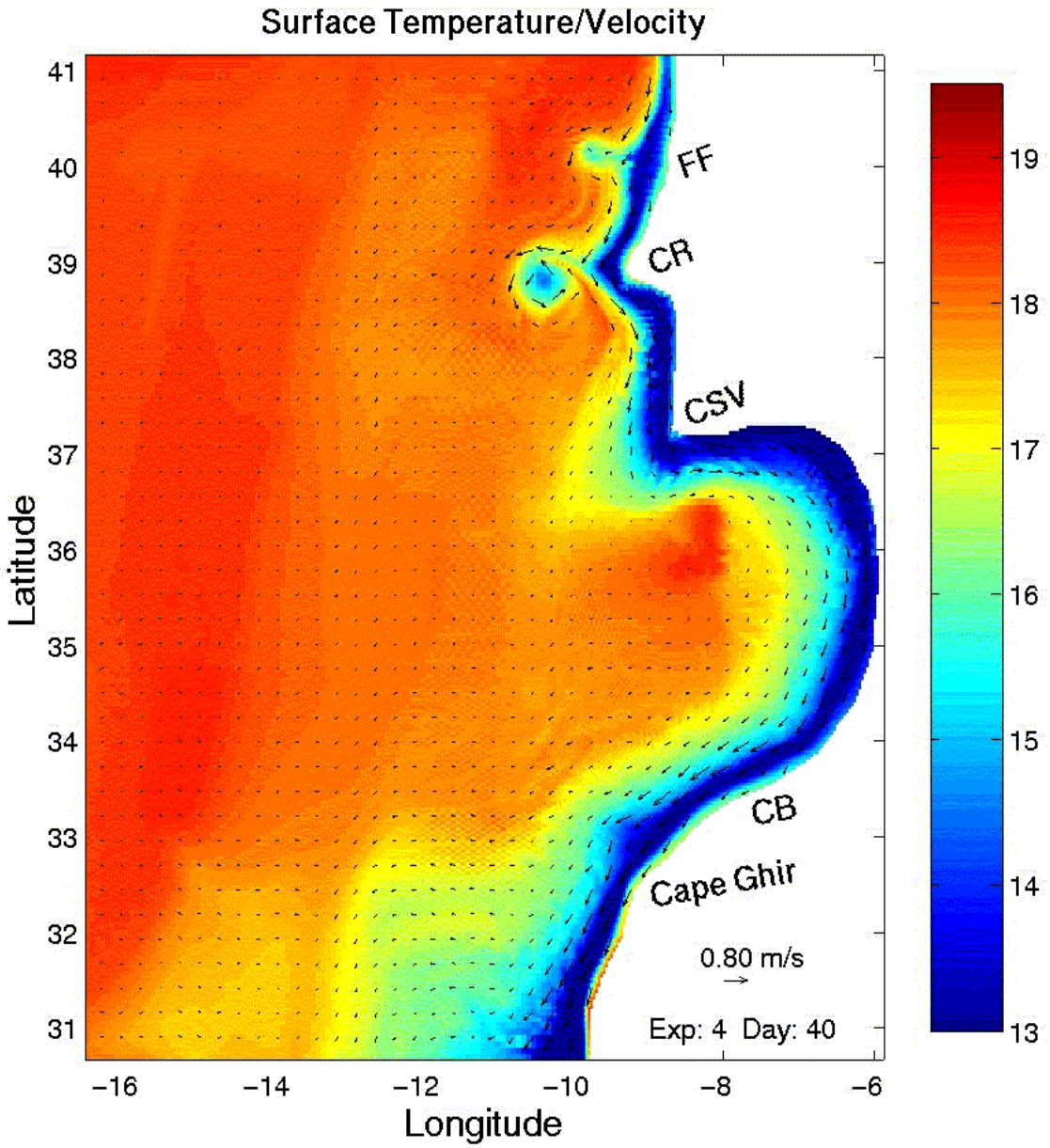

Figure 41. Surface velocity vectors (arrows) and temperatures (in color) for Experiment 4 on day 40.

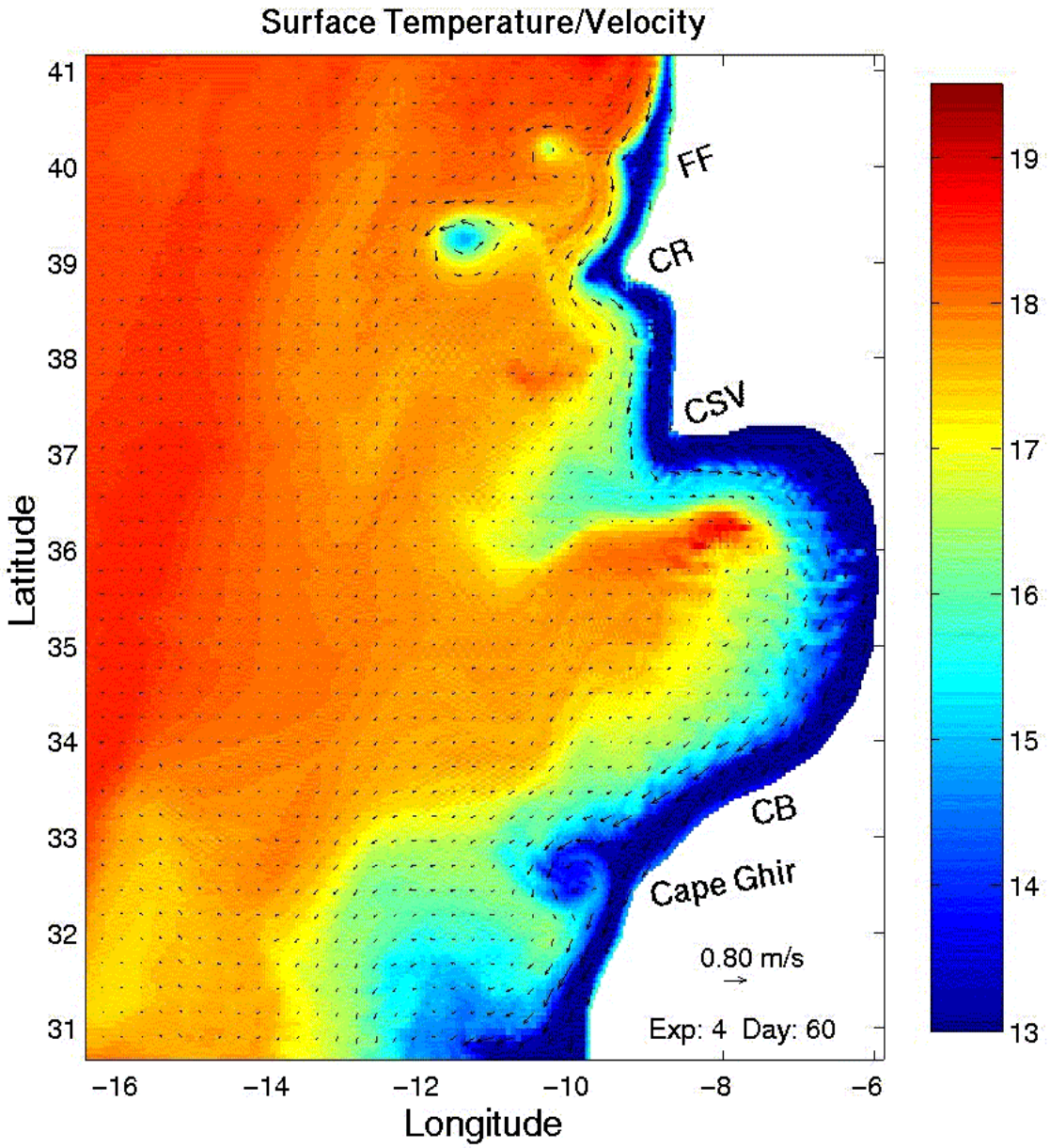

Figure 42. Surface velocity vectors (arrows) and temperatures (in color) for Experiment 4 on day 60.

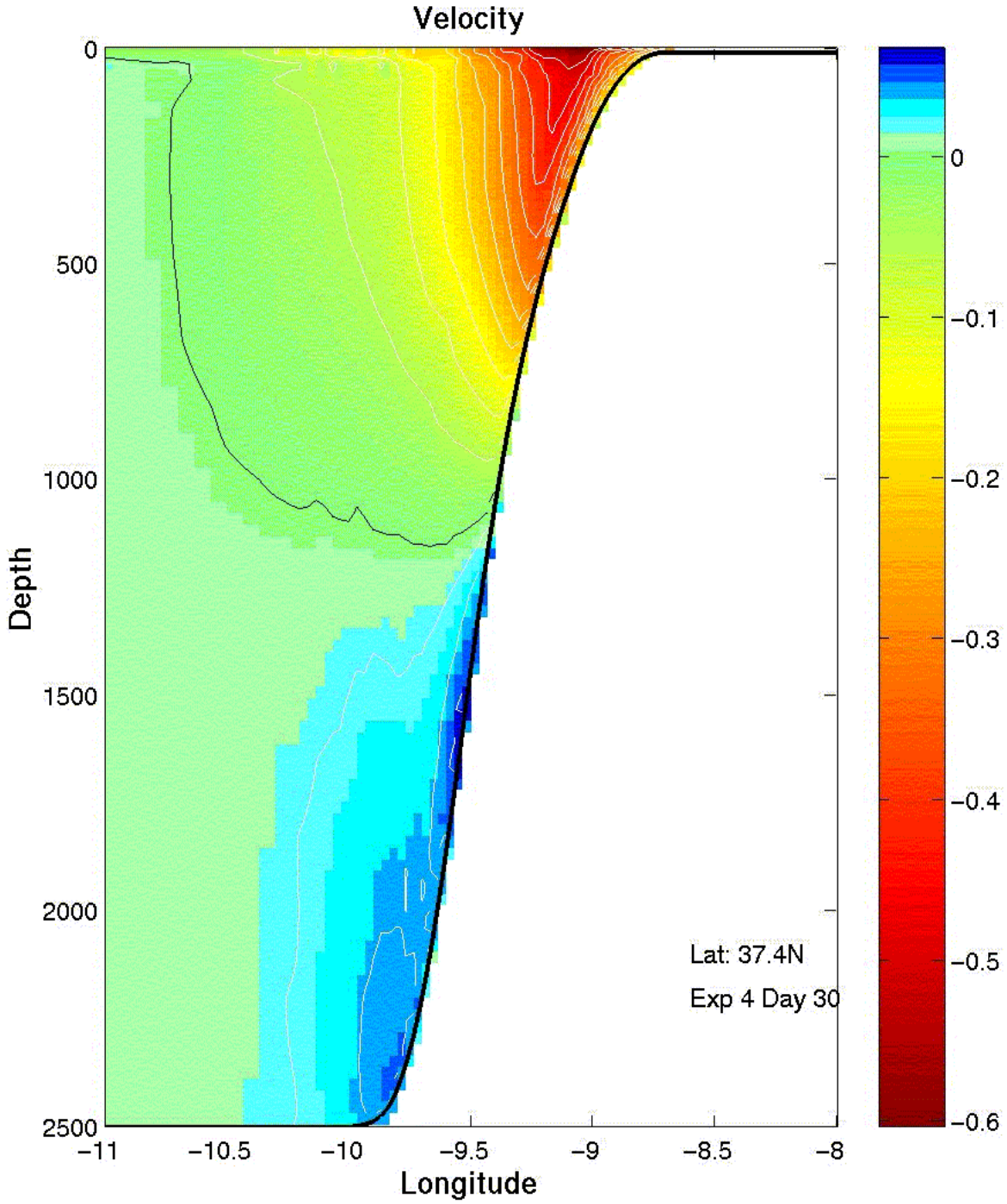

Figure 43. Cross-section of meridional velocity (v) at 37.4°N for Experiment 4 on day 30. Equatorward (poleward) flow is denoted by red (blue) color with contour intervals of 5 cm/s (2 cm/s).

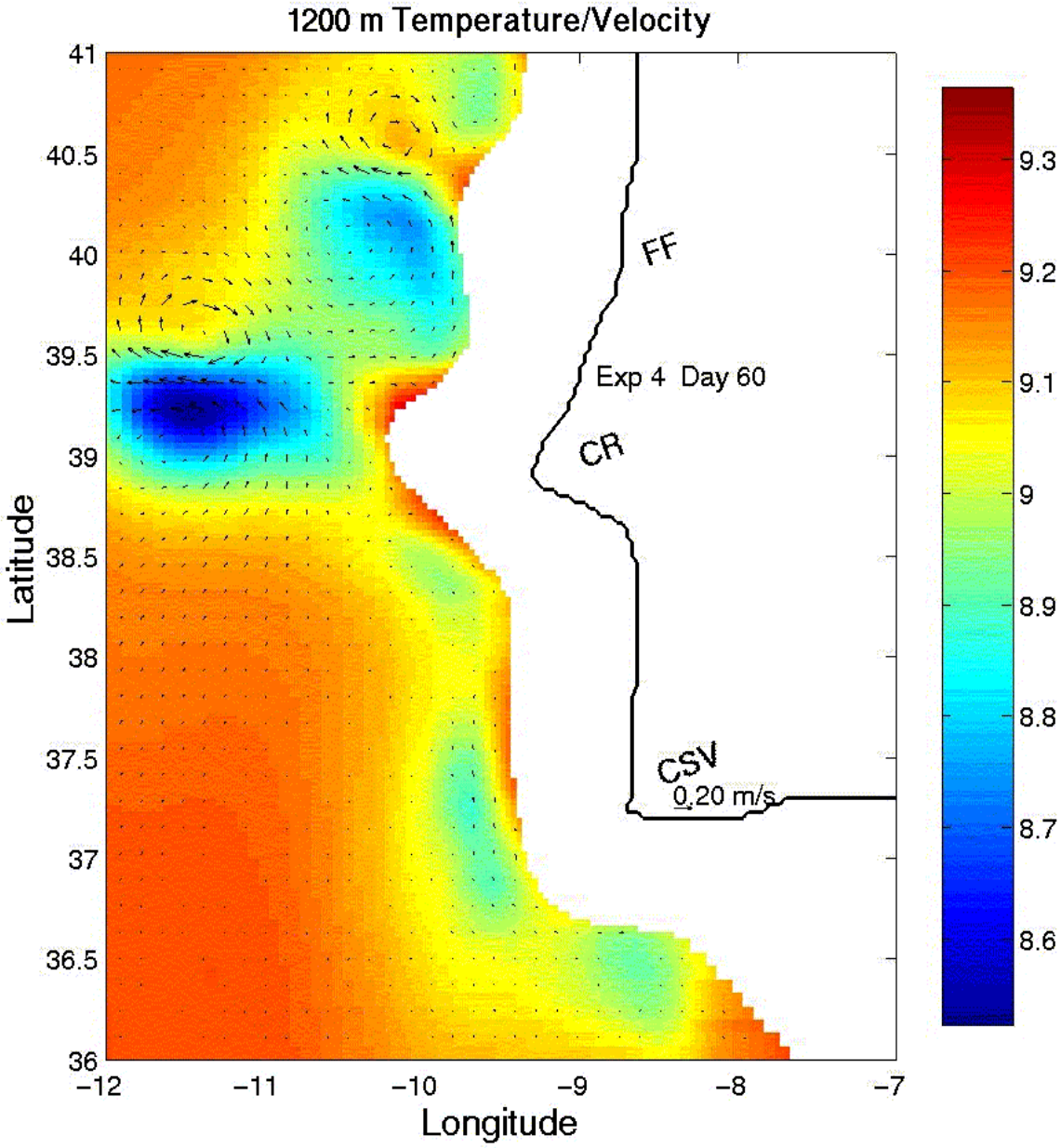

Figure 44. 1200 m velocity vectors (arrows) and temperatures (in color) for Experiment 4 on day 60.

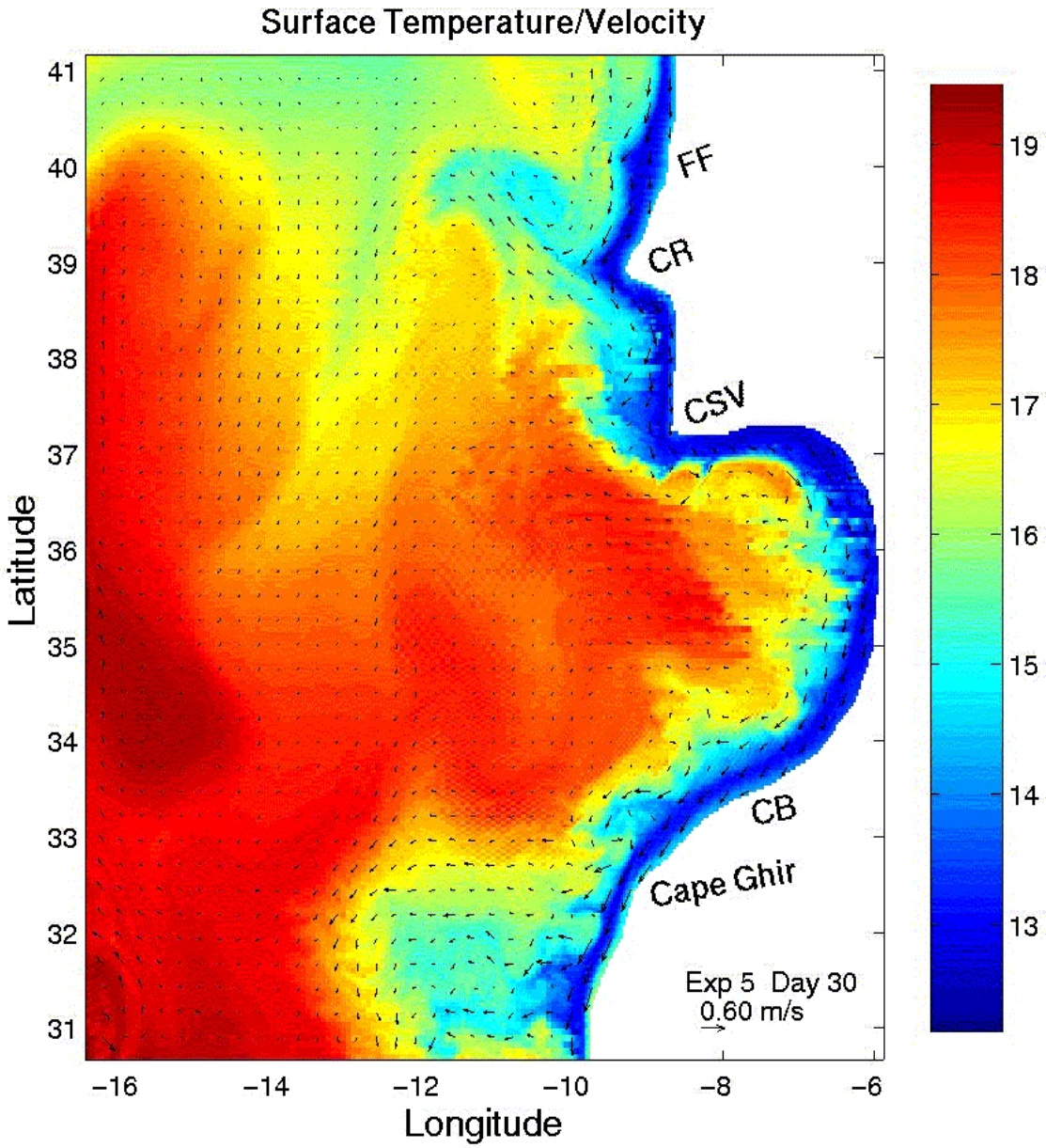

Figure 45. Surface velocity vectors (arrows) and temperatures (in color) for Experiment 5 on day 30.

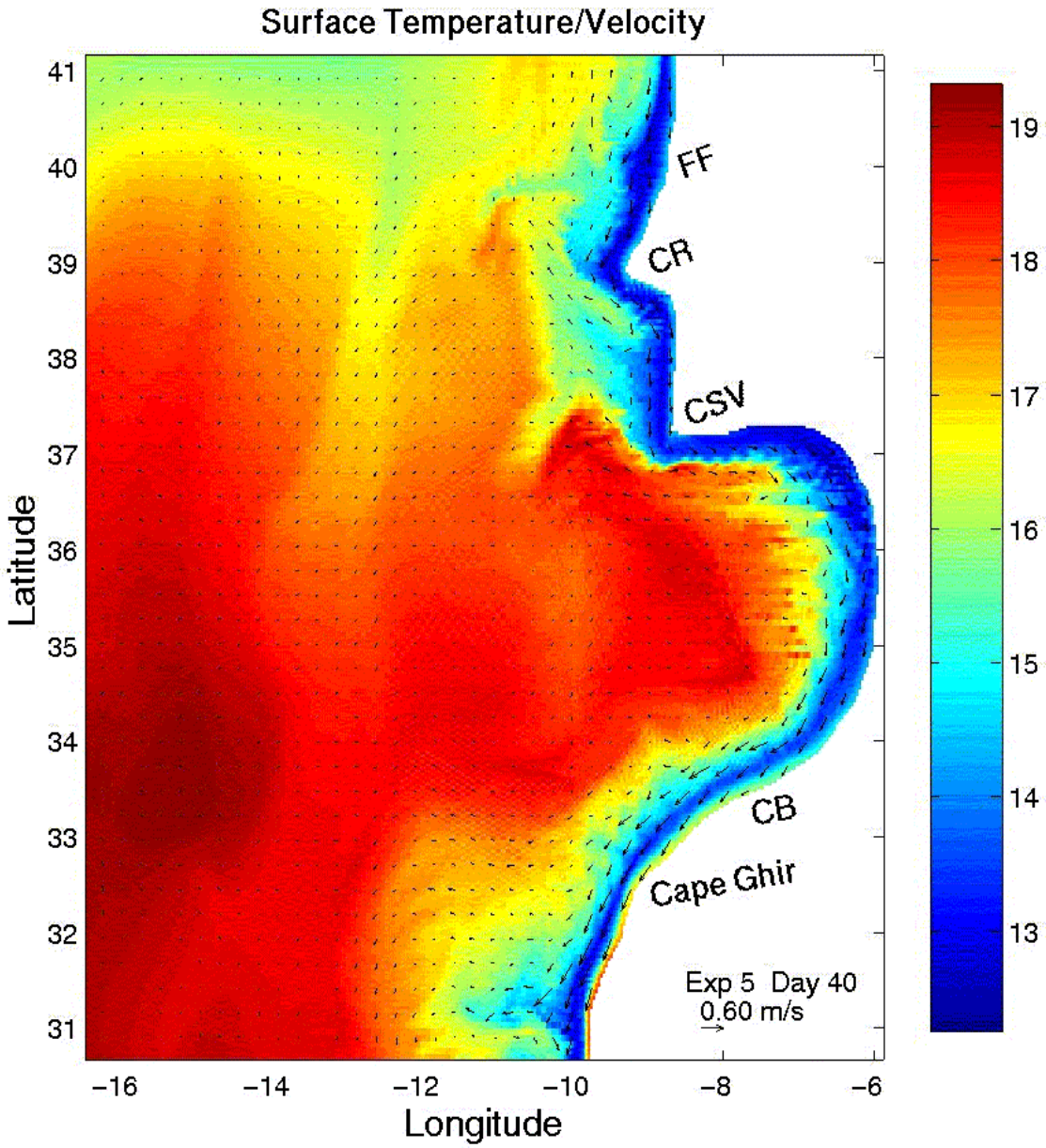

Figure 46. Surface velocity vectors (arrows) and temperatures (in color) for Experiment 5 on day 40.

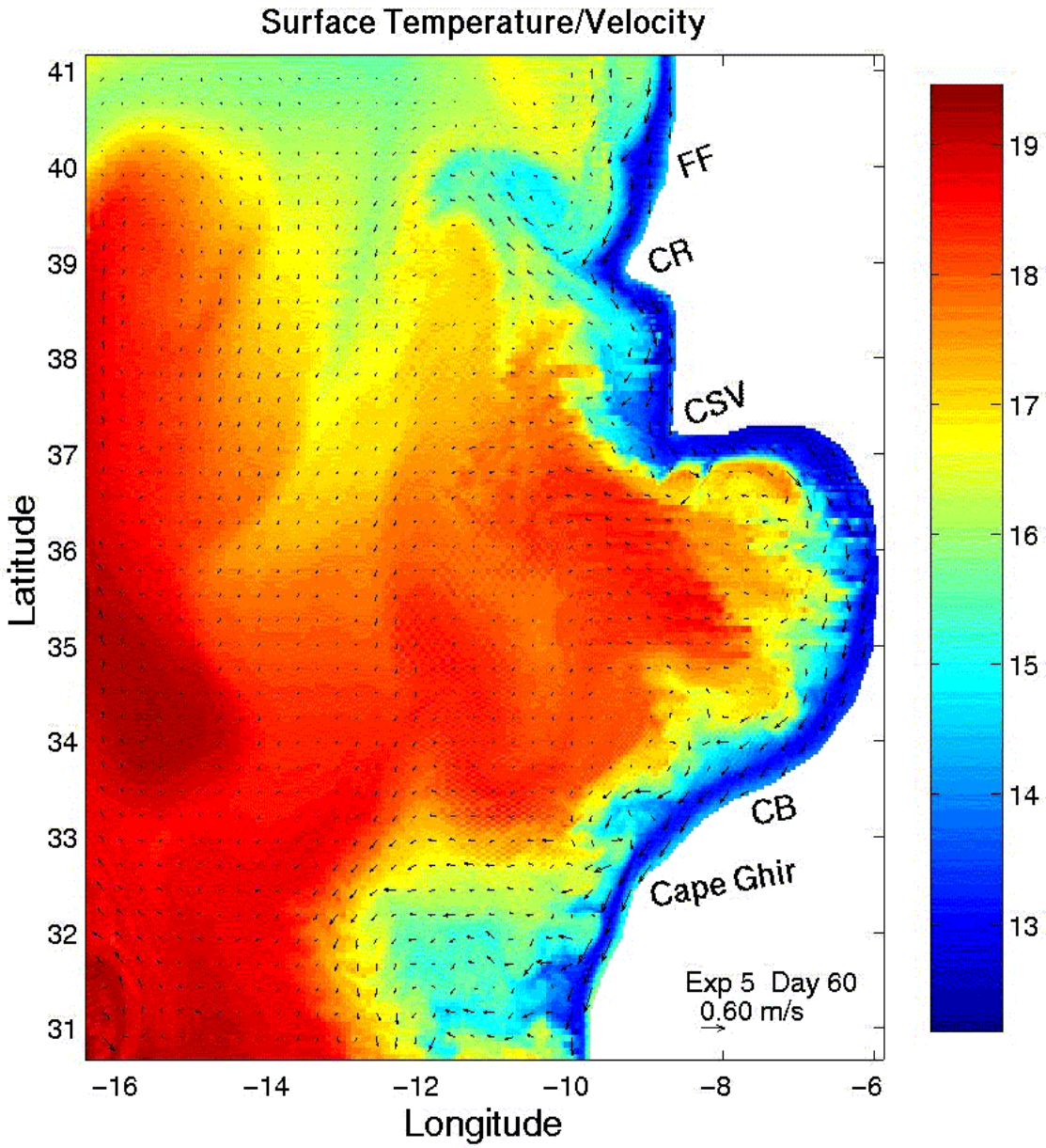

Figure 47. Surface velocity vectors (arrows) and temperatures (in color) for Experiment 5 on day 60.

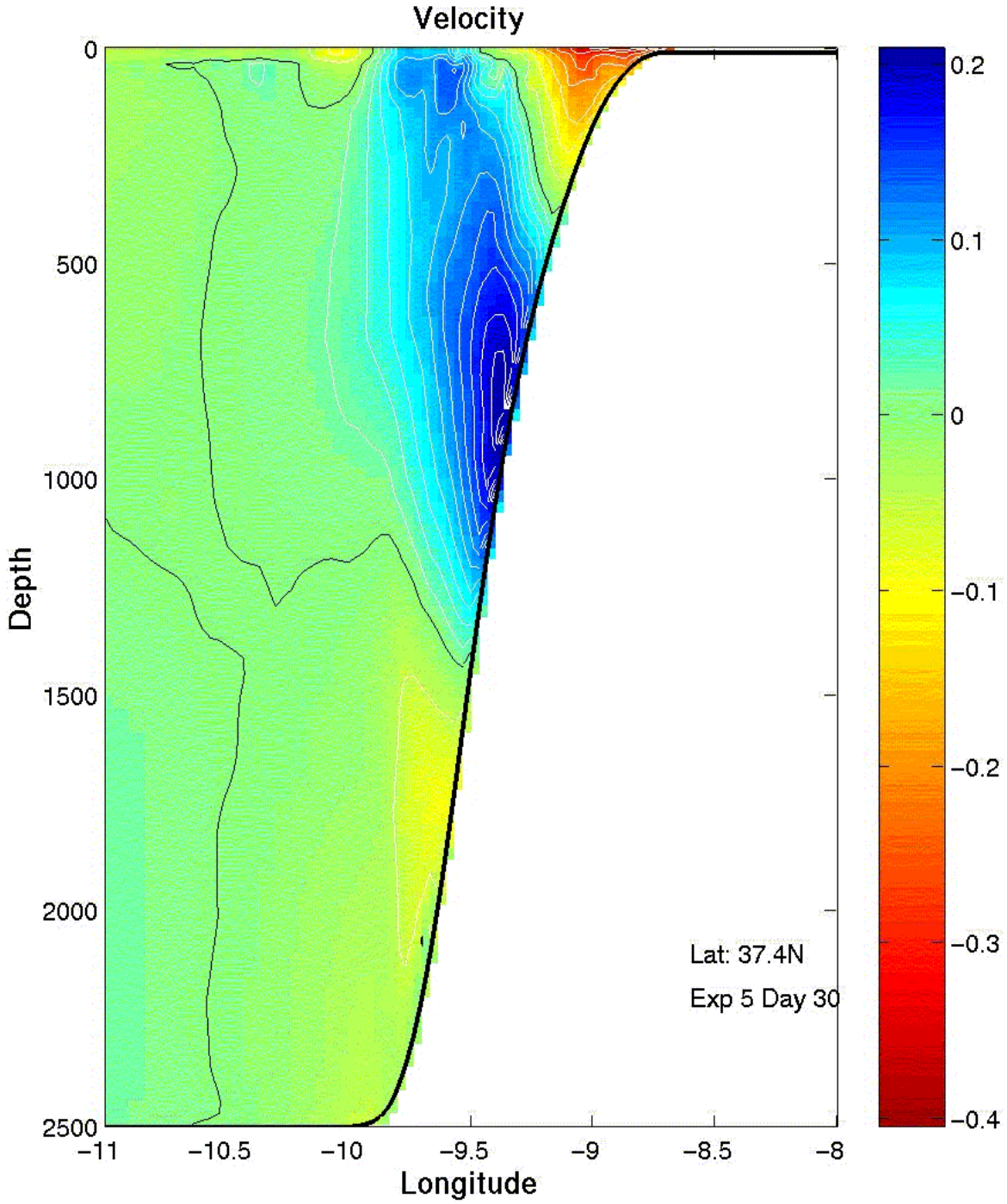

Figure 48. Cross-section of meridional velocity (v) at 37.4°N for Experiment 5 on day 30. Equatorward (poleward) flow is denoted by red (blue) color with contour intervals of 5 cm/s (2 cm/s).

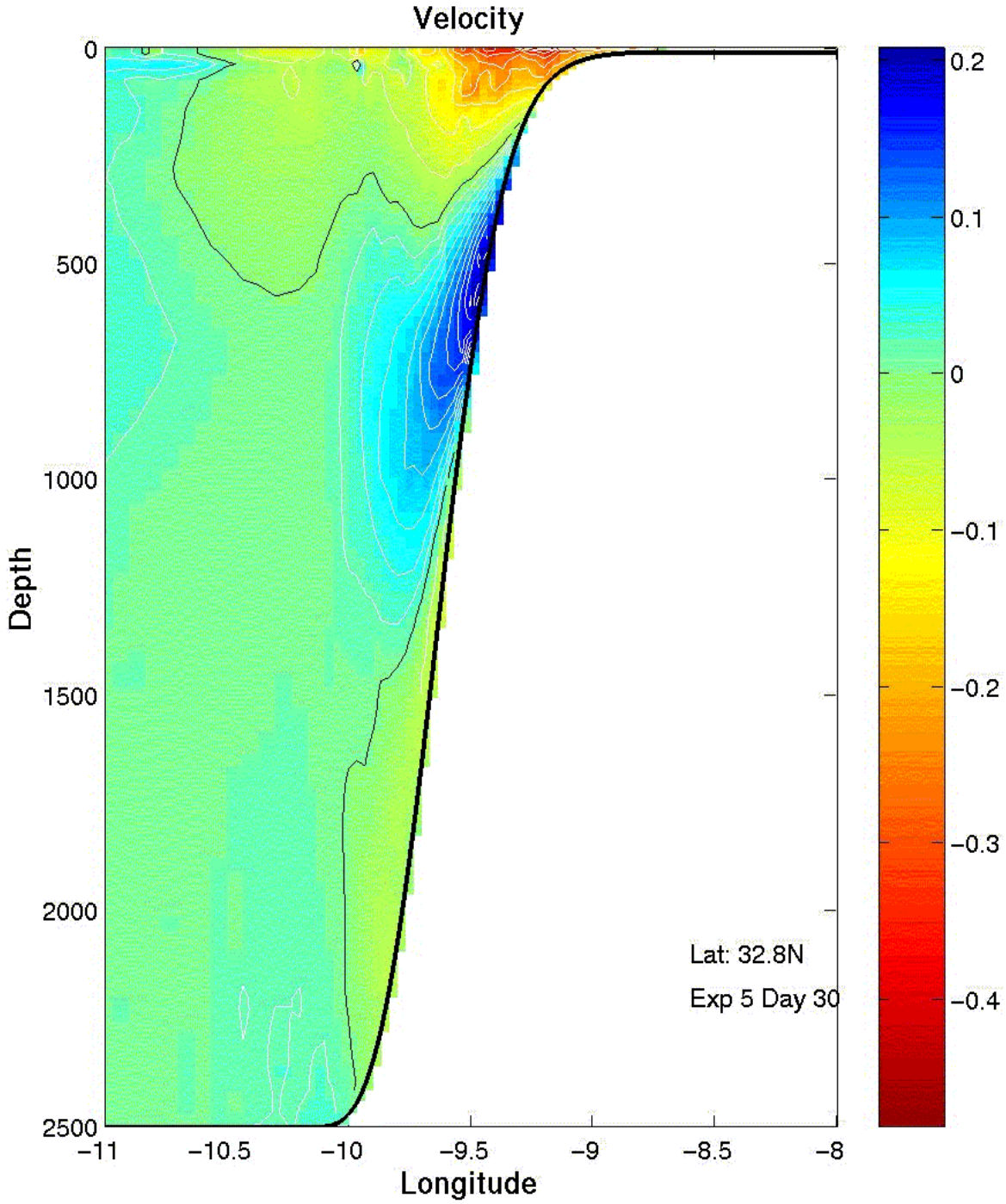

Figure 49. Cross-section of meridional velocity (v) at 32.8°N for Experiment 5 on day 30. Equatorward (poleward) flow is denoted by red (blue) color with contour intervals of 5 cm/s (2 cm/s).

THIS PAGE INTENTIONALLY LEFT BLANK

	EXP 1	EXP 2	EXP 3	EXP 4
TOPOGRAPHY	NO	NO	YES	YES
CORIOLIS PARAMETERIZATION	f – PLANE	BETA PLANE	f -PLANE	BETA PLANE

Table 1. Summary of specific experimental design in this study

Level	Depth (m)	Level	Depth (m)	Level	Depth (m)
1	0	12	300	23	1400
2	10	13	400	24	1500
3	20	14	500	25	1750
4	30	15	600	26	2000
5	50	16	700	27	2500
6	75	17	800	28	3000
7	100	18	900	29	3500
8	125	19	1000	30	4000
9	150	20	1100	31	4500
10	200	21	1200	32	5000
11	250	22	1300	33	5500

Table 2. Vertical levels and depth used by Levitus and Boyer (1994) and Levitus *et al*. (1994)

Level	Sigma Value	Level	Sigma Value
1	0	12	-0.61538
2	-0.00961	13	-0.69231
3	-0.01923	14	-0.76923
4	-0.03846	15	-0.84615
5	-0.07692	16	-0.92308
6	-0.15385	17	-0.96154
7	-0.23077	18	-0.98077
8	-0.30769	19	-0.99038
9	-0.38462	20	-0.99519
10	-0.46154	21	-1.0
11	-0.53846		

Table 3. Values of sigma levels

LIST OF REFERENCES

Ambar, I., Mediterranean Influence off Portugal, in *Actual Problems of Oceanography in Portugal, Junta Nacional de Investigacao Cientifica e Tecnologica, Lisboa*, 73-87, 1982.

Ambar, I., and M. R. Howe. Observations of the Mediterranean Outflow – 1. Mixing in the Mediterranean Outflow. *Deep-Sea Res*., 26, 535-554, 1979.

Barton, E. D., Eastern Boundary of the North Atlantic: Northwest Africa and Iberia. In *The Sea, Vol. 11, The Global Coastal Ocean: Regional Studies and Syntheses*, K. H. Brink and A. R. Robinson, eds., Wiley, New York, Chap. 22, 633-657, 1998.

Batteen, M. L., Wind-forced Modeling Studies of Currents, Meanders, and Eddies in the California Current System, *J. Geophys. Res*., 102, 985-1009, 1997.

Batteen, M. L. and Y. –J. Han, On the Computational Noise of Finite Difference Schemes used in Ocean Models, *Tellus*, 33, 387-396, 1981.

Batteen, M. L., R. L. Haney, T. A. Tielking, and P. G. Renaud, A Numerical Study of Wind Forcing of Eddies and Jets in the California Current System, *J. Mar. Res*., 47, 493-523, 1989.

Batteen, M. L., J. R. Martinez, D. W. Bryan, and E. J. Buch, A Modeling Study of the Coastal Eastern Boundary Current System off Iberia and Morocco, *J. Geophys. Res*., 105 (C6), 14,173-14,195, 2000.

Blumberg, A. F., and G. L. Mellor, A Description of a Three-Dimensional Coastal Ocean Circulation Model, *Three-Dimensional Coastal Ocean Models, Coastal Estuarine Sci*., 4, edited by N. Heaps, pp 1-16, AGU, Washington, D. C., 1987.

Chapman, D. C., Numerical Treatment of Cross-Shelf Open Boundaries in a Barotropic Coastal Ocean Model, *J. Phys. Oceanogr*., 25, 1060-1075, 1985.

Ezer, T. and G. L. Mellor, Diagnostic and Prognostic Calculations of the North Atlantic Circulation and Sea Level Using a Sigma Coordinate Ocean Model, *J.Geophys Res.*, 99 (C7), 14,159-14,171, 1994.

Ezer, T. and G. L. Mellor, Simulations of the Atlantic Ocean With a Free Surface Sigma Coordinate Ocean Model, *J. Geophys. Res*., 102 (C7), 15,647-15,657, 1997.

Fiuza, a. F. de G., The Portuguese Coastal Upwelling System, in *Actual Problems of Oceanography in Portugal, Junta Nacional de Investigacao Cientifica e Tecnologica, Lisboa*, 45-71, 1980.

Fiuza, A. F. de G., M. E. de Macedo, M. R. Guerreiro, Climatological Space and Time Variation of the Portuguese Coastal Upwelling, *Oceanologica Acta*, Vol. 5, No. 1, 31-40, 1982.

Fiuza, A. F. de G., Hidrologia e dinamica das Aguas costeiras de Portugal. Dissertacao apresentada a Universidade de Lisboa para obtencao do grau de doutor em Fisica, especializacao em Ciencias Geofisicas. Univ Lisboa, 194pp., 1984.

Fiuza, A. F. de G. and F. M. Sousa, Preliminary results of a CTD survey in the Coastal Transition Zone off Portugal During 1-9 September 1988, *Coastal Transition Zone Newsletter*, 4, 2-9, 1989.

Frouin, R., A. F. G. Fiuza, I. Ambar, and T. J. Boyd, Observations of a Poleward Surface Current off the Coasts of Portugal and Spain During Winter, *J. Geophys. Res*., 95, 679-691, 1990.

Hagen, E. C. Zulicke, and R. Feistel, Near-surface structures in the Cape Ghir filament off Morocco, *Oceanol. Acta*, 19, 6, 577-598, 1996.

Haidvogel, D. B., A. Beckmann, and K. S. Hedstrom, Dynamical Simulation of Filament Formation and Evolution in the Coastal Transition Zone, *J. Geophys. Res*., 96, 15,017-15,040, 1991.

Haynes, R. and E. D. Barton, A Poleward Flow Along the Atlantic Coast of the Iberian Peninsula, *J. Geophys. Res*., 95, 11425-11441, 1990.

Haynes, R., E. D. Barton, and I. Piling, Development, Persistence and Variability of Upwelling Filaments off the Atlantic Coast of Iberia, *J. Geophys. Res*., 98, 22681-22692, 1993.

Ikeda, M., W. J. Emery, and L. A. Mysak, Seasonal Variability in Meanders of the California Current System off Vancouver Island, *J. Geophys. Res*., 89, 3487-3505, 1984a.

Ikeda, M., L. A. Mysak, and W. J. Emery, Observations and Modeling of Satellite-sensed Meanders and Eddies off Vancouver Island, *J. Phys. Oceanogr*., 14, 3-21, 1984b.

Iorga, M. C., and M. S. Lozier, Signatures of the Mediterranean Outflow From a North Atlantic Climatology, 1. Salinity and Density Fields, *J. Geophys. Res*., 104, 25,985-26,009, 1999.

Kase, R. H., A. Beckmann, and H. H. Hinrichsen, Observational Evidence of Salt Lens Formation in the Iberian Peninsula, *J. Geophys. Res*., 94, 4905-4912, 1989.

Levitus, S., and T. P. Boyer, World Ocean Atlas 1994, Vol.4: Temperature, *NOAA Atlas NESDI 4*, 117 pp., U. S. Dept. of Commerce, Washington, D. C., 1994.

Levitus, S., R. Burgett, and T. P. Boyer, World Ocean Atlas, 1994, Vol. 3: Salinity, *NOAA Atlas NESDI 3*, 99 pp., U. S. Dept. of Commerce, Washington, D. C., 1994.

McCreary, J. P., Y. Fukamachi, and P. K. Kundu, A Numerical Investigation of Jets and Eddies Near an Eastern Ocean Boundary, *J. Geophys. Res*., 92, 2515-2534, 1991.

Meincke, J., G. Siedler, and W. Zenk, Some Current Observations Near the Continental Slope off Portugal, *"Meteor" Forsch.–Ergebn*., A, 16, 15-22, 1975.

Mellor, G. L., User's Guide for a Three-Dimensional, Primitive Equation, Numerical Ocean Model, 40 pp., Program in Atmos. And Ocean Sci. report, Princeton Univ., Princeton, N. J., 1996.

Mellor, G. L., L. Y. Oey, and T. Ezer, Sigma Coordinate Pressure Gradient Errors and the Seamount Problem, *Journal of Atmospheric and Ocean Technology*, 15, 1122-1131, 1998.

Mellor, G. L., and T. Yamada, Development of a Turbulence Closure Model for Geophysical Fluid Problems, *Rev. Geophys. Space Phys*., 20, 851-875, 1982.

Nelson, C.S., Wind Stress and Wind Stress Curl over the California Current, NOAA Tech Rep. NMFS SSFR-714, U. S. Dept. Commerce, 87 pp., 1977.

Palma, E. D., and R. P. Matano, On the Implementation of Passive Open Boundary Conditions for a General Circulation Model: The Barotropic Mode, *J. Geophys. Res*., 103 (C1), 1319-1341, 1998.

Palma, E. D., and R. P. Matano, On the Implementation of Open Boundary Conditions for a General Circulation Model: The Three-Dimensional Case, *J. Geophys. Res*., 105 (C4), 8605-8627, 2000.

Pares-Sierra, A., W. B. White, and C. –K. Tai, Wind-driven Coastal Generation of Annual Mesoscale Eddy Activity in the California Current System: A Numerical Model, *J. Phys. Oceanogr*., 23, 1110-1121, 1993.

Richardson, P. L., and A. Tychensky, Meddy Trajectories in the Canary Basin Measured During the SEMAPHORE Experiment, 1993-1995, *J. Geophys. Res*., 103, 25,029-25,045, 1998.

Sandwell, D. T., and W. F. Smith, Global Bathymetric Prediction for Ocean Modeling and Marine Geophysics, 1996.

J. Smagorinsky, S. Manabe, and J.L. Holloway. Numerical results from a nine-level general circulation model of the atmosphere. *Mon. Wea. Rev.*, 93:727--768, 1965.

Stammer, D., H. H. Hinrichsen, and R. H. Kase, Can Meddies be Detected by Satellite Altimetry?, *J. Geophys. Res*., 96, 7005-7014, 1991.

Tomczak, M. and J. S. Godfrey*, Regional Oceanography: An Introduction*, Pergamon Press, New York, 422 pp., 1994.

Trenberth, K. E., W. G. Large, J. G. Olsen, The Mean Annual Cycle in Global Ocean Wind Stress, *J. Phys Oceanogr*., 20, 1742-1760, 1990.

Van Camp, L., L. Nykjaer, E. Mittelstaedt, and P. Sclittenhardt, Upwelling and Boundary Circulation off Northwest Africa as Depicted by Infrared and Visible Satellite Observations, *Prog. Oceanog*., 26, 357-402, 1991.

Wooster, W.S., A. Bakun, and D. R. McLain, The Seasonal Upwelling Cycle Along the Eastern Boundary of the North Atlantic, *J. Mar. Res*., 34, 131-140, 1976.

INITIAL DISTRIBUTION LIST

1. Defense Technical Information Center
   8725 John J. Kingman Rd, STE 0944
   Ft. Belvoir, VA 22060-6218

2. Dudley Knox Library
   Naval Postgraduate School
   411 Dyer Rd
   Monterey, CA 93943-5101

3. Chairman (Code OC/Bv)
   Department of Oceanography
   Naval Postgraduate School
   Monterey, CA 93943-5122

4. Chairman (Code MR/Wx)
   Department of Meteorology
   Naval Postgraduate School
   Monterey, CA 93943-5114

5. Dr. Mary L. Batteen
   Department of Oceanography
   Naval Postgraduate School
   Monterey, CA 93943-5122

6. Dr. R. T. Williams
   Department of Meteorology
   Naval Postgraduate School
   Monterey, CA 93943-5114

7. LT Wendy A. Towle
   11525 76th Ave NW
   Marysville, WA 98271